UNIVERSITY OF PARDUBICE

FACULTY OF TRANSPORT ENGINEERING

LOSS OF STABILITY OF THIN-WALLED CONICAL SHELLS WITH CIRCUMFERENTIAL RING LOADED BY AXIAL FORCE

A Thesis Submitted for the Degree of Ph.D.

2018 M.Sc. Haluk Yılmaz

Programme of Study:

P3710 Technique and Technology in Transport and Communications

Branch of study:

3708V024 Technology and Management in Transport and Telecommunications

Supervisor: doc. Ing. Petr Tomek, Ph.D.

Supervisor Specialist: Prof. Ing. Petr Paščenko, Ph.D.

Doctoral dissertation topic:

Loss of Stability of Thin-Walled Conical Shells with Circumferential Ring Loaded by Axial Force

The doctoral dissertation has arisen at the supervising:

Department of Mechanics, Material and Machines Part

ABSTRACT

This dissertation is devoted to the effects of the circumferential ring on the loss of stability of the conical shells loaded by an axial force. The truncated conical shell with different shell thicknesses and base angles at the lower edge are investigated in this thesis. The main aim is a proposal a new method to calculation of load carrying capacity of the conical shell structures with a base angle less than 25° loaded by axial force. The proposed method is applicable for different radial stiffness of the circumferential ring. Two dimensionless similarity parameters are used in this method. Numerical models are created in COSMOS/M package program. The numerical analyses were performed for different angles, shell thickness and radial stiffness of circumferential ring. Empirical relationships are established based on the results of the numerical analysis.

KEYWORDS

Conical shell, Circumferential ring, Load Carrying Capacity, Axial loading, FEM

NÁZEV

Ztráta stability tenkostěnných kuželových skořepin s obvodovým prstencem zatížených osovou silou.

SOUHRN

Tato dizertační práce se zabývá vlivem obvodového prstence na ztrátu stability kuželových skořepin zatížených osovou silou. V této dizertační práci jsou zkoumány komolé kuželové skořepiny s rozdílnou tloušťkou pláště a úhlem vzepětí. Hlavním cílem je návrh nové metody pro výpočet únosnosti komolých kuželových skořepin s úhlem vzepětí nižším než 25° zatížených osovou silou. Navržená metoda je aplikovatelná pro různé radiální tuhosti obvodového prstence. V rámci této metody jsou použité dva bezrozměrné podobnostní parametry. Numerické modely jsou vytvořeny v programu COSMOS/M. Numerické analýzy byly provedeny pro různé úhly vzepětí, tloušťky pláště skořepiny a radiální tuhosti obvodového prstence. Na základě výsledků numerických analýz jsou stanoveny empirické vztahy.

KLÍČOVÁ SLOVA

Kuželová skořepina, Obvodový prstenec, Únosnost, Osové zatížení, MKP

Author's Declaration

I hereby declare:

This thesis was prepared separately. All the literary sources and the information I used in the thesis are listed in the bibliography.

I was familiar with the fact that rights and obligations arising from the Act No. 121/2000 Coll., Copyright Act, apply to my thesis, especially with the fact that the University of Pardubice has the right to enter into a license agreement for the use of this thesis as a school work pursuant to § 60, Section 1 of the Copyright Act, and the fact that should this thesis be used by me or should a license be granted for the use to another entity, the University of Pardubice is authorized to claim from me a reasonable contribution to cover the costs incurred during the making of the thesis, according to the circumstances up to the actual amount thereof.

I agree with the reference only disclosure of my thesis in the University Library.

In Pardubice on …. / …. / ….

Haluk YILMAZ

Acknowledgments

First and foremost, I would like to express my very great appreciation to my supervisor doc. Ing. Petr Tomek, Ph.D. for his patient guidance and useful critiques of this research work. I would also like to thank Prof. Ing. Petr Paščenko, Ph.D., who provided an insight into the inception of my research.

I would like to express my very great appreciation to Anadolu University of Turkey and Council of Higher Education of Turkey for the financial support to my Ph.D. study.

I would also like to extend my thanks to my colleagues in Pardubice for their help and motivation during this research.

Last but not the least, I would like to thank my family: my parents and my wife for supporting me spiritually throughout my Ph.D. study.

Haluk YILMAZ

TABLE OF CONTENT

LIST OF FIGURES

LIST OF TABLES

NOMENCLATURE

Symbols

A_{ring}	$[mm^2]$	Cross-sectional area of the circumferential ring
C_x	$[-]$	Dimensionless boundary condition parameter
D	$[Nm]$	Flexural rigidity
E	$[MPa]$	Modulus of elasticity
E_t	$[MPa]$	Tangent Modulus
F_{lim}	$[N]$	Limit load
F_{cr}	$[N]$	Critical load
$F_{Normalized}$	$[-]$	Normalized axial load
L	$[mm]$	Length of the conical shell edge
M	$[Nm]$	Moment
N	$[N]$	In-plane force
P_x	$[N]$	Primary force in x direction
P_θ	$[N]$	Primary force in θ direction
Q	$[N]$	Transverse shear force
Q_{pr}	$[-]$	Quality of production
$S_{x\theta}$	$[N]$	Primary shear force
Z	$[-]$	Shape factor
b_{ring}	$[mm]$	Width of the circumferential ring
$f_{y,k}$	$[MPa]$	Yield stress
f_u	$[MPa]$	Ultimate tensile stress
h	$[mm]$	Height of the relatively stiff pipe
k_c	$[-]$	Load factor
k_x	$[-]$	Buckling stress coefficient
l	$[mm]$	Length of the cylindrical shell
l_e	$[mm]$	Equivalent length of the conical shell
l_g	$[mm]$	Reference length (length of ruler to measure imperfections)
m	$[-]$	Number of half waves in x direction
n	$[-]$	Number of half waves in θ direction
r	$[mm]$	Middle surface radius
r_1	$[mm]$	Upper radius of the conical shell
r_2	$[mm]$	Bottom radius of the conical shell
r_e	$[mm]$	Equivalent radius of the conical shell
x	$[-]$	Axis in longitudinal direction
u	$[mm]$	Displacement in x direction
v	$[mm]$	Displacement in θ direction
w	$[mm]$	Displacement in z direction

t	$[mm]$	Middle surface thickness
t_{shell}	$[mm]$	Shell thickness of the conical shell
z	$[-]$	Axis in radial direction
Γ	$[-]$	Rigidity parameter of the circumferential ring
α_c	$[deg]$	Base angle (Angle at the lower edge)
α_x- α	$[-]$	Elastic imperfection reduction coefficient (Reduction coefficient)
β_c	$[deg]$	Half-cone angle
β	$[-]$	Plastic range factor
θ	$[-]$	Axis in tangential direction
γ_{Ml}	$[-]$	Partial safety factor
γ	$[mm/mm]$	Shear strain
σ_{xEd}	$[MPa]$	Buckling meridional membrane stress
σ_{xRcr}	$[MPa]$	Elastic critical buckling stress
σ_{xRd}	$[MPa]$	Design value of the buckling stress
σ_{xRk}	$[MPa]$	Characteristic buckling stress
λ_0	$[-]$	Squash limit relative slenderness
λ_p	$[-]$	Plastic limit relative slenderness
λ_x	$[-]$	Relative slenderness
χ_x	$[-]$	Buckling reduction factor
ω	$[-]$	Dimensionless geometric parameter
η	$[-]$	Interaction exponent
Δw_k	$[-]$	Characteristic imperfection amplitude
μ	$[-]$	Poisson's ratio
ε	$[mm/mm]$	Strain

Abbreviations

ECCS	European Convention for Constructional Steelwork
FEM	Finite Element Method
GNA	Geometrically Nonlinear Elastic Analysis
GMNA	Geometrically and Materially Nonlinear Analysis
GMNIA	Geometrically and Materially Nonlinear Analysis with Imperfection
LBA	Linear Buckling Analysis
MNA	Materially Nonlinear Analysis
NASA	National Aeronautics and Space Administration

1 INTRODUCTION

Thin-walled shells have a widespread application in aerospace, mechanical, civil and structural engineering concepts in different shapes and types such as robots, shelters, domes, tanks, silos, machinery and energy absorbers (Figure 1.1). They have also significant importance for carrying liquids, pressurized gasses, and hazardous substances in road haulage, railroad and water transports. The use of the curved skin of vehicles as a load bearing member has similarly revolutionized the construction of aircraft. In the construction of all kind of spacecraft, the idea of a thin but strong skin has been used from the beginning. The demands in the thin-walled shells are quite prevalent as stated above. However, the thin-walled shells are considerably prone to loss of stability. Therefore, there is a great concern for the designers achieving maximum strength with a cost-efficient solution in the shells.

The load carrying capacity of a structure which is computed by merely linear buckling formulations is not a reliable way regarding safety aspects for nonstandard structures. These approaches may give higher loads than the real carrying capacity. Thus, the loss of stability approach is a vital issue to simulate real system response under axial loading.

Determining the load carrying capacity of the nonstandard structure might be infeasible by referring the procedures within the context of the standards and recommendations because it is difficult to estimate the nonlinearity of the structure. Likewise, the recommendations and standard methods are based on the linear theory of the shells.

In present days, updated standards and recommendations provide useful approaches. They solve stability of the conical shells with the base angle which is higher than 25° and clamped lower end [5,6]. Nevertheless, the standard methods are not applicable for the shells which have the base angle less than 25°. Besides, the rules which are included in the recommendations can be applied only to conical shells which have clamped edges or edge with the very stiff ring. In other words, if a conical shell has either base angle less than 25° or free/flexible radial stiffness at the edges, these rules cannot be applied.

Effects of the circumferential ring on the load carrying capacity of a conical shell have a significant role. Effectiveness depends on the radial stiffness of the circumferential ring. It is quite indispensable to determine the contribution of the ring only by itself. Additionally, this implementation is an alternative way to commonly used stiffeners and similar methods against system collapse. At the same time, it is easy for manufacturing scheme. It is a robust process to optimize a structure by understanding the individual influence of each design criteria.

Numerical studies (FEM) are leading guides in developing an empirical relationship to estimate limit states of a structure as a function of primary parameters (i.e., overall geometry, slenderness, type of loading and boundary conditions). Numerical studies can be used instead of experiments. Otherwise, performing experiments for each geometrical configuration can be time and cost consuming.

a. Orion spacecraft by NASA [1]

b. Uacs typ 451.1 type four-axle wagon [2]

c. Rocketdyne F-1 rocket engine [3]

d. Double corrugated hopper mount galvanized bins [4]

Figure 1.1. Conical shells in typical usage.

This study focuses on the load carrying capacity of the conical shells with a base angle less than 25° which have flexible boundary ring under axial loading. This area has lack of knowledge in the literature. Therefore, the main goal of the study is assigned to propose of a new method to estimate load carrying capacity of the conical shell structure with a base angle less than 25° for different radial stiffnesses under axial loading. The influence of the geometrical initial imperfection is included in the proposed method. A new reduction coefficient that simulates the effect of the initial imperfection on the load carrying capacity is suggested different from the standard and recommendations [5,6]. Thus, the load carrying capacity of the conical shells which stay in the non-linear area, that is mentioned above, can be estimated without any need of numerical analysis.

The study also aims to derive two dimensionless similarity parameters. These parameters allow for evaluation of the load carrying capacity of the conical shell for numerous configuration of geometrical dimensions in a wide range. One of these parameters represents the general geometrical form of the conical shell in terms of base angle, shell thickness, and radius. The other one characterizes the radial stiffness of the circumferential ring which is located around the lower edge of the conical shell.

The range of the base angle (α_c) of the conical shell is chosen between 10° and 20°. The study also mentions the influence of the circumferential ring stiffness on the loss of stability. The boundary conditions are assigned according to fixed supported (infinite radial stiffness), simply supported (zero radial stiffness) and flexible radial stiffness at the lower edge. Numerical models and simulations are performed using FEM package program COSMOS/M [9].

2 GENERAL TERMINOLOGY ABOUT THE FIELD OF THE STUDY

2.1 General Terms

In this part, some general terms, which are included in the recommendation and the present study, are described [5].

Ideal shell

Ideal shell is defined as a structure that has perfect geometry, uniformly distributed material behavior, and absence of residual stress. That is to say, the ideal shell means a structure with no initial imperfection.

Imperfection

Imperfection is defined as the difference between ideal and real shell. Imperfection might be geometrical, such as differences between the ideal shape and the real shape of the shell. Additionally, it may be observed as a fluctuation of the shell thickness, inhomogeneous boundary conditions, residual stress, loading imbalances, non-uniformly distributed mechanical properties of the material, etc. in the real applications.

Limit load

Limit load is the load which defines limit state of the structure and it is obtained from experiments or non-linear FEM analysis. The limit load may be a smooth maximum on the curve (Figure 2.1b). However, the limit load may also be a sharp peak on the curve. The curve pattern depends on location and direction of the displacement which is shown at the abscissa [5].

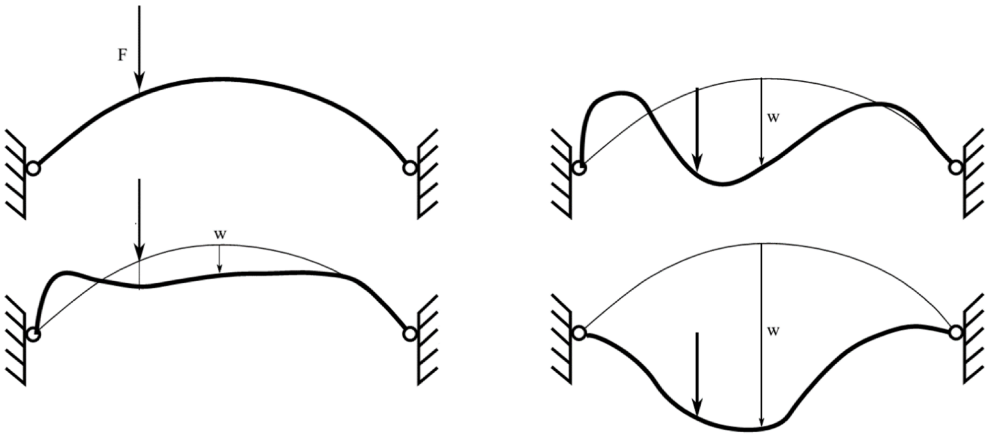

(a)

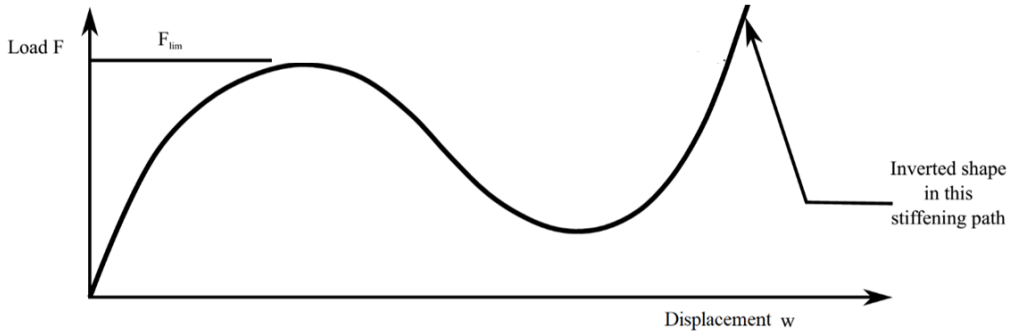

(b)

Figure 2.1. (a) Changing geometry of the structure, (b) Load-displacement response [5].

Nonstandard structure

The additional bending effect occurs in nonstandard structural elements. For instance, a conical shell with base angle higher than 25° which is clamped on the radial direction (a standard structure) under uniform axial load has almost a clear membrane stress. However, a bending state occurs at the beginning of the loading from nature of the conical shell structure with the base angle less than 25° (nonstandard structure). For this reason, linear FEM analysis or theoretical calculations cannot be used to evaluate the load carrying capacity in nonstandard structural elements (conical shells with the base angle less than 25°, spherical cap, etc.). The results may show the load carrying capacity of the structure multiple times higher than real. When designing nonstandard structures, numerical computational controls or experiments are required.

As an example, an arch with an eccentric load is illustrated in Figure 2.1. In this example, during the load increases, the shape of the structure changes. The changed shape has a lower stiffness than the original one. The structure stays stable until the loading reaches a local maximum and this local maximum is named as limit load. In this situation, the slope of the load-displacement curve equals to zero (Figure 2.1 b). At that moment, the structure attains the maximum load carrying capacity. Afterward, the lower loads cause displacement increment and, the structure becomes unstable [5]. As a consequence of this instability, the structure transforms to inverted shape its original form. Structures such as arches, spherical caps, etc. show this kind of behavior. The nonstandard structural elements always correspond to nonlinear collapse or nonlinear buckling phenomena.

Critical load

The critical load is the load which describes the limit state of the structure and it is predicted from analytical calculations or linear FEM analysis. It is seen as the critical point on the load-displacement curve. After this point, the displacement begins to grow in a new pattern which is entirely different from the pre-buckling pattern.

Standard structure

A standard structure can be considered as a simple structural element which can be described by analytical relationships. Commonly used standard structural elements include a

geometrically simple design such as a cylindrical shell, a torus, a conical shell with a base angle higher 25° and clamped edge.

The analytical solution is based on linear theory. Linear buckling is investigated only in standard construction elements. In the linear buckling, the critical point divides the compression balance into compression and bending equilibrium. Relationships for solving the linear stability of standard elements can be derived from the basic differential description in closed form. In the standard structural elements, the membrane stress is apparently superior to the bending stress. Thus, the difference between the theoretical value of the critical load and the actual strength of structure can be allowable in this case.

The analytical methods for the design of standard structural elements are laid down by the modern regulations and standards. The scope of the calculation methods for a particular design is precisely defined in the standards [5,6].

Geometric nonlinearity

When a structure has deformation under any kind of loading, its stiffness can change due to some factors. If this deviation of the stiffness of the structure is caused only by changes in the geometry, the nonlinear behavior is defined as geometric nonlinearity. Nonlinear analysis becomes necessary when the stiffness of the structure behaves nonlinearly under its operating conditions.

In other words, geometrical nonlinearity significantly affects load-displacement characteristic if the large displacement occurs (see Figure 2.2).

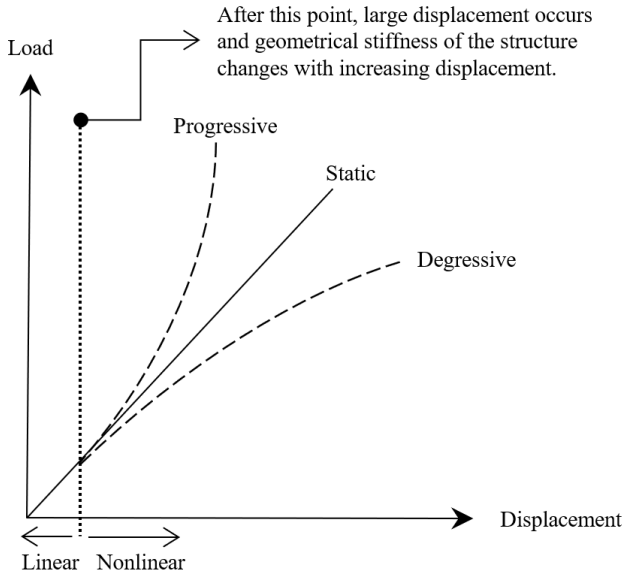

Figure 2.2. A load-displacement curve.

Material nonlinearity

If the change of the stiffness of the structure caused only by the material properties, this behavior is called material nonlinearity. A linear material model assumes the slope of the

stress-strain curve as a constant. This means, when the load is increased, stress and deformation increase linearly and if the load is removed, the structure returns to its original shape according to the slope of the curve.

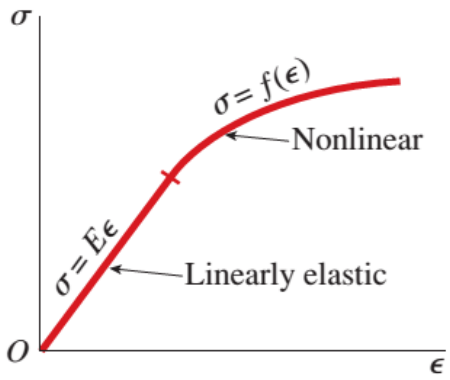

Figure 2.3. A stress-strain curve [32].

Young's Modulus is a constant of proportionality in a linear material model. It represents the slope of the linear part of the stress-strain curve (Figure 2.3). For highly nonlinear materials, this modulus may only be applicable at very low strains.

Circumferential Ring

It is the structural member which passes around the circumference of the shell. It is usually used as a tool for attachment of the shell to another structural member to increase radial stiffness of the structure.

Transverse load

The transverse load is applied perpendicular to the longitudinal axis of a member. It causes the member to bend and deflect from its original position, with internal tensile and compressive strains accompanying the change in curvature of the member. Transverse loading also induces shear forces that cause shear deformation of the material and increase the transverse deformation of the member.

2.1.1 Analysis Types

The limit state of the loss of stability can be determined using kind of analyses in FEM, according to EN 1993-1-6 [6]. These types depend on the geometry, material, and condition of the structure. They are classified as follows;

Linear Analysis (Linear Buckling Analysis LBA) determines the linear eigenvalues of the thin-walled shell structure. It gives the eigenvalue (critical load) and its corresponding shape of loss of stability. The additional bending effect, which occurs in the nonstandard structural element, is not taken into account in this analysis. Therefore, LBA numerical analysis cannot be used to evaluate the loss of stability of nonstandard structures.

Geometrically Nonlinear Analysis (Geometrically Nonlinear Elastic Analysis GNA) is applied to the ideal structure. Linear elastic material behavior is used. However, geometric nonlinearity (large displacement) is considered.

Materially Nonlinear Analysis (MNA) is applied to the ideal structure. The nonlinear elastic-plastic material model has an active role (material nonlinearity) (Figure 2.3). On the other hand, large displacement is neglected while performing the analysis. The results give plastic limit state load.

Geometrically and Materially Nonlinear Analysis (GMNA) calculates the geometric nonlinearity and the nonlinear elastic-plastic material behavior for the ideal structure. The results of the analysis show the limit load of the geometrically and materially nonlinear shell structure.

Geometrically Nonlinear Analysis with Imperfection Included (GNIA) is an analysis that includes initial imperfections (not ideal structure). Large displacement is considered, and linear elastic material behavior is used.

Geometrically and Materially Nonlinear Analysis with Imperfection Included (GMNIA) is an analysis that includes initial imperfections. Large displacement and material nonlinearity are considered. The result of the analysis is the limit load of the real structure in case of loss of stability in the elastic-plastic state. By comparing the results of the GMNA analysis, it is possible to determine the effect of initial imperfections on the strength of the structure.

2.2 Loss of Stability

The loss of stability is defined as a sudden drop in the carrying capacity of the structure. This reduction in the carrying capacity accompanies large displacement on the structure. The loss of stability happens instantaneously, and after this process, distortion on the structure often can be seen obviously with the unaided eye (Figure 2.4). In case of loss of stability, the structure takes a new equilibrium state.

The structure behaves in a new equilibrium state as before losing its stability. The load carrying capacity of the deformed structure can rise again. It can resist against higher load until further loss of stability. However, the shell structures can completely collapse even with the first stability loss (e.g. a spherical cap).

The maximum design load should never reach a level corresponding to the loss of stability of the shell structure. Loss of stability can occur due to unexpected overloading of the structure (insufficient dimensioning or mistakes under operation, etc.). In some cases, it is possible to continue to use this shell structure in a new equilibrium state until another loss of stability is reached. However, its carrying capacity must be verified. A conical roof sheet with the reinforcing ribs may be shown as an example for this case. Even after the limit state of loss of stability of the conical roof panel is achieved, the load carrying capacity of the conical roof panel may not be affected significantly.

Figure 2.4. Failure examples caused by loss of stability in practice [33, 34 and 35].

The loss of stability is investigated for the shell structures with three phenomena,

1. Nonlinear collapse
2. Nonlinear buckling
3. Linear buckling

In the nonlinear collapse, deformed shell structure has axially symmetric shape. While the load increases gradually, the shell structure deforms to its opposite position (Figure 2.6 point A). This kind of deformation is typical for thin-walled structures which do not have purely membrane stress. The bending stress is dominant on this collapse due to the form of the structure (conical shells with a base angle less than 25°, spherical caps, etc.).

In this process, the stiffness of the shell structure behaves contrary to the applied load. In case the load is sustained after the slope of the curve reaches zero value (Figure 2.6 Point A), the structure can have considerable deformation. Finally, it collapses suddenly and dramatically. This situation is explained as a term “snap-through buckling,” and it is often seen on shallow arcs and spherical caps because of their very nonlinear characteristics.

At the beginning of the loading, they deform rather small in comparison to loading increment. However, when the load reaches nearly to the limit value, deformation rate of the structure increases during the structure approaches neutral equilibrium state. Afterward, the structures reach “snap-through” and “post-buckled” status respectively. At the end of the process, they are seen as an inverted form of the original shape (Figure 2.5).

Figure 2.5. Failure of the Metrodome's roof arising from the weight of snow and ice [36].

Nonlinear buckling is a typical expression of axially asymmetric shaped deformation of the shell structure. Nonlinear buckling may occur earlier or further reaching nonlinear collapse (Figure 2.6 Points B).

Linear buckling occurs at the bifurcation point (Figure 2.6 Point C). On this type of failure, deformation starts to get higher values after it reaches the critical load or bifurcation point. Following to this point on the load-displacement curve, a new path appears that is quite different from the pre-buckling path. The structure takes a new equilibrium shape. The new deformed shape of the shell has waves. Number and characteristic of the waves depend on the loading type of the shell structure.

It needs to be determined critical load by linear (eigenvalue) analysis for the evaluation of linear buckling. Analytical solutions are based on linear shell theory. This approach is only applicable for standard structures. On the other hand, analyzing the nonlinear collapse or nonlinear buckling is necessary to assess the strength of the nonstandard structure against loss of stability [37].

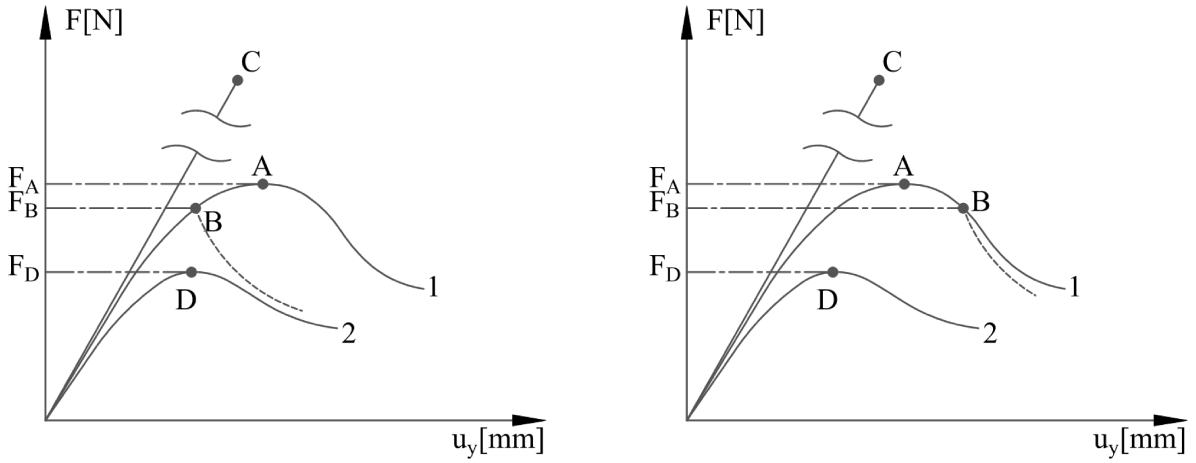

Figure 2.6. Equilibrium curves for loss of stability of a shell structure [37].

Figure 2.6 exhibits an example of equilibrium curve for loss of stability of a conical shell. By depending on the displacement of the node at the center of the conical shell, the

equilibrium curve represents the progression of the axial load. The nonlinear collapse of the structure appears at point A or D, and nonlinear buckling occurs at point B.

The first curve shows the behavior of the ideal conical shell structure and the second curve symbolizes a real application of a conical shell structure at Figure 2.6. The carrying capacity of a shell structure under operating condition may be affected by the initial imperfection.

Eigenvalue or linear buckling analysis gives a critical load of an ideal linear elastic conical shell structure at point C. This point is relatively higher than the limit load of the ideal conical shell structure.

The equilibrium curve is shown symbolically above (Figure 2.6). On the other hand, a numerical analysis result for the nonlinear collapse can be seen in Figure 2.7. In the analysis process, nonlinear collapse and nonlinear buckling of the conical shell are observed. Parameters of the conical shell are assigned as the shell thickness $t_{shell} = 1.6$ mm, the base angle $\alpha_c = 15°$, the cross-section area of the circumferential ring $A_{ring} = 30$ mm^2, the ratio $r_e/t_{shell} = 372.5$ for this numerical analysis. Axially symmetrical nonlinear collapse occurs at the 88. step consequence of increasing of the load.

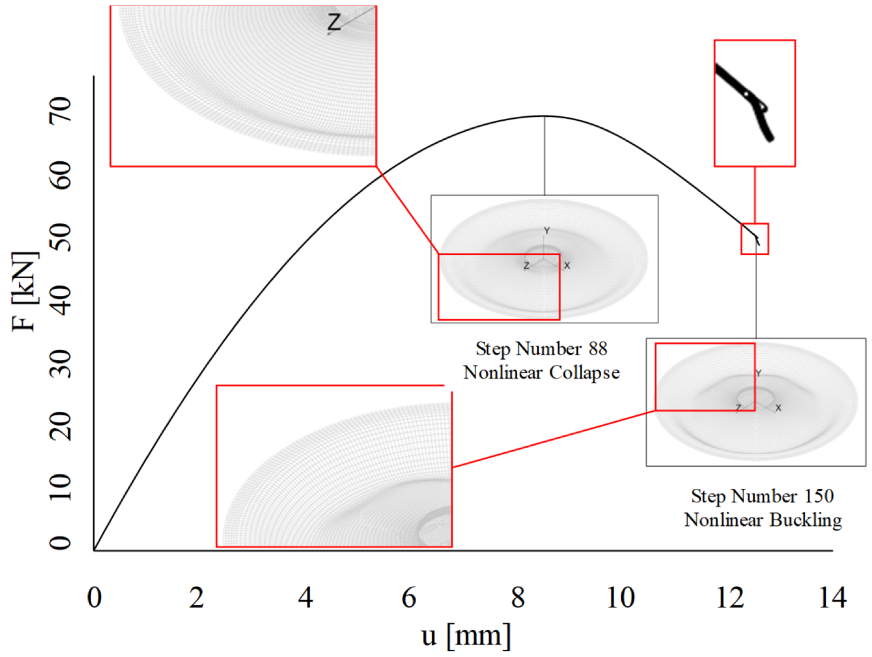

Figure 2.7. Representation of nonlinear collapse and nonlinear buckling behavior on the equilibrium curve.

Beyond the nonlinear collapse at step 150, a number of waves appear on the shell structure, and equilibrium curve starts to follow a new path. At that point, nonlinear buckling takes place.

3 LITERATURE REVIEW

Stability of the thin-walled shell structures has been studied by many prominent authors. Results of their studies are embedded in standards, regulations, and recommendations. In this dissertation, two of the most important documents of them are cited. These are "Recommendations for Design of Steel Shell Structures ECCS" [5] and the "European Standard for Design Steel Structures EN 1993-1-6-2007 [6]. On the standards and recommendations, limit state of the shell structures is given in consequence of plasticity, fatigue, cyclic plasticity, and buckling. Some of the studies which are concerned in this dissertation study are outlined below;

In one of the earliest research in the area, ***Lackman and Penzien*** experimentally investigated the buckling of conical shells under axial loading [13]. Arguing with the work of Seide [10], the authors were included the Poisson's Ratio in so-called correction factor 'C' to include the effects of small deflections and no-defects. Conical shells with 20° and 40° half-cone angles were manufactured for experiments using nickel material. Nickel was selected for experiments due to the high yield strength and good electroplating properties for manufacture. The results of the axial loading experiments were compared to proposed theory and previous studies in terms of critical buckling load and failure pattern. The conclusions were drawn on the suitability of the proposed equation, which includes a proper correction factor, to predict the critical buckling load of axially loaded conical shells. In addition, it was noted that the correction factor should be chosen according to the true radius of curvature of the base of the conical shell, rather than the mid-height curvature.

As one of the pioneers in the field, ***Weingarten et al.*** studied and discussed the stability of cylindrical and conical shells under axial loading. Both steel and Mylar polyester sheet materials were used for an extensive experimental programme. Mylar specimens have the ability to retake their shape after buckling because the buckling happened as an elastic deformation which allowed to use one specimen in more than one tests. Steel specimens exhibited diamond shaped buckles usually, but some specimens with large radius-to-thickness ratio exhibited elastic buckling just as the Mylar specimens displayed (Figure 3.1). However, this did not allow for retesting the steel specimens more than once as it was with Mylar counterparts, and this was attributed to the effects of imperfections [15].

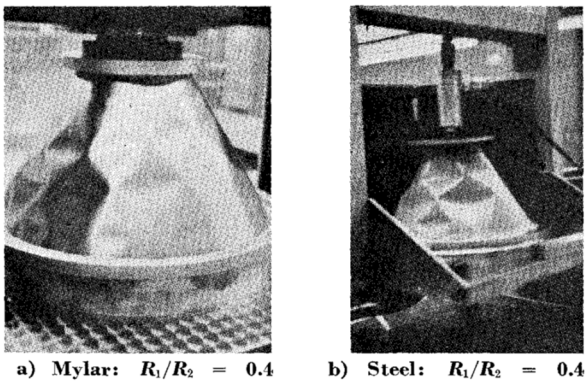

a) Mylar: $R_1/R_2 = 0.4$ b) Steel: $R_1/R_2 = 0.4$

Figure 3.1. Experimental buckle pattern for 30° conical shell [15].

Similar to the previous researchers, experimental data indicated that the buckling coefficient varied with radius – thickness ratio (Figure 3.2 (top)). They found that the analytic theory was useful in establishing the significant parameters. However, the accuracy of the theoretical approach was required to be checked experimentally. The lower bound which was established during the study was found to be applied to cylinders and conical shells (Figure 3.2 (bottom)). Although the theory correctly predicted the critical parameters involved, design carrying capacity must be found by experimental methods. Since the current theories were not sufficient to determine exact numerical values of the parametric coefficients.

In a subsequent paper, ***Weingarten et al.*** investigated the elastic stability of thin-walled cylindrical and conical shells under combined internal pressure and axial loading. The extensive experimental data indicated that elastic pressurized cylinders carry a higher amount of axial load than unpressurized cylinders. The variation of the net load with internal pressure was observed to be dependent on the radius-to-thickness ratio. Experimental carrying capacity obtained for conical shells were in good agreement with small deformation theory predictions for sufficiently high pressures. The results indicated that the end support condition might be more critical for conical shells than it is for cylinders. The authors also specified that it was possible to design curves to be recommended in the low-pressure region despite insufficient data [16].

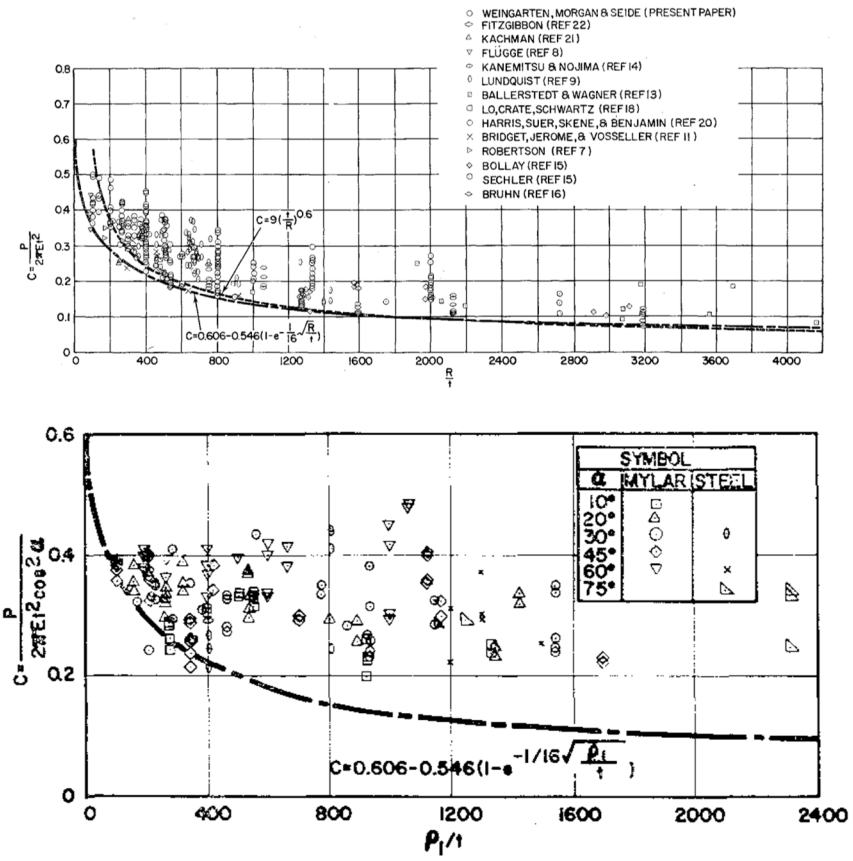

Figure 3.2. Experimental results and their comparison to the previous research data (top), and comparison of axial compression coefficients for conical shells with the lower bound curve for cylinders (bottom) [15].

Singer investigated the buckling of circular conical shells under uniform axial loading by setting Poisson's ratio equal to zero. Not much information could be drawn from the study due to the age of the resource (1965) and the way it was presented. However, as a result of the author's investigation, the instability behavior of thin conical shells under axial loading, within the bounds of linear theory, is similar to that of cylindrical shells. The author also expressed that the disagreement of the predictions of linear theory with the experimental result was also similar. However, the linear analysis has practical value in cases of combined loading for orthotropic or closely stiffened shells [17].

In mathematical analysis, ***Tani and Yamaki*** studied buckling of conical shells under axial loading in different boundary conditions. They used a methodology previously developed by the authors to solve the problem of buckling of conical shells under torsion. The problem was analyzed under four sets of boundary conditions, including both clamped and simply supported cases. Upon observing convergence problems, the authors introduced a set of additional parameters (Z and k_c). With the help of these parameters, it was observed that the effect of clamping was significant for short shells with Z less than 10. Additionally, axisymmetric buckling appears for Z less than 2, 3, and 10. Through detailed calculations, the correlations to the buckling of equivalent cylindrical shells are clarified which facilitates the estimation of critical load for any given conical shell [18].

Two different solution methods to analyze asymmetric elastic buckling of axially compressed conical shells available in the literature were extensively compared by ***Pariatmono and Chryssanthopoulos*** [19]. The authors employed the F (stress function) – W (out-of-plane displacement of the conical shell) approach similar to Tani and Yamaki [18], but with two different displacement functions were used. After explaining the approaches, which were also proposed by previous researchers as well as theirs, they presented the comparison data for simply supported conical shells in tables for both models. In terms of buckling load parameter values, overall, good correlations were obtained with Tani and Yamaki's model as well as with Baruch's model. The correlations were slightly worse for small half-cone angle values. However, they reported that there was considerable disagreement between the final modes obtained by either model (Figure 3.3). In the light of this information, the authors mentioned that the equations that Baruch developed could represent the failure modes better than Tani and Yamaki's model.

After the analysis of simply supported conical shells, the authors progressed into applying the same procedure to clamped support condition. In this condition, the difference in failure modes was not as dramatic as it was in simply supported condition. The reason was observed as the effect of clamping as it shifts the maximum amplitude region from the ends of the conical shell towards the center of it.

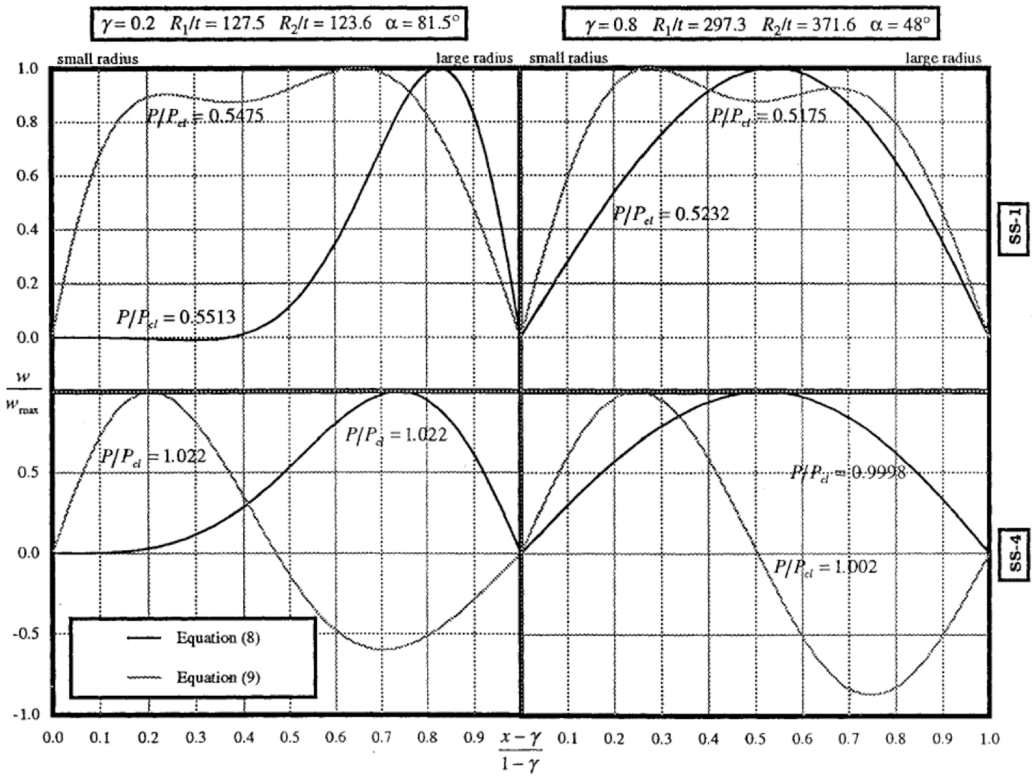

Figure 3.3. Mode composition for simply supported conical shells: Equation (8) Tani and Yamaki, Equation (9) Baruch [19].

Tavares expressed the mathematical approach to identify the stresses, strains, and displacements of complete or thin conical shells loaded along the meridian. Axisymmetric loadings were considered either distributed or concentrated. The assumptions of first-order-approximation shell theory (Kirchoff-Love hypothesis) was applied to the described model. Following the assumptions, the author described in detail the lengthy governing equations and their solutions. It was seen that a complete conical shell with lateral load could be obtained as a particular case and in a second step a conical shell with load at the vertex. As a conclusion, it was stated that the derived expressions could be used for a conical shell with edge loads taking the applied load equal to the unit and using the expressions for the second interval [20].

Teng and Barbagallo presented the buckling strength of rings attached to cone-cylinder intersections. From FEM parametric study, simple formulae were first developed which could be used to estimate the stiffness of the rotational restraint provided by adjacent shell walls. This formula was derived to predict the flexural-torsional buckling strength of rings with an elastic rotational restraint. Later, the formulae were combined with an existing closed-form solution based on thin-walled membrane theory. Numerical results were obtained using a FEM analysis which was able to model cross-section distortion. Comparisons between the two approaches showed that when the restraint stiffness is small, they agree with each other firmly. The approximation of the stiffness of the shell wall rotational restraint was suggested to be used for design purposes [21].

Chryssanthopoulos and Spagnoli studied the influence of edge constraint on the stability in nonlinear behavior. They used FEM analysis for stiffened conical shell under compressive load. In this study, the authors focused on various alternatives in specifying edge conditions. Also, the sensitivity of the response to the radial edge constraint was examined. They showed that both initial stiffness and the limit load could be severely reduced if radial edge displacements were not constrained. In this case, linear eigenvalue results could be misleading. Analogies were drawn between the conical shell and the more commonly encountered cylindrical shell. Also, the implications of these results for experimental studies and development of design formulations were discussed by authors [22].

Chryssanthopoulosa et al. studied the design of stiffened conical shells against buckling using numerical models validated by experiments of regular conical shells [24]. They stated that the stiffened conical shell structures were needed to be treated differently than cylindrical structures. Therefore, the authors presented a design-based approach using FEM models. Firstly, tests were carried out with five unstiffened, and three stringer-stiffened conical shells and the results of load, strain, and displacement were used for the validation of the FEM model as seen in (Figure 3.4). The comparison results were found satisfactory. Failure of unstiffened conical shells emerged as an axisymmetric bulge near the small-radius end, whereas stringer-stiffened conical shells displayed local panel buckling failure which is non-axisymmetric. In addition, the authors examined the imperfection sensitivity of stringer-stiffened conical shells and found out that for practical stiffening ratios. The imperfection sensitivity of stringer-stiffened conical shells appears to be appreciably lower than that of their unstiffened counterparts.

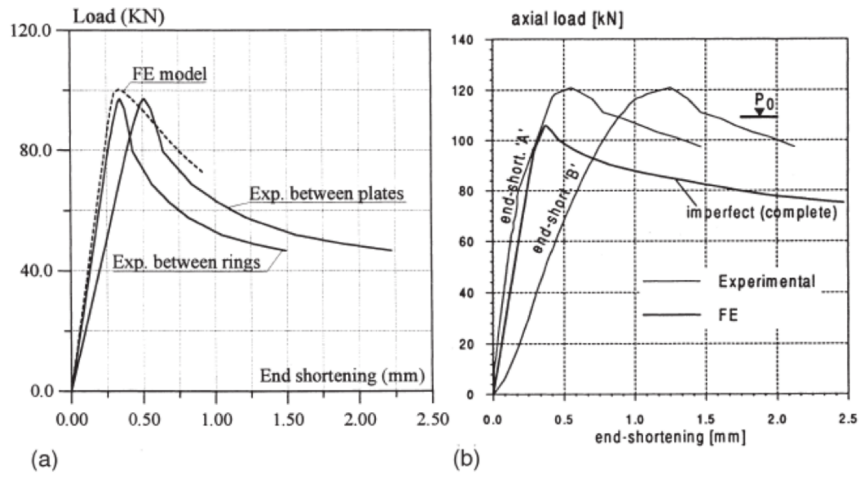

Figure 3.4. Validation of FEM model with the experiments. (a) unstiffened conical shell, (b) stringer-stiffened conical shell [24].

Spagnoli and Chryssanthopoulos investigated the effect of the different shell and stiffening parameters of conical shells under the axial loading. The authors studied the linear and nonlinear elastic carrying capacity response of the conical shell by means of an appropriate FEM model. They determined the critical load on the basis of linear analysis and also showed

the imperfection sensitivity through nonlinear analysis of imperfect conical shells. Different aspects of the behavior were quantified through suitably defined curvature parameters [25].

Chryssanthopoulos and Poggi examined experimentally strength of unstiffened conical shells under axial loading. The paper presented the results during a test program involving unstiffened steel conical shell in compression. Thinner material (0.7 – 0.9 mm) was used to exploit the geometrical effects. The majority of the tests showed that the regular axisymmetric buckle was confined close to the small-radius end. A plastic mechanism approach, including second-order effects, was described and shown to be a simple and useful tool for predicting the collapse load. In addition, the approach showed the end-shortening as well. The derivation of the theoretical expression pertaining mechanism was summarized, and some aspects regarding the solution procedures were presented by authors. The comparison of the plastic mechanism approach with the experimental programme was found significant (Figure 3.5) [26]. Finally, the authors remarked that an imperfection effect/constant assumption should be made while using the plastic mechanism approach in the absence of experimental validation data.

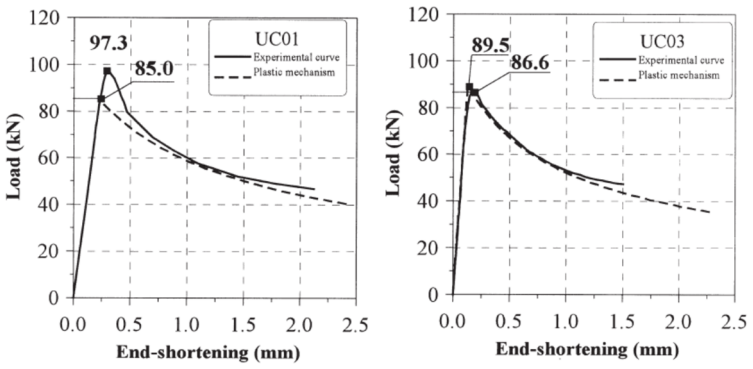

Figure 3.5. Comparison between experimental curves and mechanism approach [26].

Yu et al. researched flat-topped conical shells under the axial load through experimental and theoretical approach. Both elastic model and plastic model were proposed to describe the collapse process and to predict the load-displacement characteristics. Analytical expressions describing the load-displacement and energy-displacement relationships during the large displacement process were derived. Both elastic and plastic deformation models were proposed and formulated to describe the deformation process of the cell, and to predict the load-displacement and energy dissipation characteristics. A good agreement was shown between the theoretical predictions and experimental results by authors [27].

Thinvongpituk and El-Sobky examined the buckling behavior of aluminum conical shell under axial loading using the experiment and numerical model. The experiments were carried out with a number of specimens under quasi-static load in three different end conditions, i.e., simple support, top constraint, and base constraint. FEM models (Figure 3.6) were generated via ABAQUS software for every mode of deformation. It was revealed that the carrying capacity of the conical shell was reducing exponentially, while the mean radius to thickness ratio is increasing. Analysis results showed that the buckling mode is influenced by

the geometric parameter (R_m/t – mean radius to thickness ratio) and end condition. The end constraint was found to have a significant effect on the carrying capacity of the conical shell, such as the conical shells having a constraint at the top edge yield higher load. The result from FEM was compared to the experimental result, and good agreement was achieved [28].

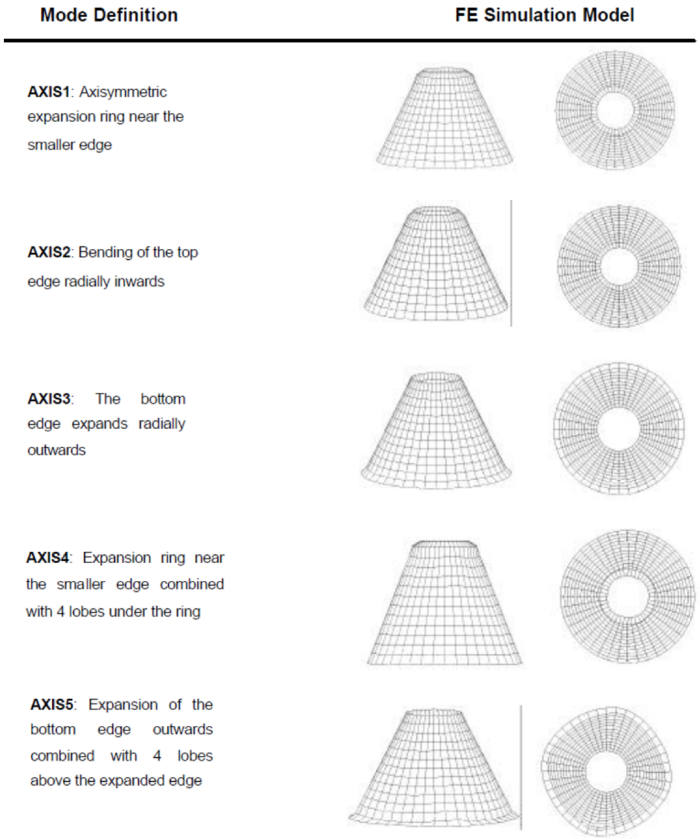

Figure 3.6. Model and definition of the axisymmetric buckling modes of constant [28].

Gupta and co-workers investigated the buckling behavior of aluminum conical shell and analyzed the behavior of rolling and stationary plastic hinges during deformation [29]. The authors used aluminum conical shells with varying top and bottom edge dimensions while keeping either of the top or bottom edge dimension as constant (Figure 3.7), resulting in 40 different specimens. These specimens were under quasi-static axial loading in order to analyze the energy absorption properties. Load-displacement curves were observed during testing from which the absorbed energy values were obtained. The authors supported their study with numerical modeling using ANSYS FEM software while taking into account the influence of rolling and stationary plastic hinges in the buckling pattern. During the axial loading, the tests were stopped periodically to measure the rolling plastic hinge radii.

It was observed from the experiments that the deformation of conical shells was governed by D_m/t and H_c/t values. The deformation resulted in a first rolling plastic hinge followed by the diamond pattern for thicker shells, and integral lobes for thinner shells. The numerical study included the nonlinearities and therefore provided consistent deformation shape results. However, the force and energy absorption values between static experiments and numerical analysis were unacceptable. Furthermore, the study was very detailed, but it lacked

critical analysis. Lastly, a previously developed analytical model by the authors [23] was tested within the study, and considerable improvement was achieved due to the equation for the radius of rolling plastic hinge obtained experimentally.

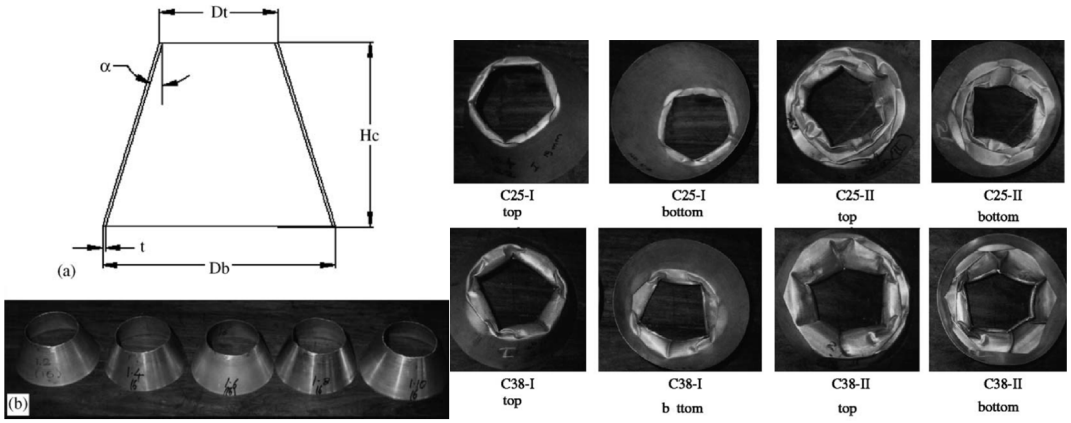

Figure 3.7. Geometrical details of conical aluminum specimens (top left), specimens before tests (bottom left), and various failure modes (right) [29].

Blachut et al. investigated the static stability of steel conical shells under axial loading, hydrostatic pressure, and the combination of these two [30]. For the experimental programme, five conical shells of 14° half-cone angle were used: two for axial loading, two for lateral pressure, and one for hydrostatic pressure. Of these specimens, the ones were under axial loading and were failed by collapse through excessive plastic straining at the top end (Figure 3.8). Other conical shells which were under combined and lateral pressure were failed by buckling as they displayed seven dimples around the hoop direction, i.e., seven circumferential waves of the eigenmode. After the experiments, several numeric models were adopted for identifying the buckling parameters and eigenmodes as well. The authors found out that stress-strain model with linear segments gave better results compared to the elastic-perfectly plastic material model in terms of buckling load prediction. However, for buckling pressure, the reverse was the case, and elastic-perfectly plastic model provided a better prediction for the conical shells under lateral pressure and combined loading. The authors stated that the predictions were satisfactory overall but advised that further investigation is required before definitive conclusions could be made.

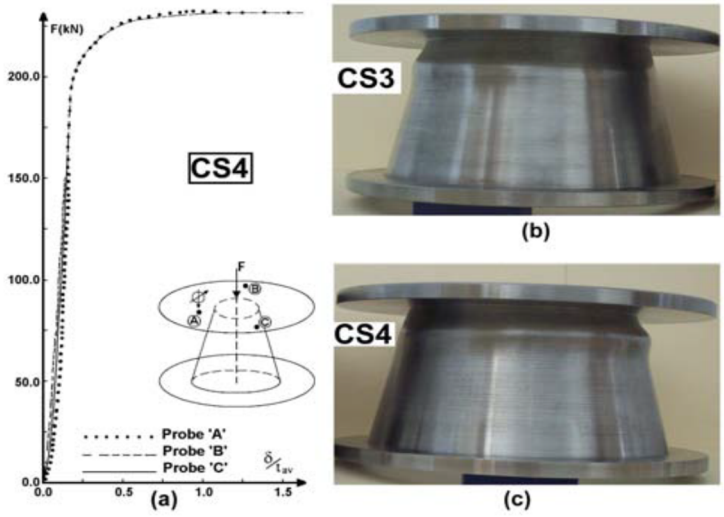

Figure 3.8. Tested conical shells after axial loading [30].

Shakouri and Kouchakzadeh investigated the buckling response of two connected conical shells (Figure 3.9) under axial loading in simply supported boundary condition [31]. Initiating the analysis with the governing equations for joined conical shells based on thin-walled shell theory and theorem of minimum potential energy, the results of the numerical study was compared to four available literary information (Figure 3.9). The comparison showed good agreement of critical buckling load values, but slight differences were observed for circumferential wave number.

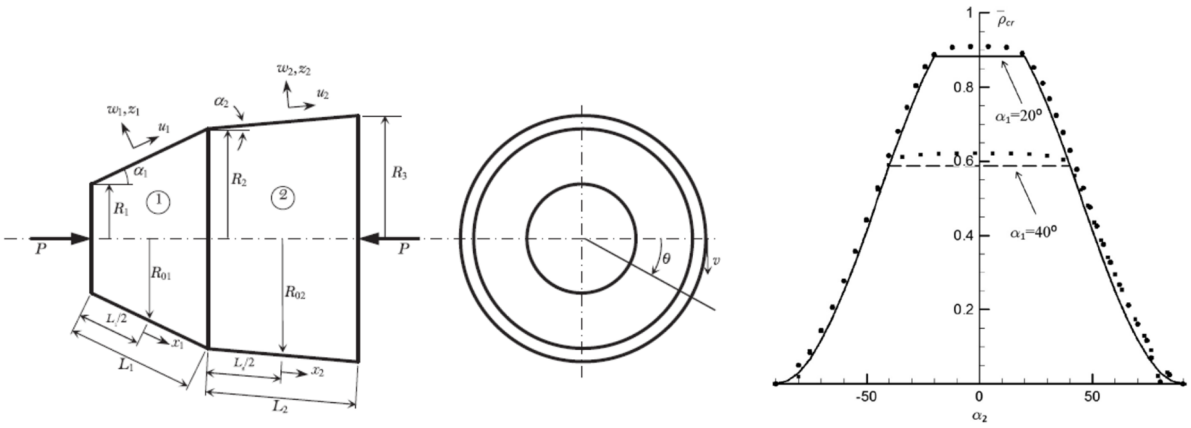

Figure 3.9. The geometry of joined conical shells (left), comparison of results (dots) with another available study (lines) [31].

The results of their work revealed that the minimum buckling load of each separate shell could be used as the buckling load of joined shells for the long conical shell ($L/R_1 > 0.3$). Other important outcomes of their research were; increasing the buckling load of joined shells when the conical shells move towards cylindrical shell. Using two joined conical shells is lightweight in the sense that it can resist higher axial loads compared to solo conical shells.

3.1 Scope of the Study

Design criteria of the standard shell structures are provided with some analytical approximations within the context of standards and regulations. Whereas, designing of the nonstandard structures requires to perform numerical analysis or experiment. Geometric stiffness may decrease in nonstandard structures with the deformation which arises because of the loading. Therefore, it should not be forgotten that nonlinearity has a considerable influence on the load carrying capacity of the thin-walled shell structures. Linear calculations may give quite higher results than actual load carrying capacity for non-standard structures.

As mentioned before, the conical shells with a base angle less than 25° behave highly nonlinear. Unfortunately, the limit load of these type of nonstandard structures is not determined in the literature, adequately. In addition to this, the standards and recommendations are not bright enough for conical shells with the low base angle which have flexible radial stiffness at the lower edge. Therefore, the standard methods are not applicable for the selected base angle and assigned boundary conditions in the study.

Additionally, effects of the circumferential ring on the load carrying capacity of a conical shell have a significant role depending on the radial stiffness of the ring. It is quite indispensable to determine the contribution of the ring on load carrying capacity. It is a robust process to optimize a structure by understanding the individual influence of each design criteria.

The main goal of this study is to propose a new method to estimate load carrying capacity of the conical shell structure with a base angle less than 25° for different radial stiffnesses under axial loading. The influence of the initial geometrical imperfection is included in the proposed method. A new reduction coefficient that simulates the effect of the initial imperfection on the load carrying capacity is suggested different from the standard and recommendations [5,6]. Thus, the load carrying capacity of the conical shells, which stay in the mentioned nonlinear area, can be estimated using the new proposed method without any need of numerical analysis.

The study also aims to derive two dimensionless similarity parameters. These parameters allow evaluation load carrying capacity of the conical shell for numerous configuration of geometrical dimensions in a wide range. Derivation of nondimensional similarity parameters makes possible to simulate real applications with a simple model. This study also aims to clarify the effect of radial stiffness of circumferential ring on the load carrying capacity under axial loading. For this reason, the study includes some topics as follows,

- Determination of the load carrying capacity of the conical shells which have a base angle of less than 25°.
- Investigation of the influence of the radial stiffness on the limit load.
- Evaluation of the effect of the initial geometrical imperfection on the load carrying capacity.
- Derivation of the dimensionless similarity parameters to evaluate limit load in a wide range of the conical shell geometries.

- Suggestion of a new methodology to estimate load carrying capacity for conical shells with a base angle less than 25°.

4 PROBLEM DESCRIPTION

4.1 Analytical Study

An analytical solution is a procedure for determining the load carrying capacity of the thin-walled conical shell structures which is described in the standards and recommendations. This method is based on the linear shell theory, and it is derived from the critical load under axial loading of the cylinder. Amount of this value is adjusted by counting in some coefficients for simulation of the real applications. These coefficients can be originated from the effect of boundary conditions, geometry, material model, initial imperfection, etc. In order to adapt the analytical approach to the conical shells for evaluating the critical load, the existing regulations are modified by finding out compatible correlation factors. *"Principles of Structural Stability Theory"* is taken as a reference for the derivation of the critical load [40].

The assumptions are given below should be carried out by deriving the shell equations;

- The thickness of the shell is smaller than the other dimensions of the shell; that is, the shell is thin.
- Lateral displacements are lower than the thickness of the shell.
- The material of the shell is homogenous, isotropic and has linear elastic material properties.
- Lines which are normal to the middle surface before bending stay also straight and normal during bending.
- The shell does not have any imperfection at any cross-section.

A thin-walled circular cylindrical shell with length L, wall thickness t, and undeformed middle surface radius r is considered, as shown in Figure 4.1. The coordinate system x, θ, and z describing any point on the middle surface together with all the displacement components u, v, and w are illustrated in Figure 4.1. The forces and moment intensities act on a shell element having in-plane forces, transverse shears, bending moments and twisting moments [40].

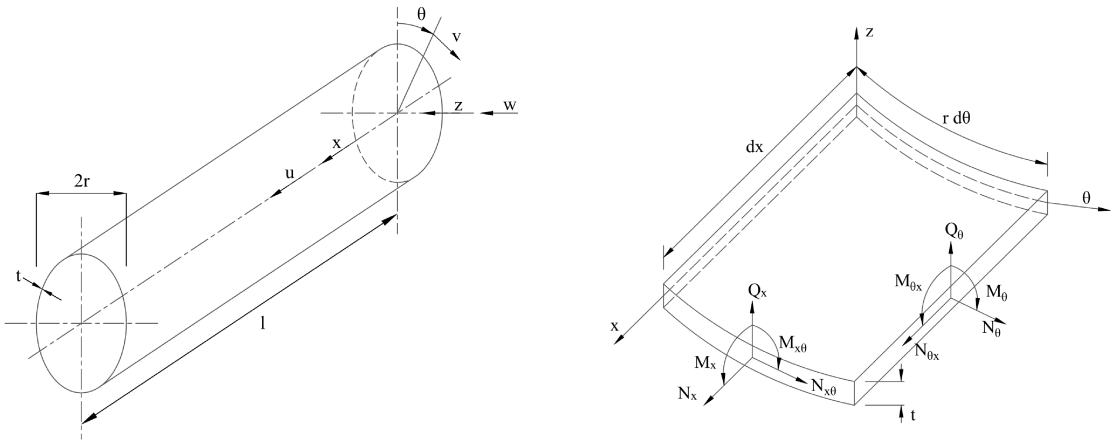

Figure 4.1. Circular cylindrical shell and cylindrical shell element [38].

The in-plane forces' components in x and θ directions are equal to their own forces, because the transverse shear forces can be neglected in these directions. Hence, it can be written as follows,

$$\frac{\partial N_x}{\partial x} + \frac{\partial N_{x\theta}}{\partial \theta} = 0 \qquad \text{Eq. 4.1}$$

$$\frac{\partial N_\theta}{\partial \theta} + \frac{\partial N_{\theta x}}{\partial x} = 0 \qquad \text{Eq. 4.2}$$

The curvature of the element should be considered to determine the equation of equilibrium in the z-direction. As a consequence of the initial curvature of the shell, the N_θ forces (Figure 4.2) include a component in the z direction. It is equal to Eq. 4.3.

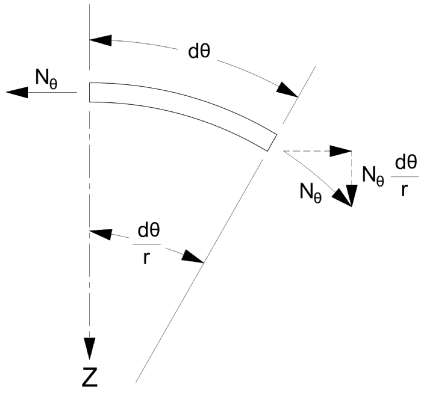

Figure 4.2. The radial component of in-plane forces due to initial curvature.

$$N_\theta \left(\frac{1}{r}\right) dx d\theta \qquad \text{Eq. 4.3}$$

However, the other in-plane forces do not have a component in the z-direction due to the initial curvature. However, all the in-plane forces have z components as a result of the curvature which is caused by bending. These components due to the bending are added to Eq. 4.3, and the in-plane forces in the z-direction is obtained as Eq. 4.4 using slightly deformed shell element (Figure 4.3b).

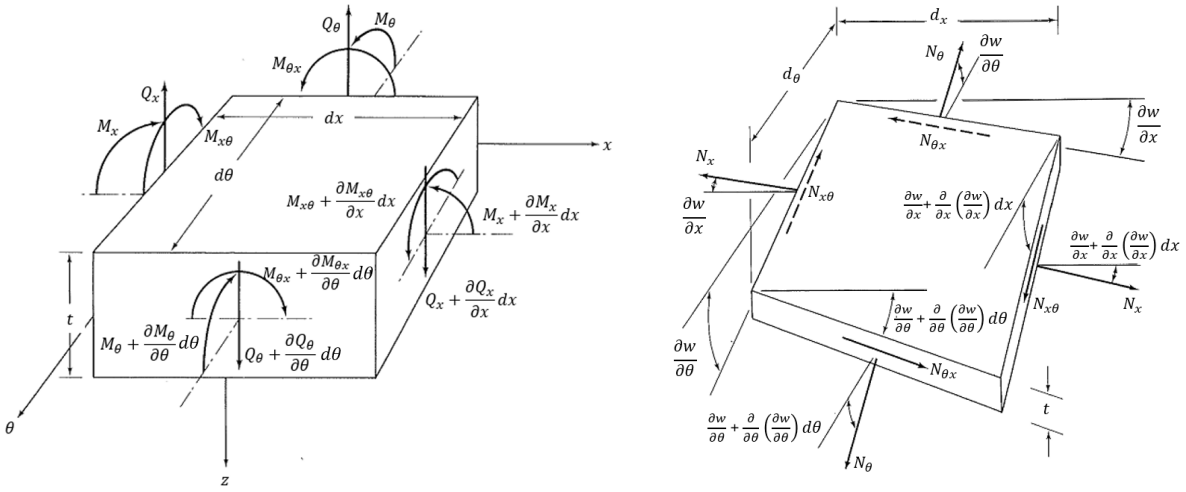

(a) (b)

Figure 4.3. (a) Bending and twisting moments, (b) In-plane and shear forces in a slightly deformed shell element [40].

$$\left[N_x \frac{\partial^2 w}{\partial x^2} + 2N_{x\theta} \frac{\partial^2 w}{\partial x \partial \theta} + N_\theta \left(\frac{\partial^2 w}{\partial \theta^2} + \frac{1}{r}\right)\right] dx d\theta \qquad \text{Eq. 4.4}$$

Transverse shear forces must be added to the z components of the in-plane forces. They are given by Eq. 4.5.

$$\left(\frac{\partial Q_x}{\partial x} + \frac{\partial Q_\theta}{\partial \theta}\right) dx d\theta \qquad \text{Eq. 4.5}$$

The shear forces in Eq. 4.5 is calculated as seen in Eq. 4.6 and Eq. 4.7 corresponding to the equation of moment equilibrium for x and θ axes in Figure 4.3a.

$$\frac{\partial Q_\theta}{\partial \theta} = \frac{\partial^2 M_\theta}{\partial \theta^2} - \frac{\partial^2 M_{x\theta}}{\partial x \partial \theta} \qquad \text{Eq. 4.6}$$

$$\frac{\partial Q_x}{\partial x} = \frac{\partial^2 M_x}{\partial x^2} - \frac{\partial^2 M_{\theta x}}{\partial x \partial \theta} \qquad \text{Eq. 4.7}$$

Eq. 4.5 can be written as Eq. 4.8 using Eq. 4.6 and Eq. 4.7.

$$\left(\frac{\partial^2 M_x}{\partial x^2} - 2\frac{\partial^2 M_{x\theta}}{\partial x \partial \theta} + \frac{\partial^2 M_\theta}{\partial \theta^2}\right) dx d\theta \qquad \text{Eq. 4.8}$$

The equation of equilibrium in the z-direction can be achieved if Eq. 4.4 and Eq. 4.8 are associated.

$$\frac{\partial^2 M_x}{\partial x^2} - 2\frac{\partial^2 M_{x\theta}}{\partial x \partial \theta} + \frac{\partial^2 M_\theta}{\partial \theta^2} + N_x \frac{\partial^2 w}{\partial x^2} + 2N_{x\theta}\frac{\partial^2 w}{\partial x \partial \theta} + N_\theta\left(\frac{\partial^2 w}{\partial \theta^2} + \frac{1}{r}\right) = 0 \qquad \text{Eq. 4.9}$$

The equations below (Eq. 4.10, Eq. 4.11 and Eq. 4.12) give the relationships of bending moments and curvatures in the shell. D is the flexural rigidity.

$$M_x = -D\left(\frac{\partial^2 w}{\partial x^2} + \mu\frac{\partial^2 w}{\partial \theta^2}\right) \qquad \text{Eq. 4.10}$$

$$M_\theta = -D\left(\frac{\partial^2 w}{\partial \theta^2} - \mu\frac{\partial^2 w}{\partial x^2}\right) \qquad \text{Eq. 4.11}$$

$$M_{x\theta} = D(1-\mu)\frac{\partial^2 w}{\partial x \partial \theta} \qquad \text{Eq. 4.12}$$

The strain of a shell in x direction can be expressed as Eq. 4.13, if deformation of the shell is relatively small.

$$\varepsilon_x = \frac{\partial u}{\partial x} \qquad \text{Eq. 4.13}$$

The strain which is caused by the transverse bending must be supplemented to obtain the strain in the θ direction for the shell ε_θ. Because of the radial displacement w, element AB is displaced to $\bar{A}\bar{B}$ (Figure 4.4) and the resulting strain is seen in Eq. 4.14.

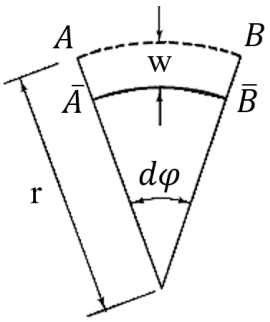

Figure 4.4. Tangential strain due to radial displacement**.**

$$\varepsilon = -\frac{AB - \bar{A}\bar{B}}{AB} = -\frac{rd\varphi - (r-w)d\varphi}{rd\varphi} = -\frac{w}{r} \qquad \text{Eq. 4.14}$$

Therefore, the total strain in the θ direction is obtained as in Eq. 4.15. Besides, the shear strain $\gamma_{x\theta}$ is shown in Eq. 4.16.

$$\varepsilon_\theta = \frac{\partial v}{\partial \theta} - \frac{w}{r} \qquad \text{Eq. 4.15}$$

$$\gamma_{x\theta} = \frac{\partial u}{\partial \theta} + \frac{\partial v}{\partial x} \quad \text{Eq. 4.16}$$

The middle surface shell forces can be stated in terms of the two-dimensional stress-strain relations as follows,

$$N_x = \sigma_x t = \frac{Et}{1-\mu^2}(\varepsilon_x + \mu\varepsilon_\theta) \quad \text{Eq. 4.17}$$

$$N_\theta = \sigma_\theta t = \frac{Et}{1-\mu^2}(\varepsilon_\theta + \mu\varepsilon_x) \quad \text{Eq. 4.18}$$

$$N_{x\theta} = \tau_{x\theta} t = \frac{Et}{2(1+\mu^2)}\gamma_{x\theta} \quad \text{Eq. 4.19}$$

Substitution of Eq. 4.13, Eq. 4.15, and Eq. 4.16 into these relations, the shell forces can be rewritten as,

$$N_x = \frac{Et}{1-\mu^2}\left(\frac{\partial u}{\partial x} + \mu\frac{\partial v}{\partial \theta} - \mu\frac{w}{r}\right) \quad \text{Eq. 4.20}$$

$$N_\theta = \frac{Et}{1-\mu^2}\left(\frac{\partial v}{\partial \theta} - \frac{w}{r} + \mu\frac{\partial u}{\partial x}\right) \quad \text{Eq. 4.21}$$

$$N_{x\theta} = \frac{Et(1-\mu)}{2(1-\mu^2)}\left(\frac{\partial u}{\partial \theta} + \frac{\partial v}{\partial x}\right) \quad \text{Eq. 4.22}$$

The middle surface forces, which are defined above, appear as a result of buckling (secondary forces), and these are not the total middle surface forces. The terms of the forces, which are caused by the applied load until buckling (primary forces), should also be considered. To separate these forces, displacements in the middle surface are assumed to occur only due to buckling and the primary forces are added to the expressions. If the primary forces are stated as below,

$$N_x = P_x \quad \text{Eq. 4.23}$$

$$N_\theta = P_\theta \quad \text{Eq. 4.24}$$

$$N_{x\theta} = S_{x\theta} \quad \text{Eq. 4.25}$$

Total middle surface forces become as seen in Eq. 4.26, Eq. 4.27, and Eq. 4.28.

$$N_x = \frac{Et}{1-\mu^2}\left(\frac{\partial u}{\partial x} + \mu\frac{\partial v}{\partial \theta} - \mu\frac{w}{r}\right) + P_x \quad \text{Eq. 4.26}$$

$$N_\theta = \frac{Et}{1-\mu^2}\left(\frac{\partial v}{\partial \theta} - \frac{w}{r} + \mu\frac{\partial u}{\partial x}\right) + P_\theta \quad \text{Eq. 4.27}$$

$$N_{x\theta} = \frac{Et(1-\mu)}{2(1-\mu^2)}\left(\frac{\partial u}{\partial \theta} + \frac{\partial v}{\partial x}\right) + S_{x\theta} \quad \text{Eq. 4.28}$$

The equilibrium equations are defined concerning displacements. Substitution of the appropriate derivatives of Eq. 4.10 through Eq. 4.12 and Eq. 4.26 through Eq. 4.28 into Eq. 4.1, Eq. 4.2, Eq. 4.9gives,

$$\frac{\partial^2 u}{\partial x^2} + \frac{1-\mu}{2}\frac{\partial^2 u}{\partial \theta^2} + \frac{1+\mu}{2}\frac{\partial^2 v}{\partial x \partial \theta} - \frac{\mu}{r}\frac{\partial w}{\partial x} = 0 \quad \text{Eq. 4.29}$$

$$\frac{\partial^2 v}{\partial \theta^2} + \frac{1-\mu}{2}\frac{\partial^2 v}{\partial x^2} + \frac{1+\mu}{2}\frac{\partial^2 u}{\partial x \partial \theta} - \frac{1}{r}\frac{\partial w}{\partial \theta} = 0 \quad \text{Eq. 4.30}$$

$$-D\left(\frac{\partial^4 w}{\partial x^4} + 2\frac{\partial^4 w}{\partial x^2 \partial \theta^2} + \frac{\partial^4 w}{\partial \theta^4}\right) + P_x\frac{\partial^2 w}{\partial x^2} + P_\theta\frac{\partial^2 w}{\partial \theta^2} + \frac{P_\theta}{r} + \frac{1}{r}\frac{Et}{1-\mu^2}\left(\frac{\partial v}{\partial \theta} - \frac{w}{r} + \mu\frac{\partial u}{\partial x}\right) + 2S_{x\theta}\frac{\partial^2 w}{\partial x \partial \theta} = 0 \quad \text{Eq. 4.31}$$

To get the critical load of a cylindrical shell a set of three equations in three unknowns, which is constituted by Eq. 4.29 together with Eq. 4.30 and Eq. 4.31, is used. However, Donnel [11] has transformed this set of equations into a single one in terms of w in Eq. 4.32. It is called as the Donnell equation. ∇^2 is the Laplace operator and it is equal to $\nabla^2 = \frac{\partial^2}{\partial x^2} + \frac{\partial^2}{\partial \theta^2}$.

$$D\nabla^8 w - \nabla^4\left(P_x\frac{\partial^2 w}{\partial x^2} + P_\theta\frac{\partial^2 w}{\partial \theta^2} + 2S_{x\theta}\frac{\partial^2 w}{\partial x \partial \theta}\right) + \frac{Et}{r^2}\frac{\partial^4 w}{\partial x^4} = 0 \quad \text{Eq. 4.32}$$

To calculate the critical load of a cylindrical shell under axial loading, the terms $S_{x\theta}$ and P_θ are assumed as zero. If the cylinder is operating against torsion, $S_{x\theta}$ is equal to the applied shear force. P_θ is equal to the hoop force caused by pressure, if it is under external pressure.

If a cylinder has clamped ends, length l, and radius r, its critical load can be determined via Donnell equation which is outlined for axial loading by Batdorf [12], Eq. 4.32. For classical solution under axial loading Eq. 4.32 is reduced as Eq. 4.33.

$$D\nabla^8 w + \frac{Et}{r^2}\frac{\partial^4 w}{\partial x^4} + \sigma_x t\nabla^4\frac{\partial^2 w}{\partial x^2} = 0 \quad \text{Eq. 4.33}$$

The boundary conditions are as below,

$$w = \frac{\partial^2 w}{\partial x^2} = 0 \qquad at \quad x = 0, l \qquad \text{Eq. 4.34}$$

The radial displacement can be expressed as Eq. 4.35,

$$w = w_0 sin\frac{m\pi x}{l} sin\frac{n\pi\theta}{\pi r} \qquad \text{Eq. 4.35}$$

m refers to the number of half waves in the longitudinal direction and n refers to the number of half waves in the circumferential direction.

$$\beta = \frac{nl}{\pi r} \qquad \text{Eq. 4.36}$$

Eq. 4.35 can be rewritten as Eq. 4.37 using Eq. 4.36 for simplification.

$$w = w_0 sin\frac{m\pi x}{l} sin\frac{\beta\pi\theta}{l} \qquad \text{Eq. 4.37}$$

Substitution of Eq. 4.37 into Eq. 4.33. gives,

$$D\left(\frac{\pi}{l}\right)^8 (m^2+\beta^2)^4 + \frac{Et}{r^2} m^4 \left(\frac{\pi}{l}\right)^4 - \sigma_x t \left(\frac{\pi}{l}\right)^6 m^2 (m^2+\beta^2)^2 = 0 \qquad \text{Eq. 4.38}$$

By dividing Eq. 4.38 to $D(\pi/l)^8$ and introducing two new parameters (Z and k_x), it can be written,

$$(m^2+\beta^2)^4 + \frac{12m^4Z^2}{\pi^4} - k_x m^2 (m^2+\beta^2)^2 = 0 \qquad \text{Eq. 4.39}$$

where,

$$Z = \frac{l^2}{rt}(1-\mu^2)^{1/2} \qquad \text{Eq. 4.40}$$

$$k_x = \frac{\sigma_x t l^2}{D\pi^2} \qquad \text{Eq. 4.41}$$

As a nondimensional parameter, Z is a shape factor which indicates the ratio of length to the radius. It is useful to classify as short or long cylinders. k_x is a buckling stress coefficient. Solving Eq. 4.39, k_x is obtained,

$$k_x = \frac{(m^2+\beta^2)^2}{m^2} + \frac{12m^2Z^2}{\pi^4(m^2+\beta^2)^2} \qquad \text{Eq. 4.42}$$

If the Eq. 4.42 is differentiated regarding $(m^2+\beta^2)^2/m^2$ and the result is set equal to zero, k_x has a minimum value when,

$$\frac{(m^2+\beta^2)^2}{m^2}=\left(\frac{12Z^2}{\pi^4}\right)^{1/2} \quad \text{Eq. 4.43}$$

Substitution of Eq. 4.43 into Eq. 4.42 gives,

$$k_x=\frac{4\sqrt{3}}{\pi^2}Z \quad \text{Eq. 4.44}$$

From Eq. 4.44, the critical stress is obtained,

$$\sigma_c=\frac{Et}{r\sqrt{3(1-\mu^2)}} \quad \text{Eq. 4.45}$$

In order to adopt this formulation to conical shells, equivalent cylinder approach has been introduced. In this model, the equivalent radius is substituted into the Eq. 4.45, and the critical stress of a conical shell under axial loading is calculated with the Eq. 4.46.

This equivalent cylinder approach grounds on the physical similarities of the bifurcation behavior and the imperfection sensitivity of cylindrical and conical shells. Both cylindrical shell and conical shell surfaces can be transformed a plane, in other words, they have developable surface [5]. Therefore, this approach can be used for conical shells.

$$\sigma_{c,cone}=\frac{Et}{r_e\sqrt{3(1-\mu^2)}} \quad \text{Eq. 4.46}$$

r_e is the equivalent radius of cylinder which is calculated by recommendation. It is stated in "Buckling of steel shells European design recommendations".

$$r_e=\frac{r_2}{cos\beta_c} \quad \text{Eq. 4.47}$$

where β_c is half-cone angle of conical shell in [Rad],

$$\beta_c=\frac{\pi}{2}-\alpha_c$$

First, Seide [14] derived an expression based on Donnell type shell theory for the critical load for an axisymmetric mode in a conical shell under axial loading. Seide's formula may be written as follows [42 and 43],

$$F_{c,con}=\frac{2\pi Et^2cos^2\beta_c}{\sqrt{3(1-\mu^2)}}=F_{cyc}cos^2\beta_c \quad \text{Eq. 4.48}$$

Thus, the critical load of a conical shell is equal to cylinder's critical load which is multiplied by the square of the cosine of the half cone angle. However, this analytical model is

not adequate to estimate the limit load for nonstandard structures due to the tremendous assumptions.

In the conical shells with the small base angle, the maximum meridional bending moment is displaced from the edge to the center of the structure under axial loading. The conical shell becomes a circular plate with the maximum bending moment in the center if $\alpha_c \rightarrow 0°$. Furthermore, it is obviously seen that it is not possible to use standard methods for calculating the load carrying capacity from Eq. 4.47 and Figure 4.5. The equivalent radius of the cylinder is dependent on $1/\sin\alpha_c$. It is calculated relatively high and approaches to the infinity value in this case. For these reasons, the critical stress is significantly distorted (Eq. 4.46).

Under axial loading, the edge of the conical shell is in the tendency to shift in a radial direction (perpendicular to the axis of rotation). In the course of loading, the meridional force F_x occurs in the wall (see Figure 4.7). Its magnitude increases as the base angle decreases, proportionally $1/\sin\alpha_c$. Theoretically, the force F_x approaches infinity value for $\alpha_c \rightarrow 0°$. When the radial component of this force F_r acts, a shifting on the shell edge in the radial direction may appear. It causes a decrement in the base angle α_c and causes a significant increment in the meridional force. Gradually, this process may result in a snap-through at the structure. For this reason, conical shells which have small base angle behave nonlinearly. The forces acting in the conical shell wall are shown in Figure 4.7.

The standard method is based on the cylinder approach and this method stipulates that the ends of the structure must be restrained against displacements in the radial direction. Therefore, the standard method is applicable to the conical shell which has clamped end or reinforced end with a very stiff circumferential ring. Besides, the conical shell must have a base angle higher than 25°.

The conical shells with $\beta_c > 65°$ prone to loss of stability in the form of nonlinear collapse. This is not covered by equivalent cylinder approach as outlined above [5]. In this study conical shells which have base angle less than 25° (in other words $65° < \beta_c$) with flexible circumferential ring, are investigated. Hence, the analytical approach is inadaptable for determining the load carrying capacity of our model (Figure 4.5).

4.2 Definition of the Model

Upper radius r_1 and bottom radius r_2 are defined 50 and 250 mm relatively for the simulations. The base angle is appointed as $10° \leq \propto_c \leq 20°$. According to these values, the equivalent radius of the conical shell is set between 730 and 1440 mm. The width of the circumferential ring b_{ring} is chosen as a constant value which is 15 mm. Applying the load directly on the upper edge of the conical shell may cause convergence error in the numerical study. Stress gradients may occur on this line with the high amount of stress values. Therefore, a very stiff pipe is used on the upper edge to apply load. The load is distributed uniformly to the body of the structure by means of this stiff pipe (auxiliary surface). On the other hand, the conical shell, which is used as a connection component, is investigated in the study. In the present case, the stiff pipe also characterizes an adjacent part to simulate real condition more

precisely. The height of the relatively stiff pipe h is assigned as 10 mm. Cross section area of the circumferential ring is evaluated between $6 \leq A_{ring} \leq 300\ \text{mm}^2$.

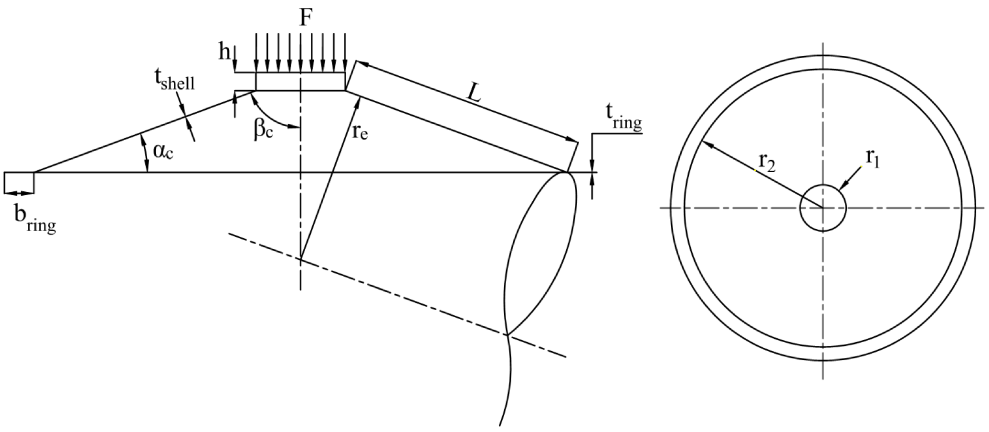

Figure 4.5. Front and top view of the conical shell (a) Front view, (b) Top view.

The thickness of the shell t_{shell} is set $0.5 \leq t_{shell} \leq 4\,mm$ interval. r_e/t_{shell} dimensionless parameter is assigned depending on the equivalent radius and the thickness of the shell between $240 \leq r_e/t_{shell} \leq 2880$. Additionally, the model is performed without ring (no radial stiffness) and with infinite stiff ring (fixed supported) in order to find ring effect on the limit load.

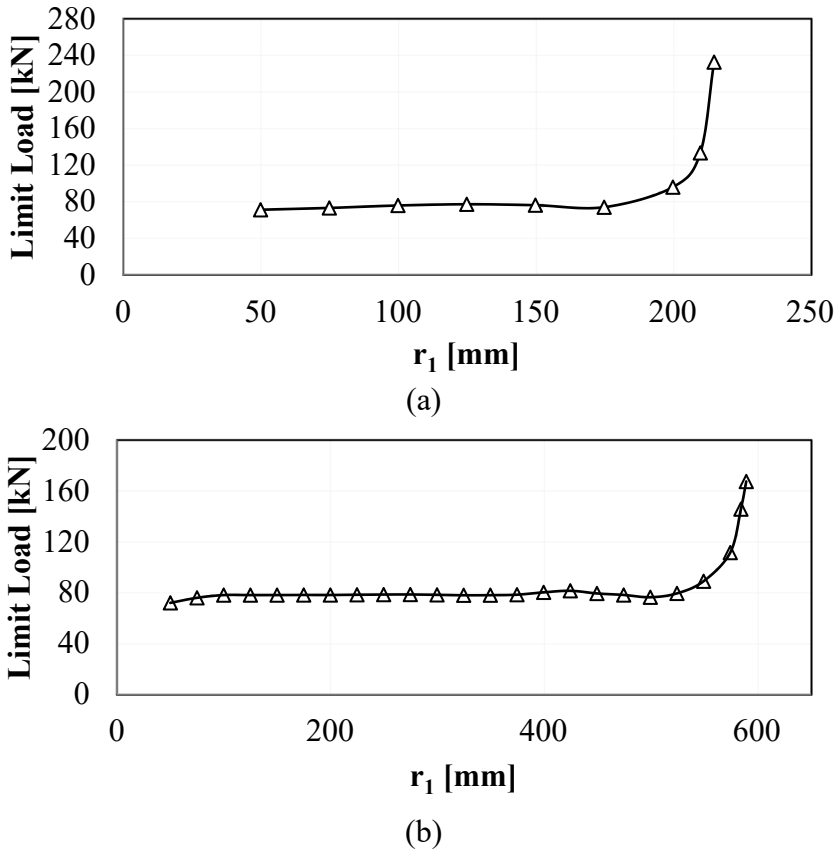

Figure 4.6. Influence of upper radius r_1 for base angle 15°. (a) r_2=250mm, t_{shell} =1.5mm, (b) r_2=650mm, t_{shell}=1.5mm.

Upper radius r_1 has a relatively small effect on the load carrying capacity of the conical shell structure under axial loading. It influences the capacity especially in the r_1/r_2 ratio is near to 1. Effective range of the r_1 take place a narrow area and it is seen in the Figure 4.6 for two different structures, for instance. One of the main aim of the study is to derivate nondimensional parameter for similarity. To achieve this goal, it is needed to be a simplification. Otherwise, the behavior characteristic of the structure under axial load can solely be expressed as a partial function and it makes the problem complicated. For this reason, the r_1/r_2 ratio excluding between 0.1 and 0.8 is neglected and it is assumed that the upper radius does not affect the limit load. Thus, the problem is simplified with a constant upper radius value (r_1=50 mm). On the other hand, the value of r_2 is selected 250 mm, initially. But, it is used in similarity parameters as a variable that can be seen in further chapters of the study. Equivalent radius of the conical shell is considered in the dissertation study as Eq. 4.47 [5].

4.3 Derivation of the Rigidity Parameter Γ

The rigidity parameter of the circumferential ring is derived to see apparently the influence of the circumferential ring on the load carrying capacity of the structure. Γ depends on the bottom edge radius of the conical shell r_2, the thickness of the shell t_{shell} and the cross-section area of the ring A_{ring}. The study "*Stabilitní Prolomení Kuželových Skořepin S Malým Vzepětím",* D. Středová [7] is taken as a reference for derivation of the Γ.

The radial stiffness of the ring

The rigidity parameter, which is required to be derived for the conical shells in this study, should be a sign to the radial stiffness of the lower end. The conical shells which have the identical Γ parameter also should have the same radial stiffness value.

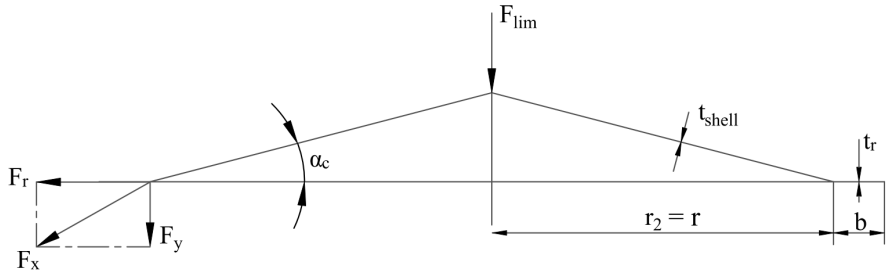

Figure 4.7. Conical shell with a circumferential ring under axial load.

However, the conical shells must be characterized with the same r_e/t parameter and the base angle $\propto_c$. Elongation of the perimeter of the ring is implied;

$$\varepsilon = \frac{2\pi(r_2 + \Delta r_2) - 2\pi r_2}{2\pi r_2} = \frac{\Delta r_2}{r_2} \qquad \text{Eq. 4.49}$$

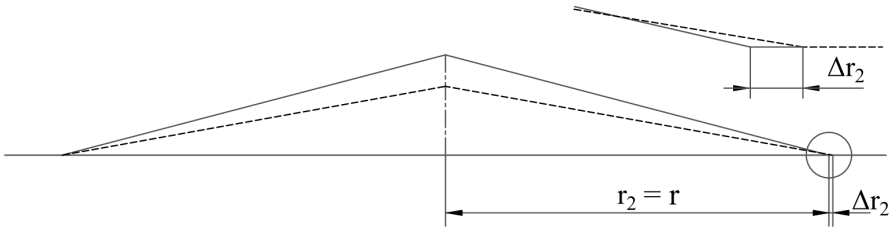

Figure 4.8. Changing the inner radius of the circumferential ring [7].

Radial force acting on the ring is expressed as,

$$F_r = \frac{F_{lim}}{tan \propto_c} \quad \text{Eq. 4.50}$$

An infinite small element of the ring is exhibited in Figure 4.9.

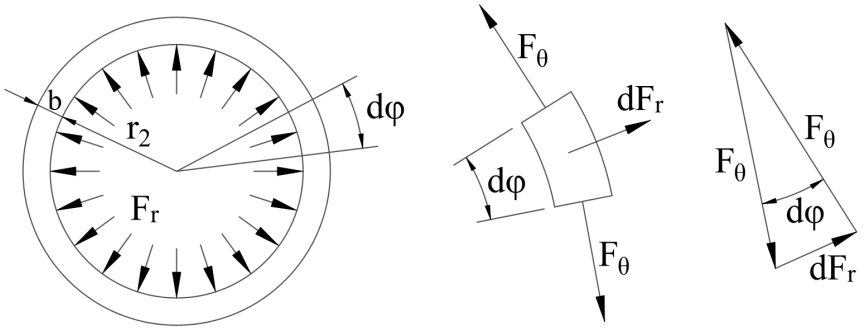

Figure 4.9. Equilibrium state of the forces on the element of the circumferential ring [7].

dF_r equalizes vector sum of the two inner circumferential forces F_θ in equilibrium. It can write as follows,

$$dF_r = F_\theta d\varphi \quad \text{Eq. 4.51}$$

and

$$dF_r = \frac{F_{lim}}{tan \propto_c} \frac{d\varphi}{2\pi} \quad \text{Eq. 4.52}$$

Value of the internal forces F_θ is obtained by utilizing expressions Eq. 4.51 and Eq. 4.52,

$$F_\theta = \frac{F_{lim}}{2\pi tan \propto_c} \quad \text{Eq. 4.53}$$

This force causes tensile stress at the inner ring,

$$\sigma_\theta = \frac{F_\theta}{t_{ring} b_{ring}} = \frac{F_\theta}{A_{ring}} = \frac{F_{lim}}{A_{ring} 2\pi tan \propto_c} \quad \text{Eq. 4.54}$$

The strain of the ring is expressed if Eq. 4.54 substitutes into Eq. 4.49,

$$\varepsilon = \frac{2\pi(r_2 + \Delta r) - 2\pi r_2}{2\pi r_2} = \frac{\Delta r}{r_2} = \frac{\sigma_\theta}{E} = \frac{F_{lim}}{2EA_{ring}\pi tan \propto_c} = constant \qquad \text{Eq. 4.55}$$

If the rings have the identical strain values, they have the same effect on the load carrying capacity. Therefore,

$\varepsilon_A = \varepsilon_B = \varepsilon_C = constant$

and

$$F_{Normalized} = \frac{F_{lim}}{2\pi r_2 t_{shell} E}$$

normalized (nondimensional) axial load previously derived in the literature [44 and 45] is substituted for F_{lim}, and Eq. 4.55 becomes,

$$\frac{2F_{Norm.}\pi r_{2,A} t_{shell,A} E}{2EA_{ring,A}\pi tan \propto_c} = \frac{2F_{Norm.}\pi r_{2,B} t_{shell,B} E}{2EA_{ring,B}\pi tan \propto_c} = \frac{2F_{Norm.}\pi r_{2,C} t_{shell,C} E}{2EA_{ring,C}\pi tan \propto_c} = constant \qquad \text{Eq. 4.56}$$

It is expected to obtain same load carrying capacity for the conical shells having the identical base angle, modulus of elasticity, and rigidity parameter. Therefore, Eq. 4.56 can simplify as seen in Eq. 4.57.

$$\frac{r_{2,A} t_{shell,A}}{A_{r,A}} = \frac{r_{2,B} t_{shell,B}}{A_{r,B}} = \frac{r_{2,A} t_{shell,A}}{A_{r,A}} = constant = \Gamma \qquad \text{Eq. 4.57}$$

Dimensionless Γ parameter depends on the radius of the lower edge of the conical shell, the thickness of the shell and the cross-sectional area of the ring. This parameter expresses the influence of the circumferential ring on load carrying capacity of the conical shells corresponding to the same base angle $\propto_c$.

$$\Gamma = \frac{r_2 t_{shell}}{A_{ring}} \qquad \text{Eq. 4.58}$$

4.4 Numerical Study

Numerical models and simulations are performed using FEM program COSMOS/M [9]. For the numerical analysis, large displacement module and Quadrilateral thick Shell element (SHELL4T) are assigned [41]. The nodal input pattern of the SHELL4T element is illustrated in Figure 4.11. Models are generated for three base angles α_c (10°, 15°, and 20°). Basic sketch of the structure is illustrated in Figure 4.5 with dimension parameters.

Considering complexity and size of the described problem, using the only experimental method in order to examine the stability of the thin wall structure is very expensive and has various difficulties. Performing numerical analysis gives an opportunity for the investigation of the conical shell structures in a wide range of geometric parameters without consuming cost and time.

In this study, geometrically nonlinear analysis (GNA) is performed, and the elastic limit load is carried out. At the first step of the study, the two limit conditions, which are fixed and simple supported conical shells, are evaluated (Figure 4.10). It is important to see the extremities of the load carrying capacity.

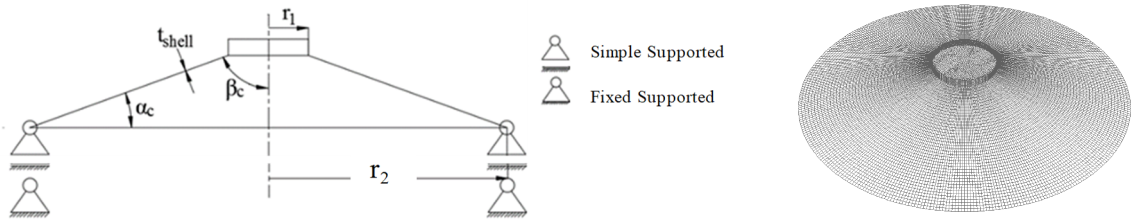

Figure 4.10. Schematic representation and numeric model of extremities.

In further studies, the limit load of the conical shell for various radial stiffnesses, which is represented by a circumferential ring, is investigated. The influence of the radial stiffness on the load carrying capacity is one of the central parts of this study. Schematic representation of the conical shell with the dimensions is illustrated in Figure 4.15 for this case. Models are axially loaded with 320 N at the initiation of the analysis. Because the upper edge is divided into 320 nodes and the load is assigned as 1 N for each node to make post-processing easy. The arc-length algorithm controls the loading increment step by step during the solution process.

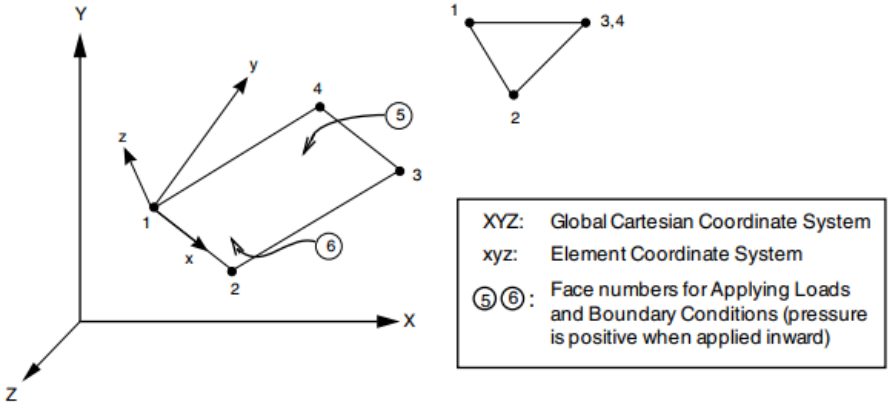

Figure 4.11. The nodal input pattern for a SHELL4T element [41].

4.4.1 Mesh Study

A number of analyses are performed to evaluate dependency of the results to mesh structure. Thus, a conical shell which has current dimensions (Table 4.1) is modeled with different element sizes.

Table 4.1. Geometric dimensions and number of elements of the models.

Notation	$\propto_c$ [°]	r_1 [mm]	r_2 [mm]	t_{shell} [mm]	b_{ring} [mm]	t_{ring} [mm]	Γ	Number of element	F_{lim} [kN]	u [mm]
M_1	15	50	250	0.5	15	0.4	20.8	11002	6.778	3.72
M_2								20720	7.131	4.81
M_3								33308	7.101	4.18
M_4								49020	7.087	4.21

The load carrying capacity and the displacements in the vertical direction at the limit point can be seen in Figure 4.12 and Table 4.1. Displacement values are taken from same data point at which the top of the conical shell for all analysis.

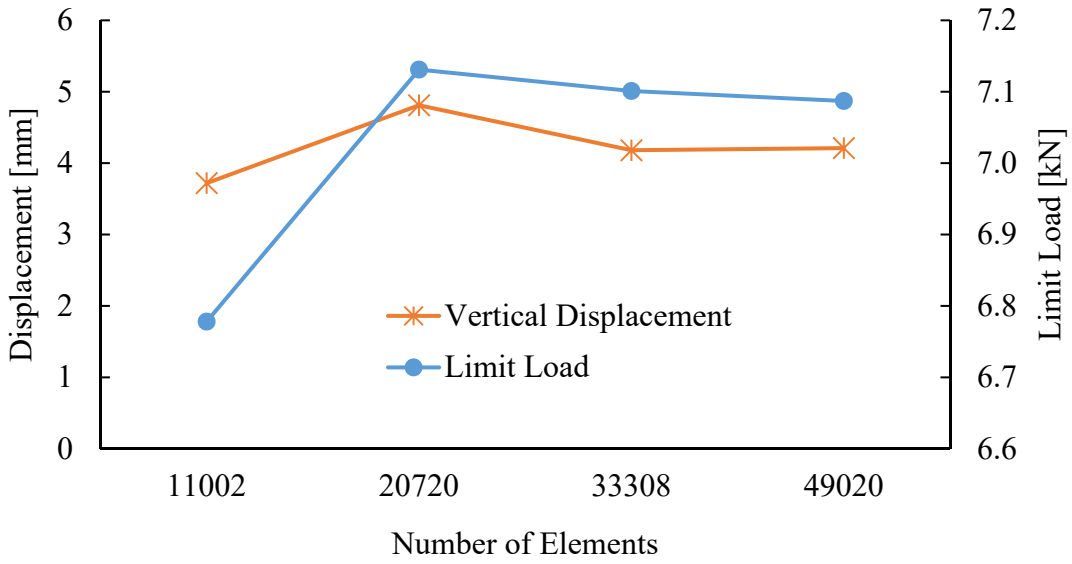

Figure 4.12. The results of the mesh study.

The results do not change over 1% between the models created with 2.6 mm (M_3) and 2.1 mm (M_4) element sizes. Therefore, the element size is chosen 2.6 mm for the numerical study considering computer supplement and time-consuming.

4.4.2 Boundary Condition

In this study, the conical shells which are used as a connection component for the structure are investigated. Simple cone–cylinder connections are the most common form of connections. They are found in steel silos and tanks with a conical roof, elevated conical water tanks with cylindrical shell support, large tubular members, pipes with a conical transition between two cylinders of different diameters and pressure vessels with a conical end closure.

When the structure has a structural weakness (e.g. connection), a ring is often provided to strengthen it. This ring may be in the form of an annular plate, a T-section or an angle section.

It should be pointed out that if a ring is provided, the radial stiffness of this ring often dominates the load carrying capacity of the structure under axial loading. In this study, the effect of the circumferential ring on load carrying capacity is also investigated as a consequence of the importance of the connection. Therefore, typical practical usage of a conical shell structure which have a circumferential ring with a cylindrical shell is modeled (Figure 4.13).

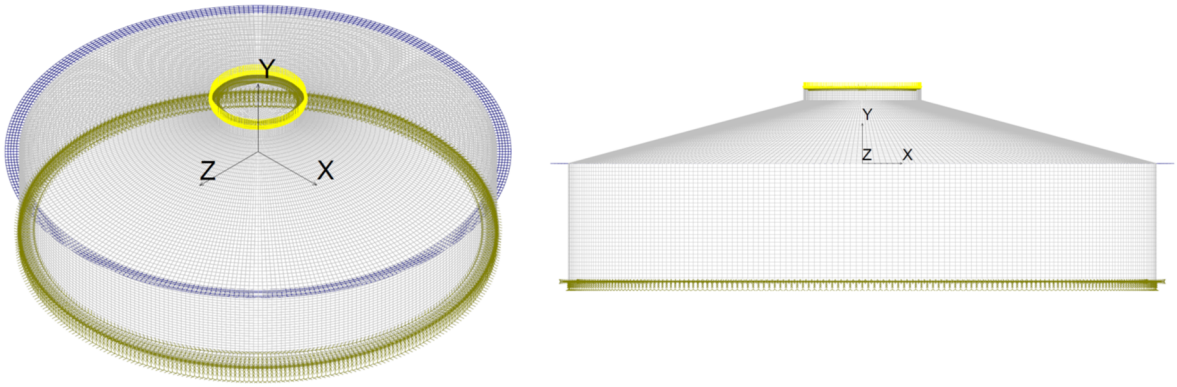

Figure 4.13. Full scaled numerical model.

Assignment of the boundary conditions is a critical step in the numerical study. Concerning the solution time and mesh structure, the full scaled numerical model is simplified in the numeric analysis (Figure 4.14). This simplification provides decreasing the solution time and getting better mesh structure quality with lower computational system requirement.

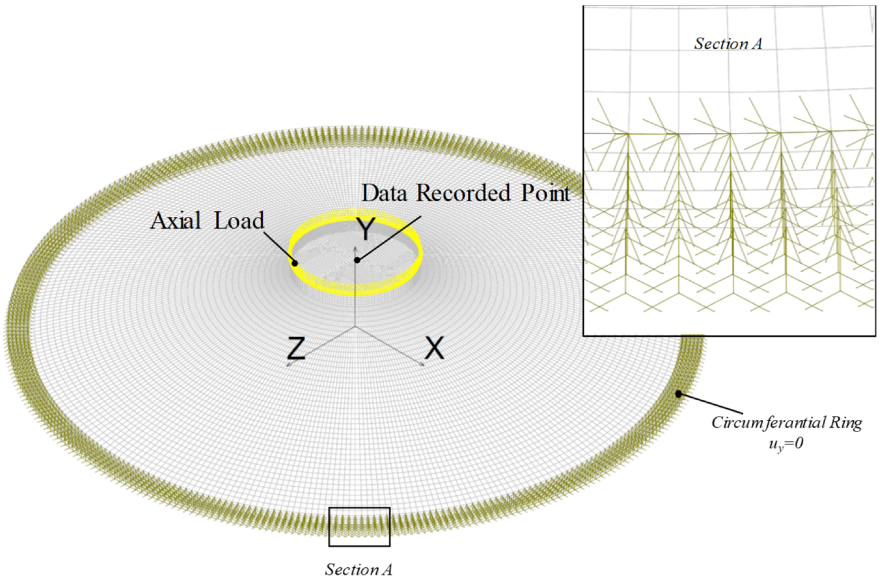

Figure 4.14. Simplified numerical model.

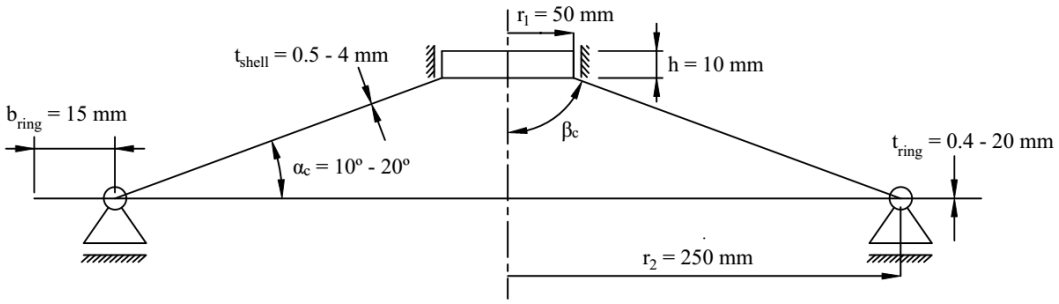

Figure 4.15. Schematic representation of the conical shell with the circumferential ring.

For this purpose, a simplified numerical model is performed for base angle 15°(Figure 4.14). This step is vital to ensure whether the simplified model is simulated the full scaled one accurately or not.

Table 4.2. Geometric parameters and the limit load of the numerical models.

Notation	$\mathbf{r_e/t_{shell}}$	Γ
C_1	1931.8	49.7
C_2	965.9	39.7
C_3	603.7	31.8
C_4	321.9	14.9

	$F_{lim}[N]$			
	C_1	***C_2***	***C_3***	***C_4***
Simplified. Model	7431.84	28498.88	72620.8	272617.6
Full Scaled Model	7494.72	29658.56	74268.8	272595.2

The results show that the simplified models can simulate the full scaled model for various dimensionless parameters (r_e/t_{shell} and Γ. see Table 4.2). Four different models are generated, and they are illustrated with "*C_*" notation.

Limit loads of the conical shell structures are substantially same for different parameters. Thus, the simplified model is used instead of a full scaled model in the study hereinafter. This numerical model can be seen in Figure 4.14. The schematic representation of the conical shell with geometric parameters and boundary conditions are illustrated in Figure 4.15.

4.4.3 Γ Parameter Validation

The rigidity parameter, Γ assumes identical relative extension of the circumferential ring if the conical shells have the same base angle of α_c and dimensionless r_e/t_{shell} parameter.

Proposed function of the Γ is tested via numerical analysis for five different the conical shell geometries in this chapter (Table 4.3).

According to results, a similarity between load carrying capacities of the conical shells regarding geometrical parameters is tried to derive. Since distributed line load is applied to the structures, it is hard to express similarity in terms of limit load for different conical shell geometries. To achieve this purpose, the load is normalized by a constitutive relation with respect to the cross-section area of the lower edge. Therefore, normalized axial load (Eq. 4.59) is adapted to the results as exhibited in the literature before [44 and 45]. This definition also used for derivation of the rigidity parameter of the circumferential ring (see section 4.3). It is a function of limit load and geometrical parameters of the structure; besides, it represents the limit load in nondimensional form. The limit load of the structure can be calculated easily from this nondimensional form. In the other words, if the structures have the same rigidity parameter of the ring Γ, the ratio of r_e/t_{shell} and, base angle α_c, they should have a same normalized load.

$$F_{Normalized} = \frac{F_{lim}}{2\pi r_2 t_{shell} E} \qquad \text{Eq. 4.59}$$

Table 4.3. Dimensions of the compared conical shells.

Notation	$\propto_c$ [°]	r_1 [mm]	r_2 [mm]	t_{shell} [mm]	r_e/t_{shell}	b_{ring} [mm]	t_{ring} [mm]	A_{ring} [mm^2]	$\Gamma = \frac{r_2 t_{shell}}{A_{ring}}$
A	15	50	250	1.5	643.9	15	6.0	90	4.167
B	15	50	400	2.4	643.9	40	5.76	230.4	4.167
C	15	50	500	3.0	643.9	50	7.2	360	4.167
D	15	50	700	4.2	643.9	75	9.4	705	4.167
E	15	50	1000	6.0	643.9	50	28.8	1440	4.167

The numerical results for five configurations are given in Table 4.4. Normalized axial loads of the conical shell structures are almost identical. The results show that the rigidity parameter works within this relation. The values of the load carrying capacity vary maximally around %3.

Table 4.4. Results of the numerical analyses.

Notation	$F_{Normalized}$*10^6 [-] (Nondimensional)
A	142.1
B	145.8
C	146.4
D	145.6
E	144.9

Diverse types of circumferential ring (square, cylinder, T profile, etc.) implementation is seen in practical applications. Circumferential rings which have different shapes, but equal cross-sectional areas have only different moment of inertia values.

According to the results of the analysis (for full-scale model), it is observed that the circumferential ring, which is located on the connection of the cylinder and the conical shell, does not have any rotation (Figure 4.16). That means the shape of the ring does not influence the strength of the structure under these conditions. Thus, the cross-section area of the ring A_{ring} can be included in the relationship of the rigidity parameter for various kind of ring profiles.

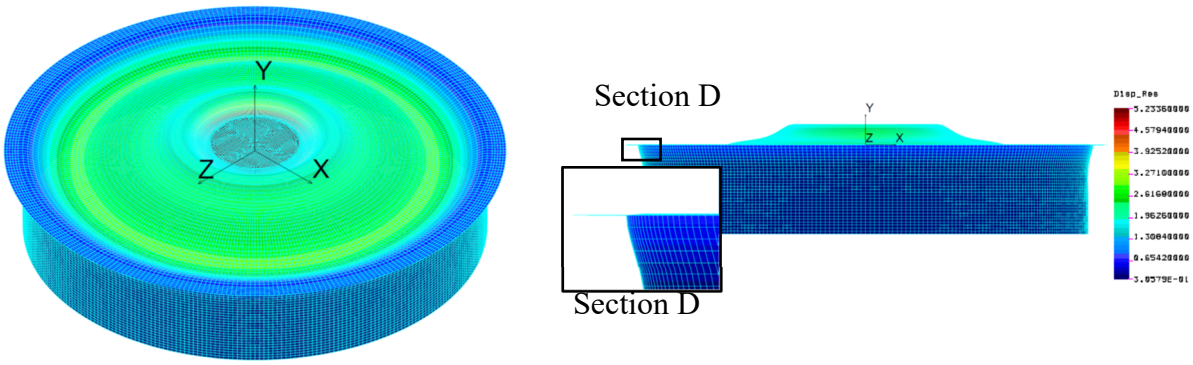

Figure 4.16. Deformed shape of the full scaled model.

4.5 Influence of Material

In the European Recommendation [5], the design procedure for buckling stress involves the following steps for the cylindrical shell which under axial load;

- Estimation of the linear elastic stress field caused by the applied load which leads to membrane stress field σ_{xEd}.
- Determination of the elastic critical buckling stress σ_{xRcr} for the perfect shell at any possible buckling location on the structure.

- Specification of the relative slenderness parameter of the shell λ_x. This parameter relates the yield stress to the elastic critical buckling stress.
- Calculation of the elastic imperfection reduction coefficient for membrane stress component α_x and elastic buckling stress for the imperfect shell $\alpha_x \sigma_{xRcr}$.
- Obtaining the buckling strength reduction factor χ_x as a function of its relative slenderness parameter λ_x in order to take account into plasticity effects. Therefore, the elastic buckling stress for the imperfect shell is simplified to calculate the characteristic buckling stress σ_{xRk}.
- Application the partial safety factor γ_{Ml} on resistance in order to find design value of the buckling stress σ_{xRd}.

The following relationships are used to check the design of the shell under axial loading. These relationships are taken from the European recommendations ECCS [5] and represent the results of many experiments by several researchers. They consider the effect of a plastic material behavior and the effect of initial imperfections. Design resistance in the axial direction must comply with the condition,

$$\sigma_{xEd} \leq \sigma_{xRd}$$

wherein σ_{xEd} is a design value of the buckling membrane stress in the axial direction, and σ_{xRd} is the meridional design buckling stress. This value depends on the material characteristics and the geometry of the shell according to the relation,

$$\sigma_{xRd} = \sigma_{xRk}/\gamma_{Ml} \qquad \text{Eq. 4.60}$$

Expression of σ_{xRk} is the characteristic buckling stress in the axial direction, γ_{Ml} is the partial safety factor. It is recommended that the value of the γ_{Ml} should not be taken as smaller than $\gamma_{Ml} = 1.1$.

The characteristic buckling stress is given by multiplying the yield strength and the buckling reduction factor,

$$\sigma_{xRk} = \chi_x f_{y,k} \qquad \text{Eq. 4.61}$$

where $f_{y,k}$ is the yield strength of the material, and χ_x is the buckling reduction factor which represents the effect of plasticity on the load carrying capacity of the shells under axial loading.

Relationships for buckling reduction factor are presented in Table 4.5. Buckling reduction factor χ is a function of the relative slenderness of the shell λ. α is the elastic imperfection reduction coefficient, β is the plastic range factor, η is the interaction exponent, and λ_0 is the squash limit relative slenderness.

Table 4.5. Buckling reduction factor [5].

Region of the loss of stability	Buckling reduction factor χ	Relative slenderness of the shell
Plastic	$\chi = 1$	$\lambda \leq \lambda_0$
Elastic-Plastic	$\chi = 1 - \beta \left[\frac{\lambda - \lambda_0}{\lambda_p - \lambda_0}\right]^{\eta}$	$\lambda_0 \leq \lambda \leq \lambda_p$
Elastic	$\chi = \frac{\alpha}{\lambda^2}$	$\lambda_p \leq \lambda$
Note: η value is recommended for the shell structures $\eta = 1.0$		

Figure 4.17 shows the form of the capacity curve. This form depends on the values of the parameters λ, β, η and λ_0 for every geometry and load conditions. These parameters vary according to shell geometry, loading type, amplitude of the imperfection and boundary conditions.

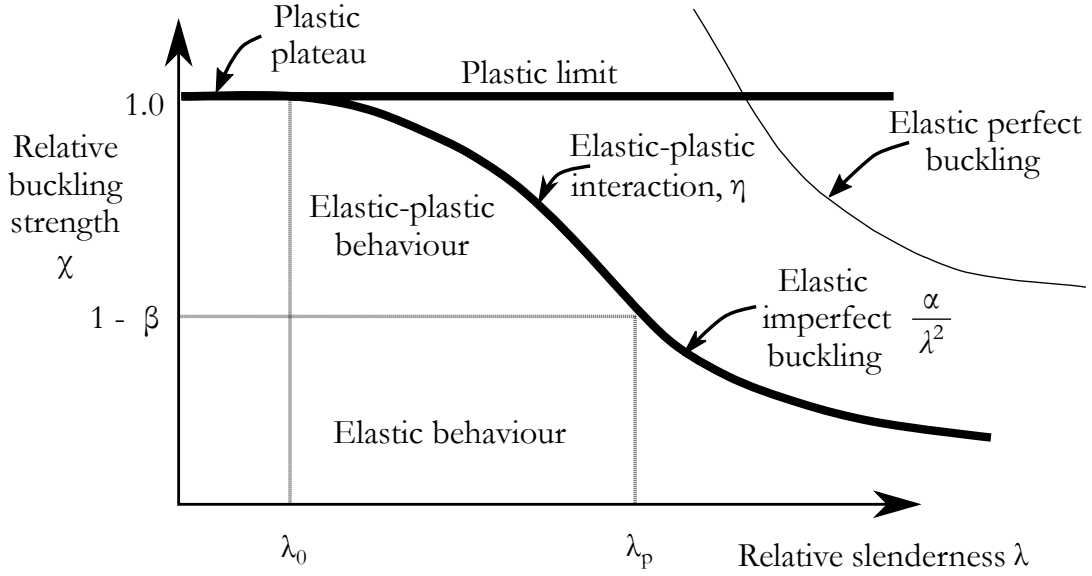

Figure 4.17. Capacity curve and the parameters, α, β, λ_0 and η [5].

The relative shell slenderness λ_x is defined depending on the yield strength of the material $f_{y,k}$ and the meridional elastic critical stress σ_{xRcr}.

$$\lambda_x = \sqrt{f_{y,k} / \sigma_{xRcr}} \qquad \text{Eq. 4.62}$$

The value of the plastic limit relative slenderness λ_p,

$$\lambda_p = \sqrt{\frac{\alpha_x}{1 - \beta}} \qquad \text{Eq. 4.63}$$

The values of the parameters λ_0 and β are achieved from the results of many experiments cylindrical shells under axial loading,

$\lambda_0 = 0.20, \quad \beta = 0.60$

In the plastic region where $\lambda_x \leq \lambda_0$, the effect of initial imperfections is not taken into account. Plastic limit state occurs and the characteristic buckling stress in the axial direction is equal to the yield strength of the material.

$\sigma_{xRk} = \chi_x f_{y,k} = 1\, f_{y,k}$

In region $\lambda_0 \leq \lambda_x \leq \lambda_p$, plastic behavior and initial imperfection influence the characteristic buckling stress. Characteristic buckling stress in the axial direction is given by,

$$\sigma_{xRk} = \chi_x f_{y,k} = 1 - \beta \left[\frac{\lambda_x - \lambda_0}{\lambda_p - \lambda_0}\right]^{\eta} f_{y,k}$$

where the influence of initial imperfections is reflected in the parameter λ_p.

When the parameters correspond $\lambda_x \geq \lambda_p$ (in the elastic region), nonlinear behavior of the material does not affect the characteristic buckling stress in the axial direction. Characteristic buckling stress is written as stated below in this case,

$$\sigma_{xRk} = \chi_x f_{y,k} = \frac{\alpha}{\lambda_x^2} f_{y,k} = \alpha_x \sigma_{xRcr}$$

Influence of initial imperfections on the load carrying capacity of the shell under axial loading is expressed by reducing with a coefficient. The coefficient of elastic imperfections reduction coefficient is denoted as α_x in the axial direction. Its value depends on the quality of production Q_{pr}.

$$\alpha_x = \frac{0.62}{1 + 1.91(\,\Delta w_k/t)^{1.44}} \qquad \text{Eq. 4.64}$$

where Δw_k is characteristic imperfection amplitude,

$$\Delta w_k = \frac{1}{Q_{pr}} \sqrt{\frac{r_e}{t_{shell}}}\, t_{shell} \qquad \text{Eq. 4.65}$$

The characteristic buckling stress, which is obtained from ECSS, for the conical shell with the given parameters in Table 4.6 is visually presented in Figure 4.18.

Table 4.6. Geometrical parameters and mechanical properties of the conical shell.

α_c[°]	r_2[mm]	$f_{y,k}$[MPa]	E [MPa]	Q_{pr}[-]	r_e[-]	η [-]	β [-]	λ_0 [-]
20	340	355	20E5	40	1000	1	0.6	0.2

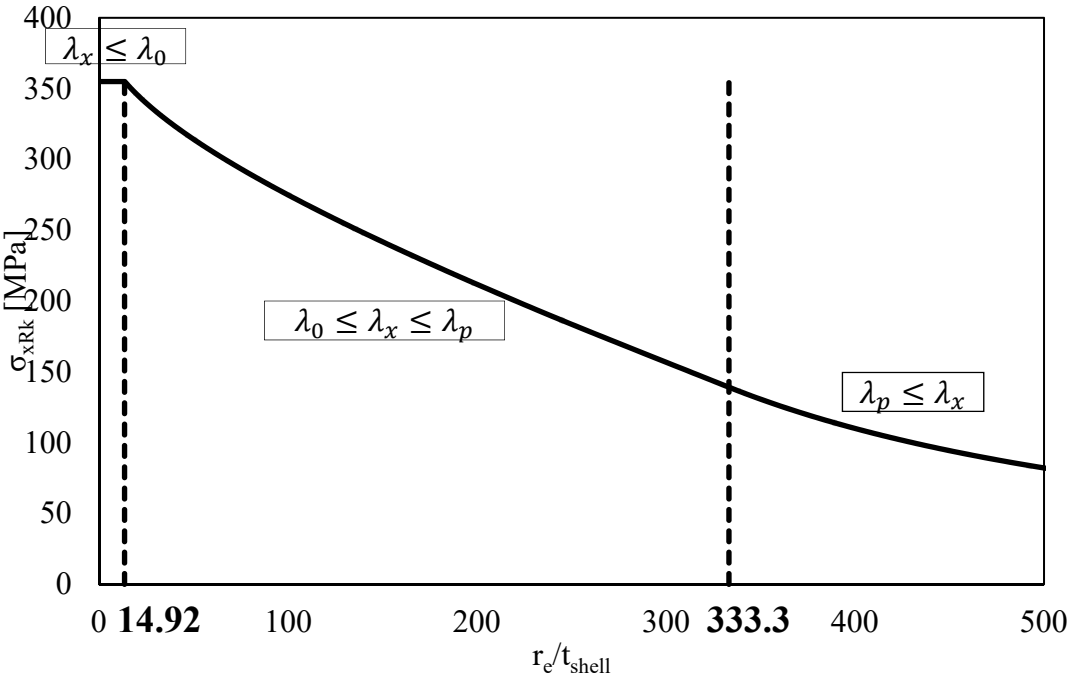

Figure 4.18. Influence of plasticity for selected conical shell in Table 4.6.

Figure 4.18 shows a curve that describes the characteristic critical stress as a function of the r_e/t_{shell} parameter. The curve is calculated for a conical shell with a yield stress of 355 MPa and modulus of elasticity of 20E5 MPa.

In case of $r_e/t_{shell} \leq 14.92$, the conical shell reaches the limit state of plasticity. In this interval, the influence of geometric initial imperfections is not considered.

In the interval $14.92 \leq r_e/t_{shell} \leq 333.3$ the loss of stability occurs in the elastic - plastic region. The load carrying capacity of the structure is determined by the limit state of loss of stability and the non-linear material behavior (plasticity) is taken into account. On the other hand, if the conical shell structure is in the area of $333.3 \leq r_e/t_{shell}$, the loss of stability occurs in the elastic region. Therefore, the effect of nonlinear material behavior is negligible in this case.

Table 4.7. Values of fabrication quality parameter Q_{pr} [5].

Fabrication tolerance quality class	**Description**	$\boldsymbol{Q_{pr}}$
Class A	Excellent	40
Class B	High	25
Class C	Normal	16

The value of the elastic critical stress under axial loading, σ_{xRcr} (Eq. 4.66) is based on the linear shell theory in the European recommendations. Its value is already adjusted depending on boundary conditions and geometry. The effect of geometry and boundary conditions on the critical stress value are considered by means of C_x (Table 4.8).

Table 4.8 Dimensionless parameters ω and C_x [5].

Type of the cylindrical shell	Dimensionless parameter ω	Dimensionless parameter C_x
Short	$\omega < 1.7$	$C_x = 1.36 - \frac{1.83}{\omega} + \frac{2.07}{\omega^2}$
Medium	$1.7 < \omega < 0.5\frac{r_e}{t}$	$C_x = 1$
Long	$\omega > 0.5\frac{r_e}{t}$	$C_x = max\left\{1 + \frac{0.2}{C_{xb}}\left[1 - 2\,\omega\frac{t}{r_e}\right]; 0.6\right\}$

Note: Dimensionless parameter C_{xb} and boundary conditions should be evaluated based on Table 4.9 and Table 4.10.

$$\sigma_{xRcr} = 0.605EC_x\frac{t_{shell}}{r_e} \qquad \text{Eq. 4.66}$$

where C_x is a function of dimensionless parameter ω which depends on the geometry of the shell structure according to the following relationship,

$$\omega = \frac{l_e}{\sqrt{r_e t_{shell}}} \qquad \text{Eq. 4.67}$$

moreover, the value of the C_x parameter is seen in the Table 4.8.

The effect of plasticity on the critical stress can be taken into account as a coefficient which depends on the structure as mentioned above. Thereby, in the numerical part of the study, it is assumed that material behavior is linear and elastic.

Table 4.9. Dimensionless parameter C_{xb} [5].

Case	Cylinder end	Boundary condition	C_{xb}
1	end 1	BC1	6
	end 2	BC1	
2	end 1	BC1	3
	end 2	BC2	
3	end 1	BC2	1
	end 2	BC2	

Table 4.10. Boundary conditions for shells [5].

Boundary Condition Code	Normal displacement	Meridional displacement
BC1	$w = 0$	$u = 0$
BC2	$w = 0$	$u \neq 0$
BC3	$w \neq 0$	$u \neq 0$

5 RESULTS AND DISCUSSION

The primary purpose of this chapter is to determine the load carrying capacity of the conical shells under axial loading within two limit boundary conditions. In addition to this, the influence of the circumferential ring on the load carrying capacity of the conical shell is investigated. These limit conditions simulate the ring which allows unlimited radial displacement or entirely prevents against the radial displacement of the lower edge (Figure 5.1).

5.1 Numerical Solution

The main part of this chapter contains a series of numerical analyses of the thin-walled conical shell structures with the base angle $\propto_c = 10°, 15°, 20°$. Moreover, different shell thicknesses corresponding to dimensionless r_e/t_{shell} parameter are assigned. Rigidity parameter of the circumferential ring is considered with respect to the cross-sectional area of the ring A_{ring}, shell thickness t_{shell} and lower radius r_2 of the conical shell. The range of the area of the ring, shell thickness and equivalent radius of the conical shell are kept between $6 - 300\ \text{mm}^2$, $0.5 - 4\ \text{mm}$ and $240 - 2880\ \text{mm}$, respectively, in the numerical analyses. On the other hand, the upper radius and the lower radius of the conical shell are assigned $r_1 = 50\ \text{mm}$ and $r_2 = 250\ \text{mm}$.

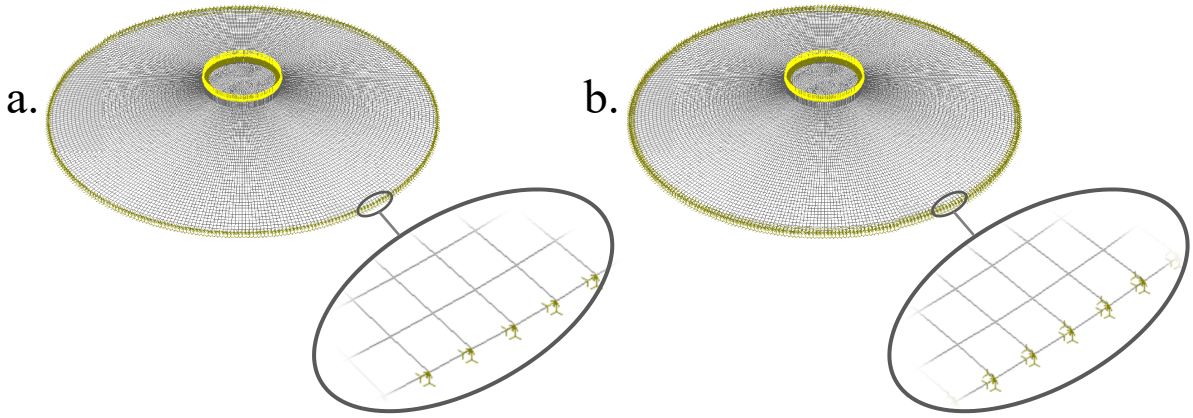

Figure 5.1. Illustration of the supports on the numerical model. (a) Simple supported, (b) Fixed supported.

Figure 5.2 exhibits the displacement curve of the selected node number 21, which located at the top of the conical shell, depending on the axial load. During the axial load increase, the structure reaches the limit state and loses its stability gradually. The load carrying capacity of the structure in parallel with geometrical stiffness decreases after this point.

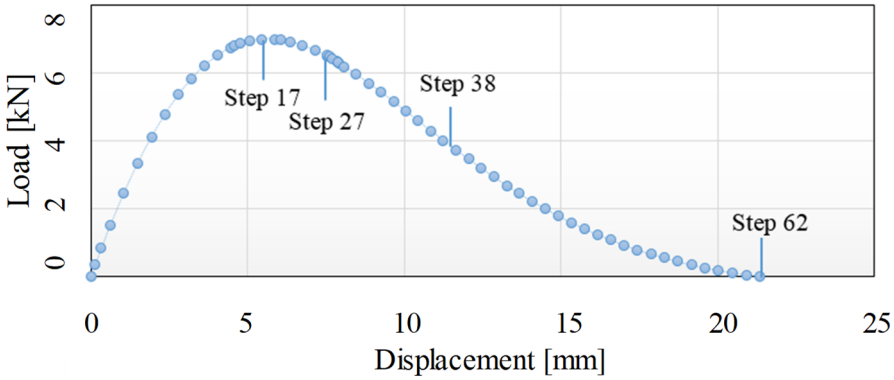

Figure 5.2. Load-displacement characteristic for nodal point 21.

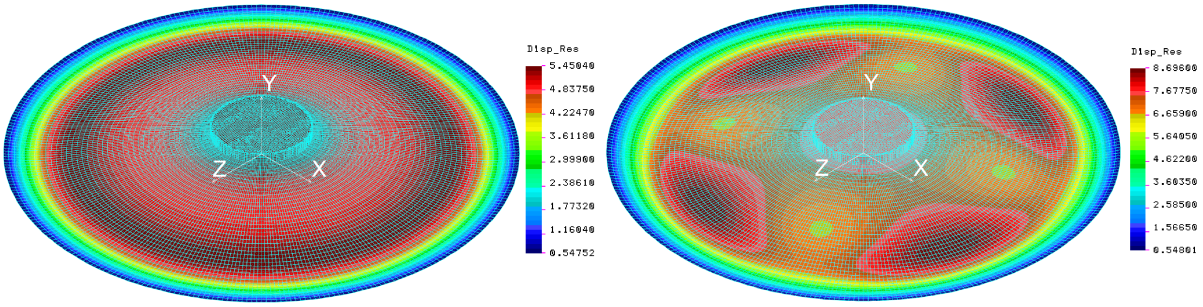

a. Resultant displacement – step number 17 **b.** Resultant displacement – step number 27

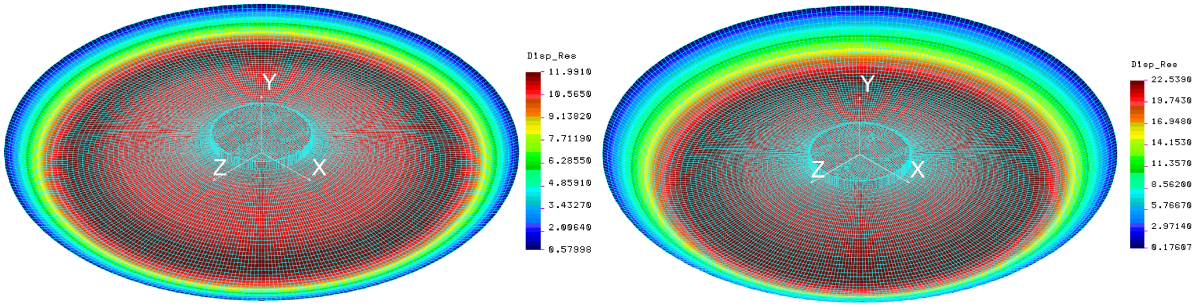

c. Resultant displacement – step number 38 **d.** Resultant displacement – step number 62

Figure 5.3. Resultant displacement of the simple supported conical shell for α_c=10°, t_{shell}=1.2 mm.

The shape of the deformed structure is plotted in Figure 5.3. At step 17, axially symmetric deformation and nonlinear collapse occur, in this case, the top of the conical shell has 5.45 mm vertical displacement under an axial load of 6.58 kN. At step 27, possible bifurcation point that is mentioned before (nonlinear buckling) occurs and it leads to the formation of four axially symmetric waves. During the subsequent process such as step 38, the load carrying capacity of the conical shell still decreases in the post-buckling process. The structure has axially symmetric deformation. Finally, at step 62, deformation propagation needs nearly zero load value. The structure gets invert shape when it is compared to initial shape at this point.

5.2 Influence of Boundary Conditions

The results of the numerical analysis for the conical shells show the limit load of the structure. The limit load is substantially dependent on selected boundary conditions (Figure 5.4). Possible displacement at radial direction causes a reduction in load carrying capacity of the structure.

The significance of the boundary condition against the load carrying capacity of the conical shell increases, especially at the lower r_e/t_{shell} values. The results of the fixed supported conical shell (wholly restricted radial displacement) suggest that the circumferential ring stiffness is quite efficacious on the limit load of the structure. The relation between the limit load and r_e/t_{shell} parameter of the fixed supported conical shell is illustrated in Figure 5.4.

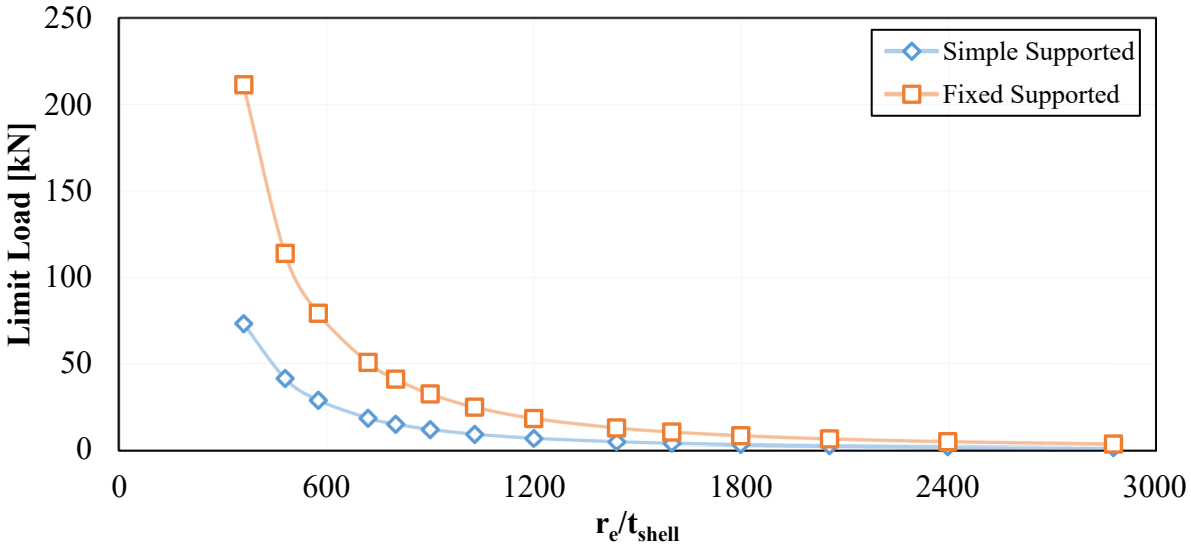

(a)

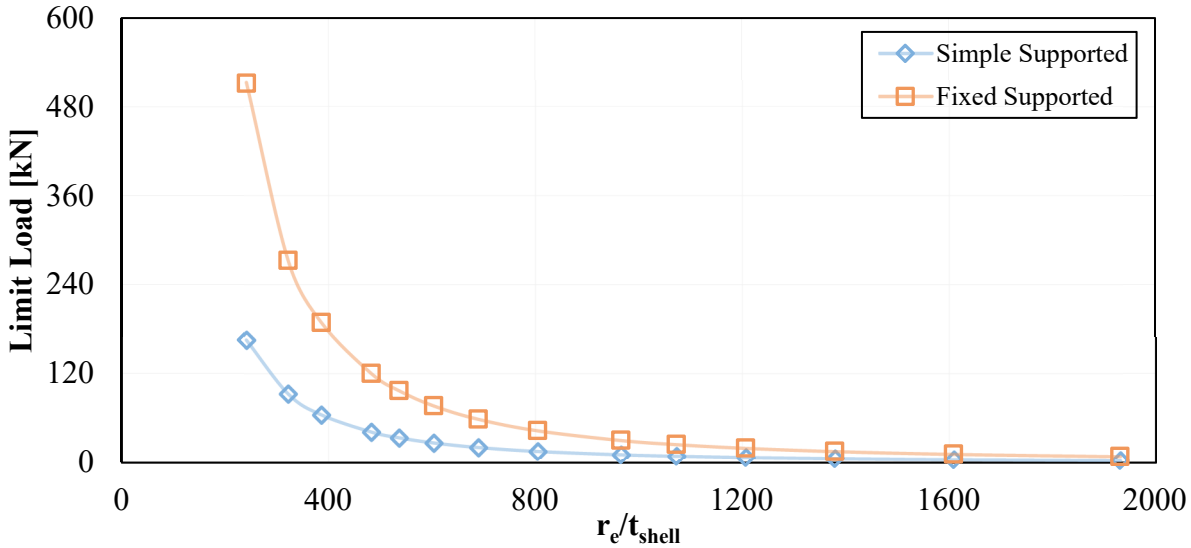

(b)

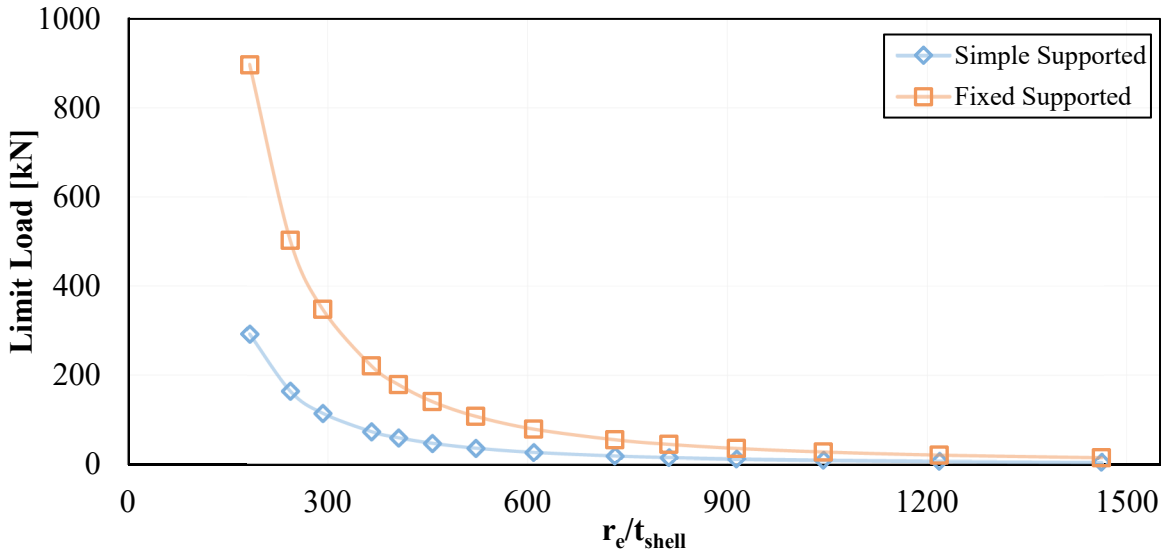

(c)

Figure 5.4. Influence of the boundary conditions on the load carrying capacity of the conical shell for different base angles, (a) Base angle 10°, (b) Base angle 15°, (c) Base angle 20°.

It is possible to derive regression curves as a power function of r_e/t_{shell} parameter using the data points (Eq. 5.1). The curve is relatively dependent on r_e/t_{shell}. The limit load of the conical shell regarding the r_e/t_{shell} parameter is in good agreement with regression curve without considering elastic-plastic behavior. For this purpose, Eq. 4.66 can be used to get a function draft,

$$F = 2\pi r_e t_{shell} 0.605 E C_x \frac{t_{shell}}{r_e}$$

In this equation, if we say the expression $(2\pi r_e t_{shell} 0.605 E C_x)$ is equal to K' then limit load can be rewritten as;

$$F_{lim} = K'(t_{shell}/r_e)^{m'} \quad or \; F_{lim} = K'(r_e/t_{shell})^{-m'} \qquad \text{Eq. 5.1}$$

where the coefficient K' depends on the modulus of elasticity, shell geometry, and the dimensionless factor C_x (Table 4.8).

The Eq. 5.1 uses to create the regression curves as a power function and data from GNA analyses are taken into consideration. Coefficients K' and m' are shown in Table 5.1 considering the linear elastic behavior of the fixed supported conical shell.

Table 5.1. The coefficients of the regression curves for the fixed supported conical shell.

Base angle $\propto_c$ [°]	Range of dimensionless r_e/t_{shell} parameter	Coefficients	
		K' [kN]	m'
10	480 - 2880	$3x10^7$	1.995
15	320 - 1930	$3x10^7$	1.999
20	240 - 1460	$3x10^7$	1.992

The load carrying capacity of the simple supported conical shell (utterly allowable radial displacement) is relatively low when compared to the fixed one at the same r_e/t_{shell} value. These differences are caused by the radial stiffness of the structures. This means, the carrying capacity of the structure is relatively dependent on the radial stiffness.

Table 5.2. The coefficients of the regression curves for the simple supported conical shell.

Base angle $\propto_c$ [°]	Range of dimensionless r_e/t_{shell} parameter	Coefficients	
		K'[kN]	m'
10	480 - 2880	$1x10^7$	2.000
15	320 - 1930	$9x10^6$	1.996
20	240 - 1460	$1x10^7$	1.996

Relations between the limit load and r_e/t_{shell} parameter of the simple supported conical shells for various base angles are illustrated in Figure 5.4. It is possible to derive regression curves using the data points as mentioned above for the fixed supported conical shells. The limit load of the conical shells and regression curves are well matched. Coefficients K' and m' are shown in Table 5.2 considering the linear elastic material behavior for the simple supported conical shells.

5.3 Influence of Base Angle

In order to compare the influence of the base angle at the same shell thickness on load carrying capacity, Figure 5.5 is illustrated. The figure shows the dependence of limit load on the thickness of the shell with different base angle $\propto_c$. From the curves, it is obviously seen that the conical shell with a higher base angle for the same shell thickness has a relatively larger amount of load carrying capacity.

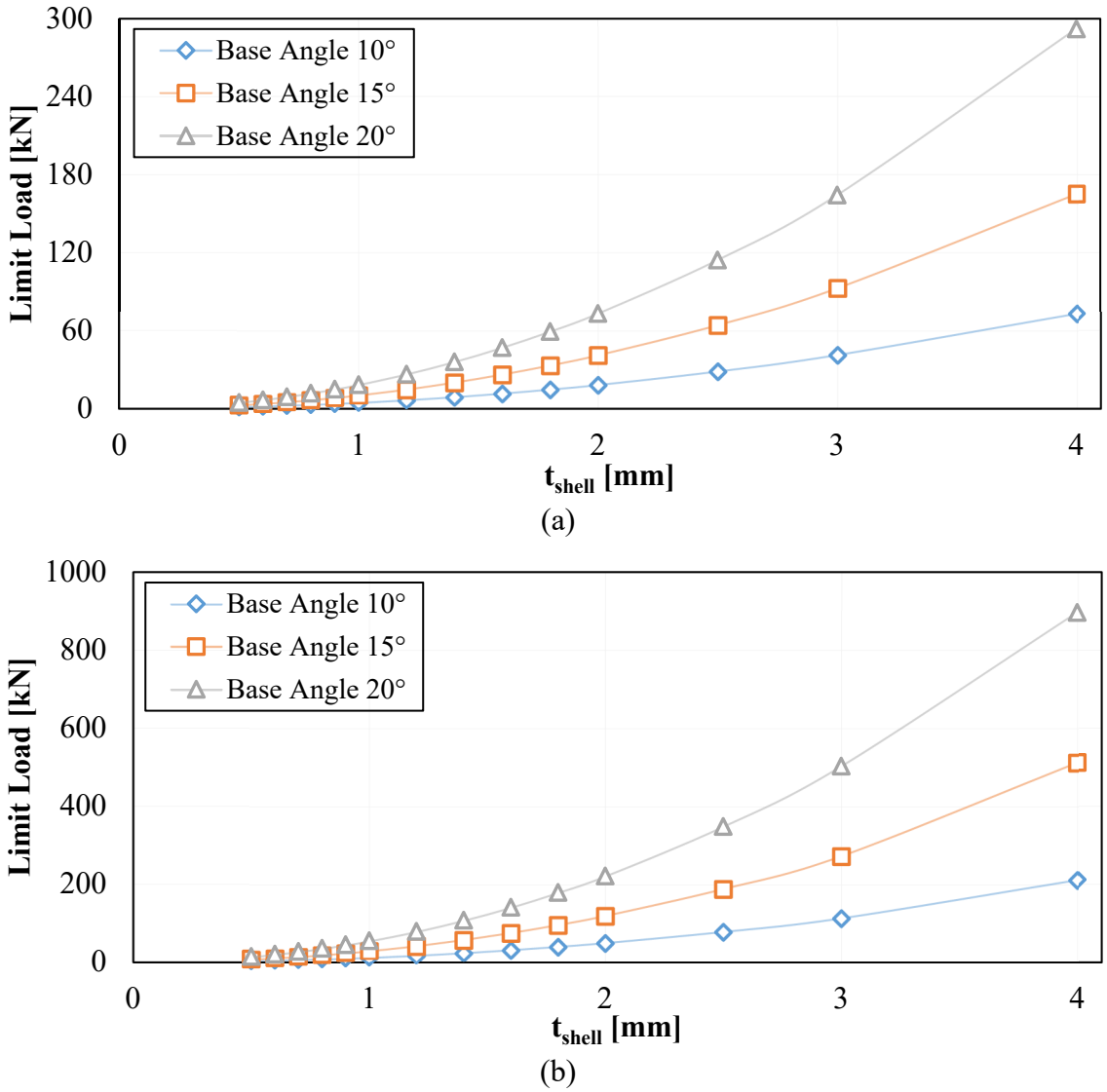

Figure 5.5. Effect of the base angle of the conical shell on the load carrying capacity. (a) Simple supported, (b) Fixed supported.

The strength of the structure against axial loading increases with both the shell thickness and the base angle. The limit load of the structure is nearly related to the square of the shell thickness. Data are well matched with a second order power function of the shell thickness. On the other hand, the increment of the base angle, even just one degree, gives a serious contribution to the limit load, positively. Since the increment of the base angle provides reducing the bending state effect which is caused by the nature of the structure. The proportion of the radial component of the force at the lower edge also decreases as base angle increasing.

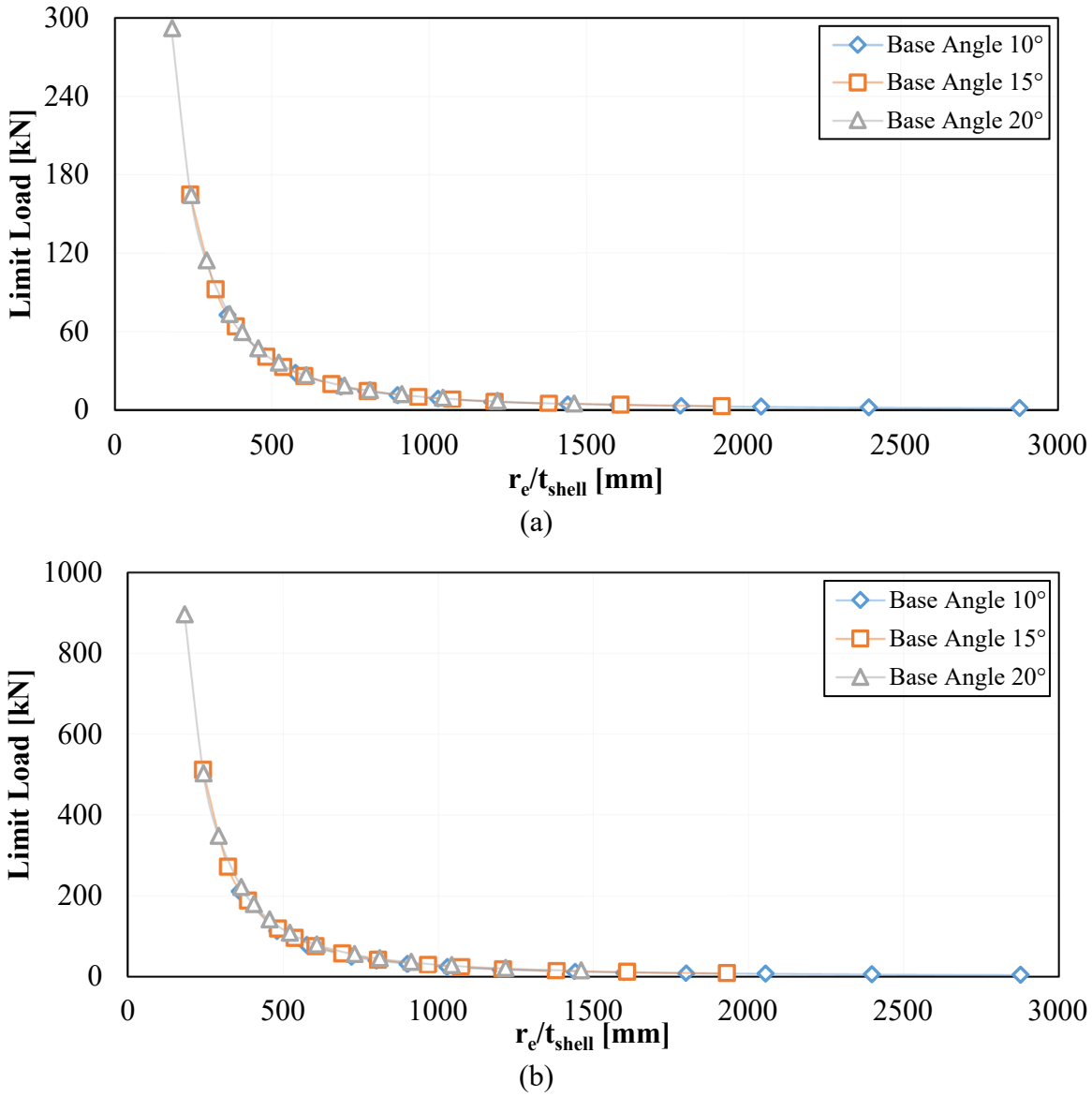

Figure 5.6. Limit loads of the conical shells with the different base angle. (a) Simple supported, (b) Fixed supported.

Figure 5.6 gives the limit load F_{lim} for a different base angle with respect to r_e/t_{shell}. It is interesting that the conical shells with a different base angle on the same r_e/t_{shell} ratio have the approximately same load carrying capacity value. The equivalent radius is derived via Eq. 4.47 for the conical shells. The conical shell which has a smaller base angle than the other one takes greater dimensionless r_e/t_{shell} parameter value, although they have the same shell thickness. If two conical shells have same parameter of r_e/t_{shell}, the conical shell which has smaller base angle must have thicker shell wall. Hence, using the r_e/t_{shell} parameter instead of the shell thickness in the graphs results in a reduction of differences between curves for a various base angle in terms of limit load. Therefore, this dimensionless parameter can be used as a similarity tool.

5.4 Conical Shell with Circumferential Ring

In the previous chapter, relationships and coefficients are mentioned to calculate the load carrying capacity of the simple supported and fixed supported conical shells. These boundary conditions at the lower edge are the representations of the extremities. However, in the practical applications, the conical shell is used with the boundary conditions which are located between two extremities (with a circumferential ring). This part of the study aims to derive simple relationships corresponding to geometrical parameters again. The conical shell is evaluated for the base angle $\propto_c = 10, 15, 20°$. Cross-sectional area of the circumferential ring A_{ring} is kept between $6 \div 300\ \text{mm}^2$.

The following figures are exhibited the limit load depending on r_e/t_{shell} for different circumferential ring stiffnesses. As expected, the curves which belong to various ring cross-sectional areas (different radial stiffness) are positioned between two extremities. It is interesting that the ring area even $A_{ring} = 6\ \text{mm}^2$ contributes significantly positive effect to the load carrying capacity of the conical shell. On the other hand, $A_{ring} = 300\ \text{mm}^2$ provides nearly same contribution with the infinite stiff case. Graphs for three different base angles are seen below (Figure 5.7). In addition to these, the limit load values can be seen in the section of appendices which is found at the end of the study.

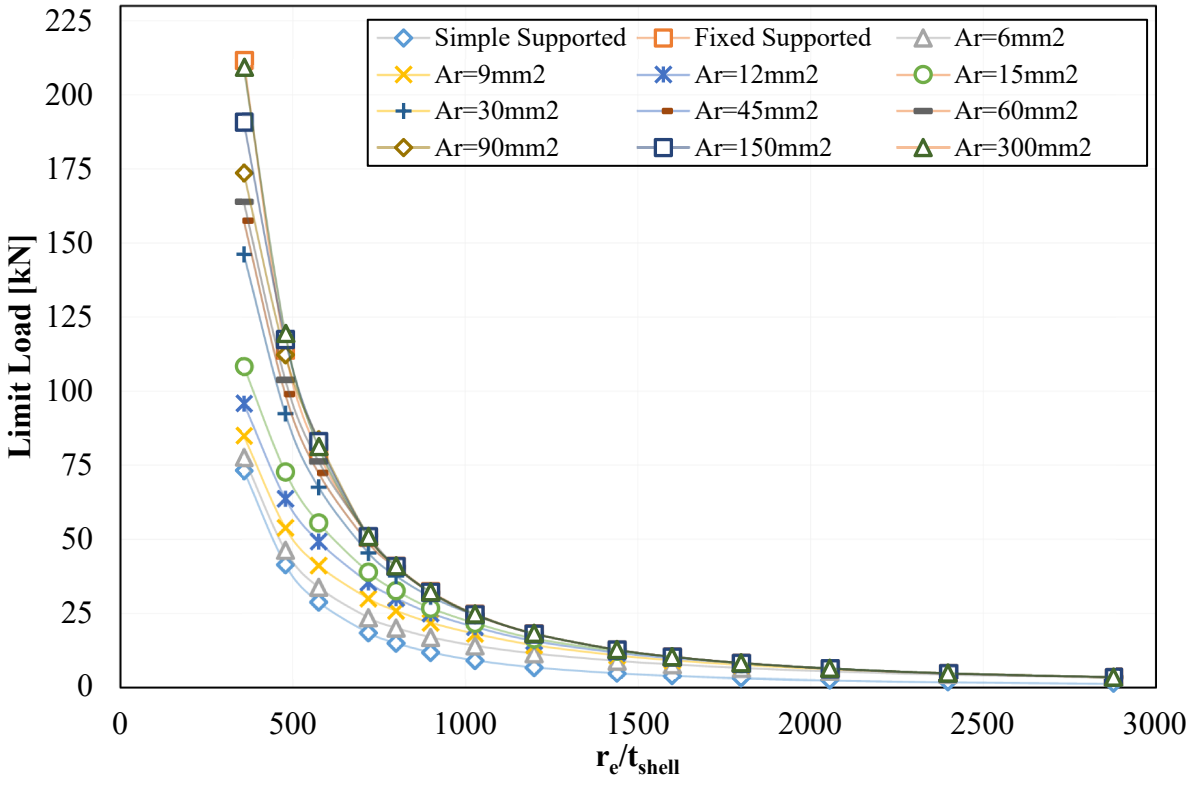

(a)

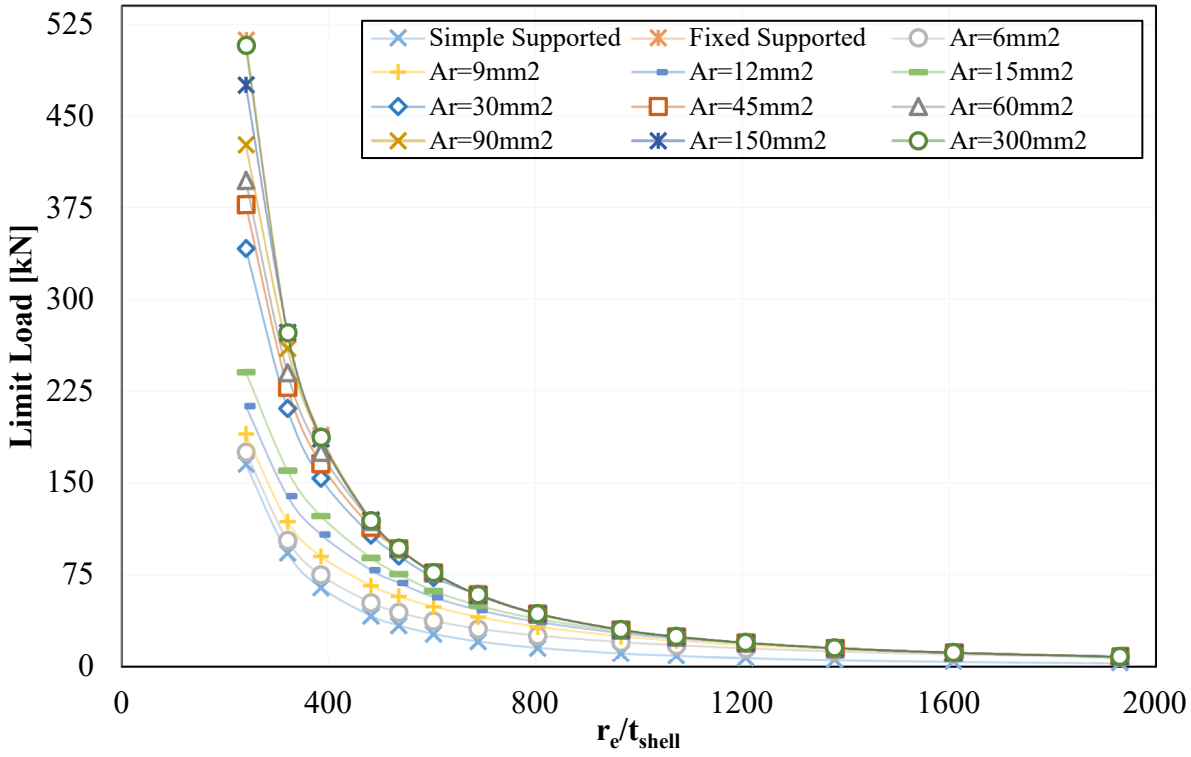

(b)

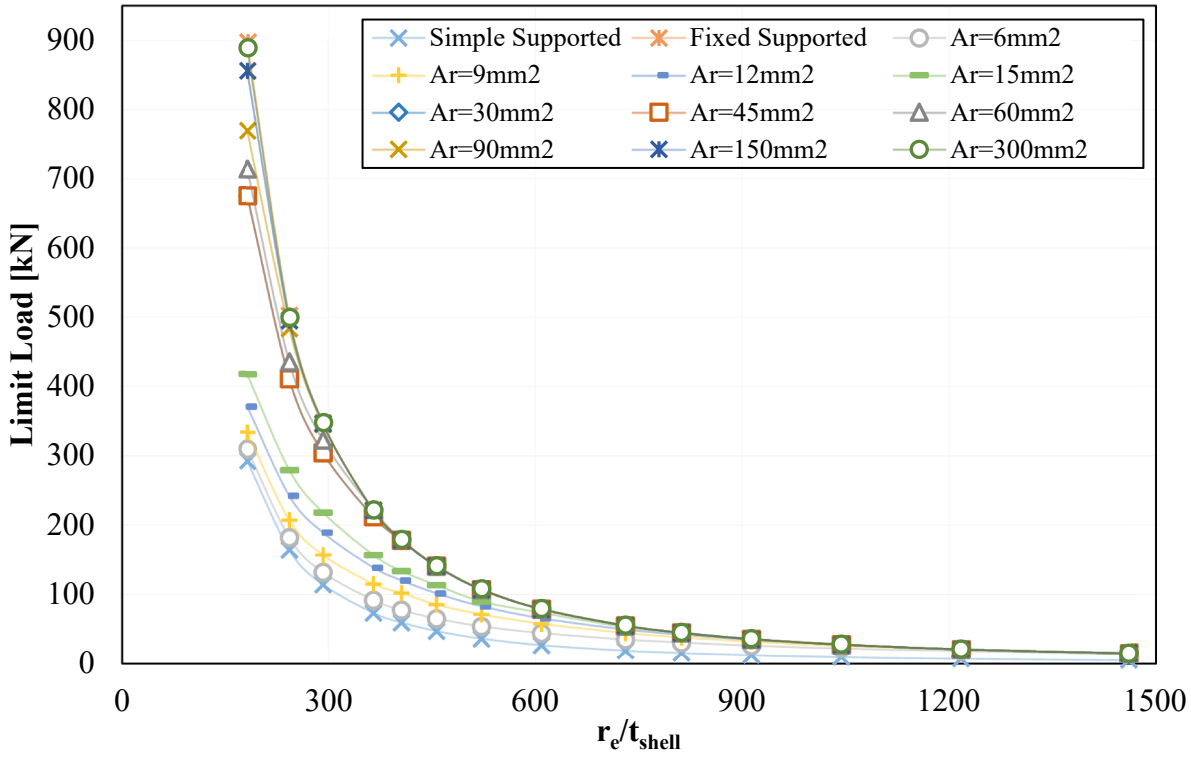

(c)

Figure 5.7. Limit loads of the conical shell for different radial stiffness. (a) Base angle 10°, (b) Base angle 15°, (c) Base angle 20°.

It is apparently seen that the importance of the radial stiffness on the conical shell structures which have a base angle less than 25°, in Figure 5.8. The capability of load carrying can reach three times higher in the comparison between the structures which have a cross-sectional area of the circumferential ring of $A_{ring} = 300\ \text{mm}^2$ and $A_{ring} = 6\ \text{mm}^2$ in the lower r_e/t_{shell} ratios. However, this difference decreases in higher r_e/t_{shell} ratios. This situation is related to the slenderness of the structure. In higher r_e/t_{shell} ratios, the expected limit load is relatively low. Therefore, the circumferential ring with $A_{ring} = 6\ \text{mm}^2$ also behaves stiff enough against the radial displacement until the nonlinear collapse occurs. Hence, the limit loads of the structures with $A_{ring} = 6\ \text{mm}^2$ and $A_{ring} = 300\ \text{mm}^2$ become nearly same in case of quite high amount of r_e/t_{shell} values.

Additionally, the values, which are obtained from analytical formulation based on the linear theory, are illustrated in Figure 5.8. They are notated with "Linear Theory." It is clear that these calculations are quite higher than the limit load values for two different radial stiffness values. This representation shows that the influence of the bending state must be taken into account in nonstandard structure evaluation. Together with this, the change in the geometric stiffness must be considered. It should be pointed out the linear theory assumes there is no radial displacement at the lower edge of the conical shell. The bars show the differences between the critical loads which are calculated analytically and limit loads which are obtained numerically of the conical shell structures. Analytical results give carrying capacity 80% higher than the model which has a circumferential ring with a cross-sectional area of 300 mm^2. Also, they get results up to 400% deviation from the limit load for the model which has a circumferential ring with a cross-sectional area of 6 mm^2. The deviation decreases with higher r_e/t_{shell} ratios. These bars evince that the linear theory approach cannot use for the conical shell structures which have either base angle less than 25° or flexible circumferential ring.

Examined coefficients of regression curves for all the cases are shown in the following table (Table 5.3). Limit load of the conical shells with base angles of 10°, 15°, and 20° can be calculated for different values of the cross-sectional area of the circumferential ring using Eq. 5.1. The parameters K' and m' are derivated via the Least Square method with a feasible regression coefficient.

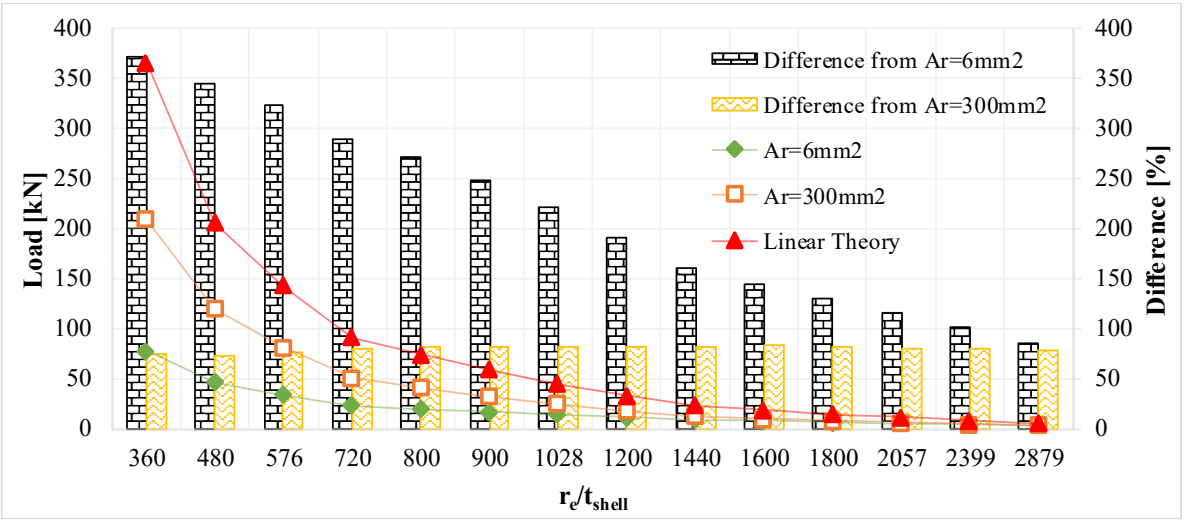

(a)

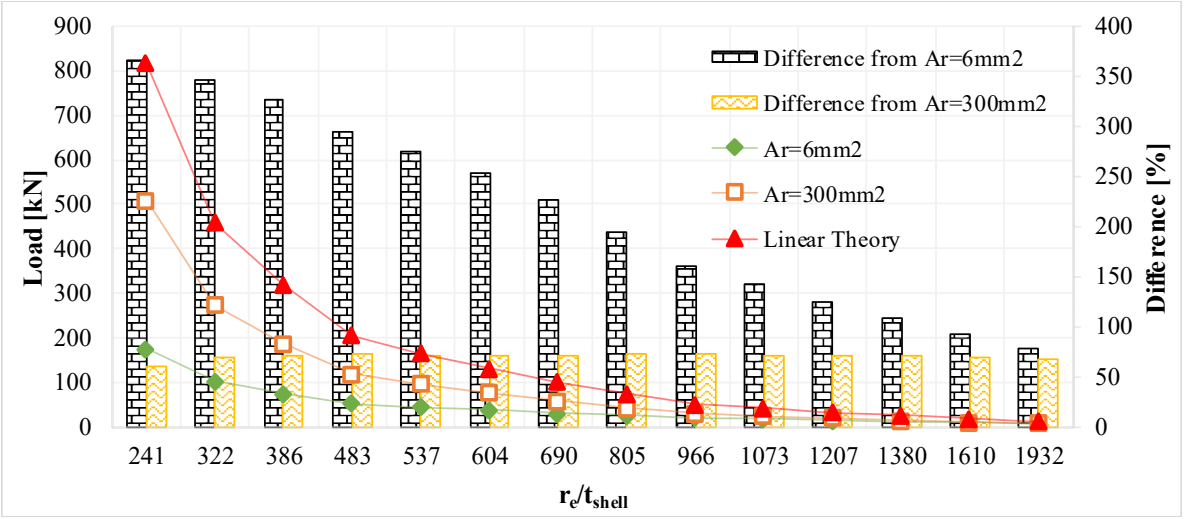

(b)

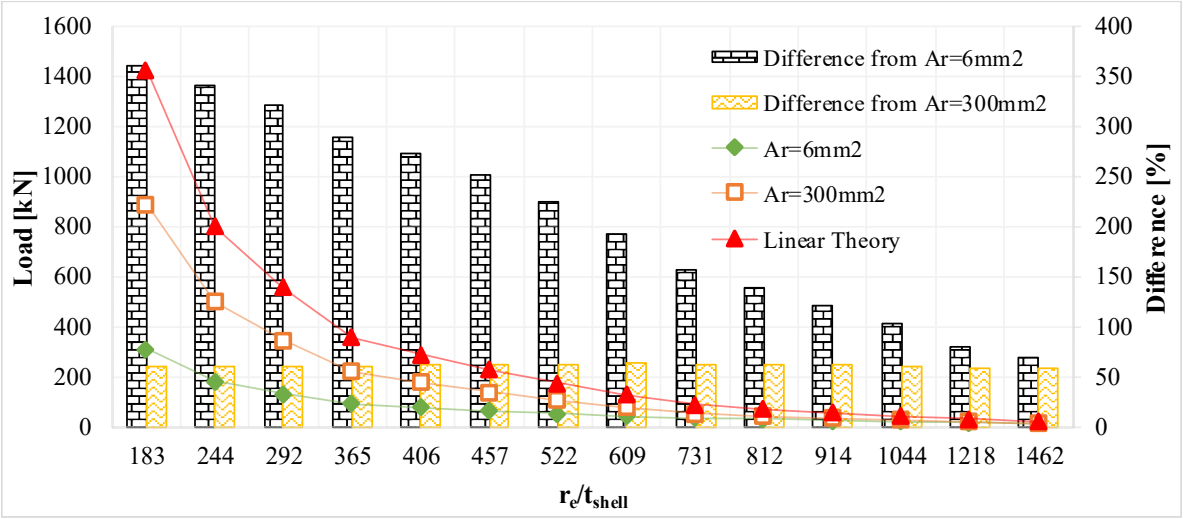

(c)

Figure 5.8. Comparison of the theoretical calculation with the limit loads of A_{ring}=6 mm2 and A_{ring}=300 mm2 cases. (a) Base angle 10°, (b) Base angle 15°, (c) Base angle 20°.

Table 5.3. Coefficients of the regression curves for the conical shell with circumferential ring.

Base Angle $\propto_c$ [°]	Range of r_e/t_{shell} parameter	Cross section area of the ring A_{ring} $[mm^2]$	Coefficients	
			K' [kN]	m'
10	480 - 2880	6	389340	1.473
		9	834171	1.555
		12	$2x10^6$	1.661
		15	$4x10^6$	1.740
		30	$1x10^7$	1.892
		45	$2x10^7$	1.944
		60	$2x10^7$	1.970
		90	$3x10^7$	2.004
		150	$3x10^7$	2.013
		300	$3x10^7$	2.013
15	320 - 1930	6	400795	1.444
		9	702258	1.499
		12	$2x10^6$	1.605
		15	$3x10^6$	1.707
		30	$1x10^7$	1.868
		45	$2x10^7$	1.922
		60	$2x10^7$	1.951
		90	$3x10^7$	1.984
		150	$3x10^7$	1.998
		300	$3x10^7$	1.996
20	240 - 1460	6	411277	1.421
		9	648337	1.460
		12	$1x10^6$	1.565
		15	$3x10^6$	1.655
		30	$2x10^7$	1.909
		45	$2x10^7$	1.909
		60	$2x10^7$	1.944
		90	$3x10^7$	1.983
		150	$3x10^7$	1.989
		300	$3x10^7$	1.996

5.5 Similarity Criteria

The load carrying capacity of the conical shell which has r_1=50 mm and r_2=250 mm is investigated until this part in the present study. The influence of the geometrical parameters on the limit load of the structure is examined separately. But, this section mentions about the derived similarity parameter which is one of the main aim of the study. Thus, the load carrying capacity of many different configurations of the conical shells can be estimated. For instance, a large conical shell which is used under operation can be simulated with a simple model using similarity parameters. In addition to this, the load carrying capacity of the structure can be calculated via Eq. 5.2 and Table 5.7 non-dimensionally without any need of a numerical analysis.

The recommended equation and coefficients in the table are obtained from the numerical analyses outputs. A number of power curves fitted to the FEM results using Least Square method. The normalized load (Eq. 4.59) is a representation of the limit load of the structure non-dimensionally.

The function that is seen in Eq. 5.2 gives results in maximum 15% variation when it is compared to FEM. The normalized load can calculate with this equation using a and b from Table 5.7 corresponding to base angle and rigidity parameter Γ. In addition to this, if the rigidity parameter of the structure is not found in the Table 5.7, linear interpolation is used to get coefficients.

$$F_{Normalized} = a\left({}^{r_e}/_{t_{shell}}\right)^{-b} \qquad \text{Eq. 5.2}$$

The aforementioned non-dimensional similarity parameters are r_e/t_{shell} and Γ. They are calculated as seen below. If these parameters are identical for the same base angle, the normalized loads of these structures are expected to be equal (see Table 5.4, Table 5.5 and Table 5.6).

$$r_e = \frac{r_2}{cos\beta_c}$$

$$\Gamma = \frac{r_2 t_{shell}}{A_{ring}}$$

The numerical analyses results and obtained values from Eq. 5.2 for randomly selected conical shell structures are seen in Table 5.4, Table 5.5 and Table 5.6. The structures which are expected to operate in real applications have different upper and bottom radii.

Table 5.4. FEM and analytical results for the conical shells with base angle 10°

	$\propto_c$ [°]	r_1 [mm]	r_2 [mm]	t_{shell} [mm]	r_e/t_{shell}	Γ	$F_{Normalized}$*10^6 [-] FEM	$F_{Normalized}$*10^6 [-] Analytical (Eq. 5.2)
A_1	10	100	500	5	575.88	20	83.54	86.3
A_2	10	250	500	5	575.88	20	82.80	86.3
A_3	10	300	2000	20	575.88	20	86.81	86.3
A_4	10	800	2000	20	575.88	20	87.53	86.3
A_5	10	700	5000	50	575.88	20	86.95	86.3
A_6	10	2000	5000	50	575.88	20	88.04	86.3

Table 5.5. FEM and analytical results for the conical shells with base angle 15°.

	$\propto_c$ [°]	r_1 [mm]	r_2 [mm]	t_{shell} [mm]	r_e/t_{shell}	Γ	$F_{Normalized}$*10^6 [-] FEM	$F_{Normalized}$*10^6 [-] Analytical (Eq. 5.2)
B_1	15	200	750	3	965.93	5	126.3	112.7
B_2	15	350	750	3	965.93	5	125.5	112.7
B_3	15	600	2500	10	965.93	5	127.1	112.7
B_4	15	1100	2500	10	965.93	5	126.9	112.7
B_5	15	450	4000	16	965.93	5	127.2	112.7
B_6	15	2100	4000	16	965.93	5	128.1	112.7

Table 5.6. FEM and analytical results for the conical shells with base angle 20°.

	$\propto_c$ [°]	r_1 [mm]	r_2 [mm]	t_{shell} [mm]	r_e/t_{shell}	Γ	$F_{Normalized}$*10^6 [-] FEM	$F_{Normalized}$*10^6 [-] Analytical (Eq. 5.2)
C_1	20	175	600	1.5	1169.5	40	92.25	91.41
C_2	20	330	600	1.5	1169.5	40	92.68	91.41
C_3	20	470	1500	3.75	1169.5	40	93.63	91.41
C_4	20	690	1500	3.75	1169.5	40	93.65	91.41
C_5	20	320	3500	8.75	1169.5	40	94.82	91.41
C_6	20	1450	3500	8.75	1169.5	40	95.18	91.41

It is seen that Eq. 5.2 meets with the FEM results, besides, the similarity parameters are well matched. The structures with various geometrical dimensions but same similarity parameters have a similar normalized load.

Table 5.7. Coefficients of the regression curves of the conical shell for different rigidity parameter.

Base Angle $\propto_c$ [°]	Range of r_e/t_{shell} parameter	Rigidity Parameter $\Gamma = \frac{r_2 t_{shell}}{A_{ring}}$	Coefficients	
			a	b
10	480 - 2880	Fixed Supported	0.0696	0.995
		Simple Supported	0.0190	1.001
		1	0.1652	1.067
		5	0.1173	1.066
		10	0.0569	0.987
		20	0.0286	0.913
		40	0.0371	0.957
		60	0.0508	1.015
		80	0.0546	1.044
		100	0.0417	1.015
15	320 - 1930	Fixed Supported	0.1141	0.999
		Simple Supported	0.0289	0.998
		1	0.1697	1.032
		5	0.1320	1.028
		10	0.0814	0.979
		20	0.0424	0.899
		40	0.0515	0.948
		60	0.0700	1.008
		80	0.0730	1.032
		100	0.0614	1.025
20	240 - 1460	Fixed Supported	0.1526	0.991
		Simple Supported	0.0375	0.996
		1	0.2634	1.038
		5	0.2036	1.033
		10	0.1230	0.984
		20	0.0566	0.880
		40	0.0730	0.946
		60	0.0936	1.006
		80	0.0937	1.023
		100	0.0650	0.992

5.6 Influence of Initial Imperfection

When researching thin-walled shell structures, the influence of initial imperfections on the loss of stability cannot be ignored. The membrane stiffness of the shells is much higher than the flexural stiffness. Initial imperfections may cause bringing the structure into bending state at the beginning of loading. The bending state may also arise due to the nature of the structure (e.g. conical shells with a base angle less than 25°). Therefore, the sensitivity of initial imperfection is less pronounced in nonstandard structures than the structures with membrane stress dominantly (e.g. a cylindrical shell).

Initial imperfections may be seen in several types, for example, imperfections in shape, structural attachment, non-uniform loading on the structure, residual stresses, uneven distributions of mechanical properties of the material, etc. One of the most notable imperfection is called initial geometrical imperfection. Initial geometrical imperfections may be caused during manufacturing or transportation of equipment. In some cases, initial imperfections are entirely embedded in the design, intentionally. The purpose of inserting the imperfection is to control the deformation progress of the structure. Controlled deformation of the structure is advantageously used in the design of deformation zones in the transport means [37].

Only the influence of geometrical initial imperfections on the load carrying capacity is investigated in the present study. The recommendation ECCS evaluates the initial geometrical imperfections as follows.

- Out of roundness
- Eccentricities
- Local dimples

Size of the characteristic imperfection amplitude Δw_k is measured using the ruler for measuring of initial geometric imperfections. The rulers are devised to relate to the size of buckles that are expected to form under each of the different basic load cases. The length of the ruler is determined by $l_g = \sqrt{4r_2 t_{shell}}$ in axial loading (Figure 5.9). It should be noted that, appropriate gauge length relationship should be used regarding to the shell geometry [5]. The influence of other geometrical imperfections (out of roundness and eccentricity) is less pronounced therefore, they are not investigated in this study.

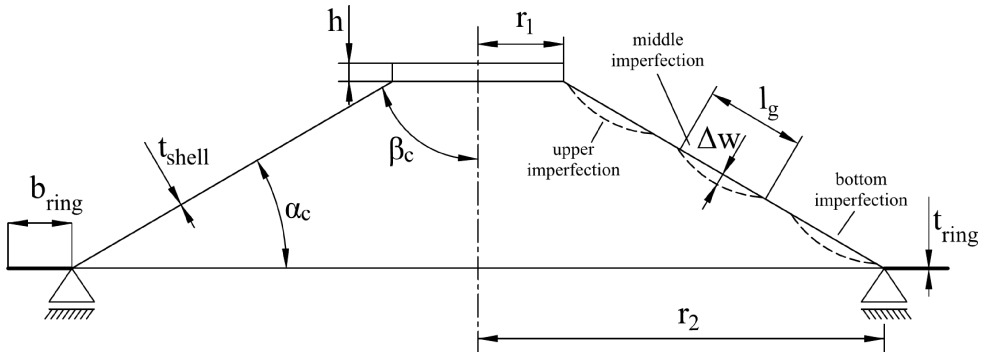

Figure 5.9. Characteristic imperfection amplitude (depth of dimple) and geometrical parameters symbolically.

The characteristic imperfection amplitude, Δw_k expresses the maximum permitted depth of the dimple. Its value depends on the quality of production and the geometrical dimensions of the conical shell.

$$\Delta w_k = \frac{1}{Q_{pr}} \sqrt{\frac{r_e}{t_{shell}}} t_{shell} \qquad \text{Eq. 5.3}$$

where, Q_{pr} is the influence of fabrication quality parameter from Table 4.7.

The maximum allowed characteristic imperfection amplitude is illustrated in Figure 5.10 for each production quality class. It is obviously seen that the maximum allowable depth gets deeper as dimensionless r_e/t_{shell} parameter decreases.

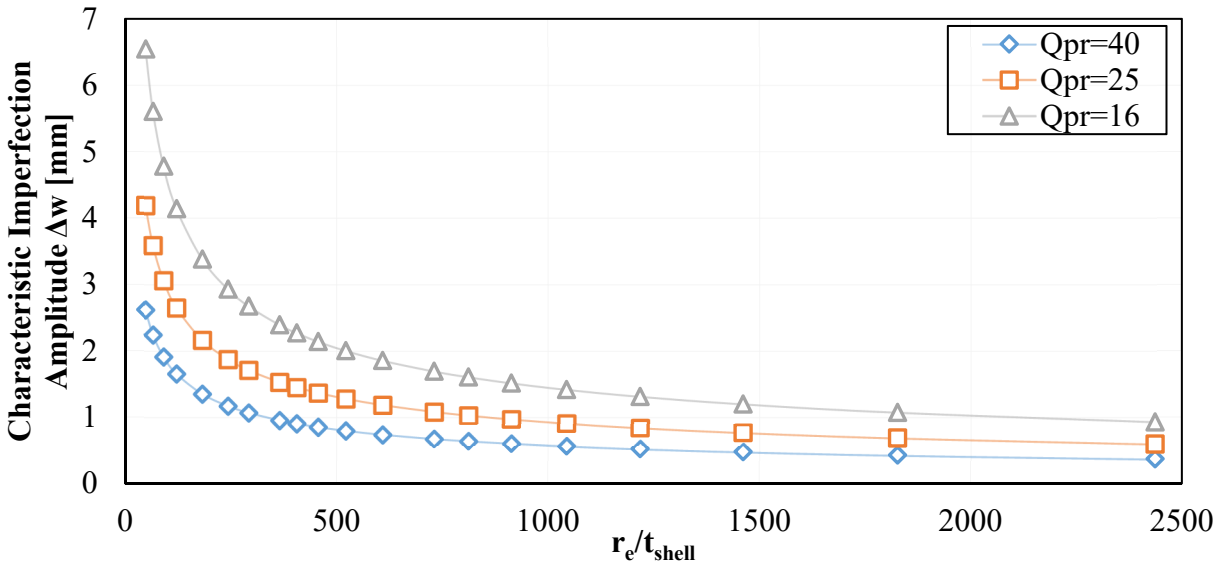

Figure 5.10. The progress of the characteristic imperfection amplitude for each quality class.

The influence of the initial geometric imperfection on the load carrying capacity of the shell structure is expressed by the reduction coefficient α. In order to calculate the reduction coefficient, the ECCS [5] states the relationship as follows,

$$\alpha = \frac{0.62}{1 + 1.91(\Delta w_k / t_{shell})^{1.44}} \qquad \text{Eq. 5.4}$$

where

Δw_k is the characteristic imperfection amplitude.

Changing of the reduction coefficient α is shown in Figure 5.11 depending on r_e/t_{shell}. The figure apparently shows that the structure with higher r_e/t_{shell} parameter is more sensitive to initial geometrical imperfection where the reduction coefficient α decreases.

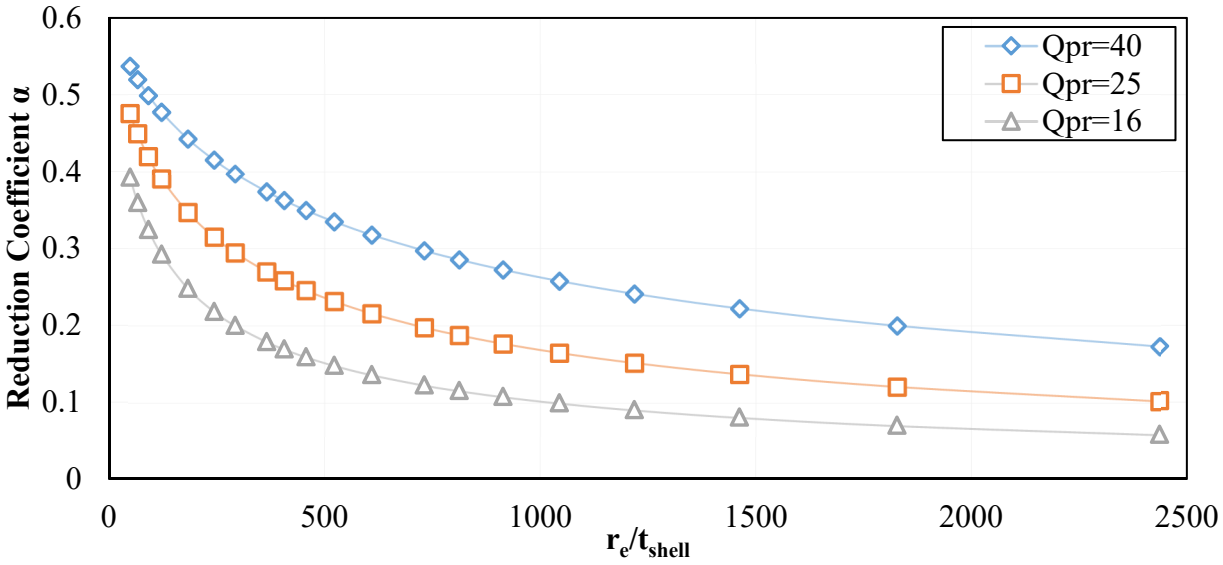

Figure 5.11. The change of the reduction coefficient.

The reduction coefficient is presented in the ECCS for a fixed supported conical shell (infinite radial stiffness) under axial loading. The bending effect is higher for simple supported conical shell than a fixed supported conical shell. Therefore, it can be assumed that the reduction coefficient specified in the ECCS is too conservative for the simple supported structure. For this reason, it is important to determine the dependence of the reduction coefficient on the radial stiffness of the conical shell.

5.6.1 Assessment of the location of the initial geometrical imperfection on the loss of stability

This chapter aims to determine imperfection location effect on the loss of stability of the conical shell. It is expected to see the most sensitive location is middle of the lateral face for an ideal conical shell under axial loading (i.e. without any imperfections). Therefore, it is possible to assume the imperfection that is in this area will have the greatest influence on the load carrying capacity. Despite this assumption, the influence of the imperfection location on the load carrying capacity of the conical shell should be investigated.

Three various locations of the initial geometrical imperfection are compared. The imperfections are located in the middle, upper, and bottom sides of the lateral surface of the structure (Figure 5.9). Influence of imperfections is evaluated using numerical analyzes of the GNIA and GNA types. Material model is considered as linear and elastic. Randomly selected two conical shells with radius $r_2 = 250$ mm are considered (see Table 5.8 and Table 5.9). The influence of the initial imperfection on the load carrying capacity of the conical shell is expressed by the α.

$$\alpha = \frac{F_{GNIA}}{F_{GNA}} \qquad \text{Eq. 5.5}$$

where

F_{GNIA} is limit load of a conical shell structure which contains initial imperfection.

F_{GNA} is limit load of an ideal conical shell structure.

Table 5.8. Reduction coefficients of the conical shell with imperfection, t_{shell}=0.6 mm.

t_{shell} [mm]	Γ	α_c [°]	Δw [mm]	Δw/ t_{shell}	l_g	Imperfection Position	α (F_{GNIA}/F_{GNA})
0.6	5	15	1.629	2.715	49	Middle	0.944
						Upper	0.976
						Bottom	0.983

Table 5.9. Reduction coefficients of the conical shell with imperfection, t_{shell}=3.0 mm.

t_{shell} [mm]	Γ	α_c [°]	Δw [mm]	Δw/ t_{shell}	l_g	Imperfection Position	α (F_{GNIA}/F_{GNA})
3	10	15	1.629	0.543	109.5	Middle	0.793
						Upper	0.824
						Bottom	0.834

Table 5.8 and Table 5.9 suggest that the conical shells with a circumferential ring are more sensitive to imperfections that are in the middle of the wall. Hence, the dimples are positioned to the middle region of the wall surface to simulate initial geometric imperfection hereinafter in the study.

5.6.2 Numerical modeling of the conical shell with a local dimple

An initial imperfection is formed as a dimple on the central region of the conical shell's wall in the numerical model. The dimple is created by a static analysis. The whole area of the structure except the dimple is fixed and an external pressure value is applied to only the area of the dimple. The appropriate pressure value is chosen to create predetermined imperfection depth Δw. The numerical model with an initial geometrical imperfection as a result of this static analysis is shown in Figure 5.12.

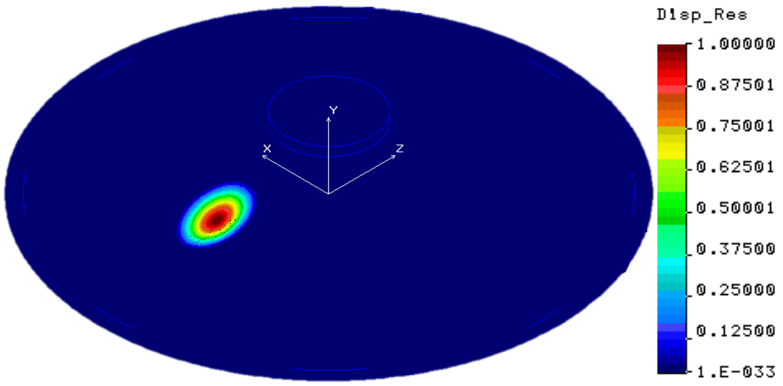

Figure 5.12. A numerical model with initial imperfection.

The deformed geometry is stored and the following numerical analysis of the GNIA type takes place on the modified model. The model consists of a base angle $\alpha_c = 20°$, shell thickness $t_{shell} = 0.6$ mm, cross-sectional area of the circumferential ring $A_{ring} = 150$ mm^2, and depth of the dimple $\Delta w = 1$ mm. The circumferential ring is constrained against only to vertical direction and an axial load is applied to the numerical model. To control iterative process, arc-length computational procedure is used. Figure 5.13 shows a deformed numerical model after loss of stability for conical shell which includes initial geometric imperfection. Six pieces of buckles occurs and the largest one is observed around the imperfection.

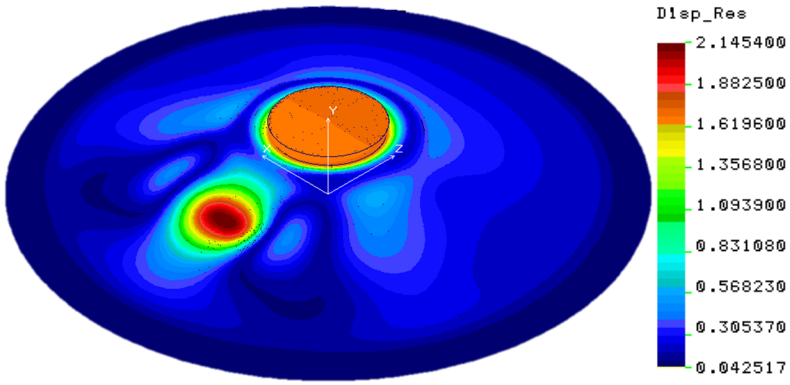

Figure 5.13. Result of GNIA analysis - resultant displacement.

Table 5.10 shows the results of numerical analyzes of the conical shells with a base angle of $\alpha_c = 15°$, shell thickness $t_{shell} = 1.4$ mm, and several radial stiffnesses.

Table 5.10. Reduction coefficients of conical shells with base angle α_c = 15°, radius of lower edge r_2=250 mm, shell thickness t_{shell}=1.4 mm, and various types of boundary conditions (zero to infinite radial stiffness).

Δw [mm] / Γ	0.153	0.307	0.537	0.767	1.073	1.380	1.840	2.300
5	0.984	0.977	0.934	0.912	0.913	0.915	0.902	0.927
10	0.998	0.999	0.810	0.797	0.790	0.790	0.791	0.788
25	0.884	0.883	0.879	0.826	0.778	0.796	0.823	0.820
60	0.947	0.992	0.991	0.929	0.941	0.993	0.816	0.817
100	0.987	0.987	0.987	0.988	0.998	0.998	0.999	0.990
Simple Supported	0.975	0.976	0.976	0.977	0.977	0.977	0.978	0.978
Fixed Supported	0.988	0.983	0.969	0.960	0.958	0.964	0.975	0.983

It is necessary to evaluate how the value of the reduction coefficient varies regarding the depth of imperfection. When creating numerical models with different depths of the imperfection, the pressure applied to the surface of the dimple is changed. Table 5.10 shows one of the calculated cases. The depth of imperfection varies with $\Delta w = 0.153 - 2.3$ mm.

The maximum reference length and depth of imperfection are dependent on shell thickness, radius, and production quality according to ECCS. Therefore, the values of the reduction coefficient given in the table above are only indicative. However, there is one critical point to be drawn from the results. The reduction coefficient does not drop below $\alpha = 0.70$ for different combinations of shell thickness and radial stiffness (see Figure 5.15).

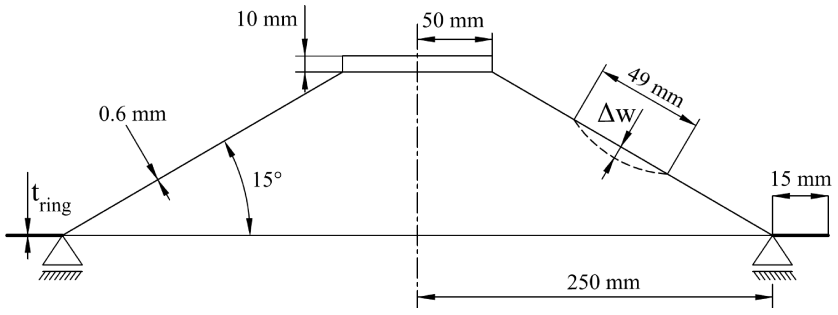

(a)

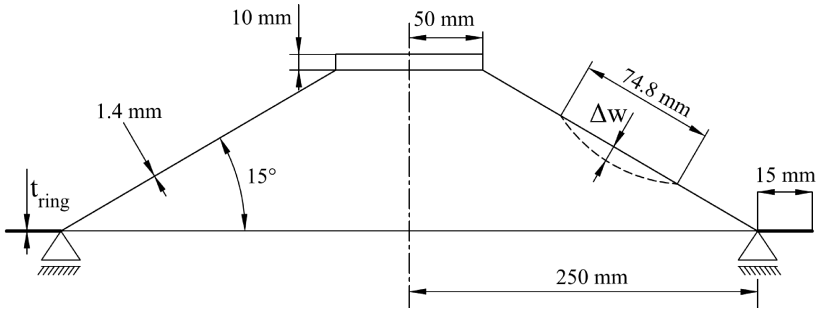

(b)

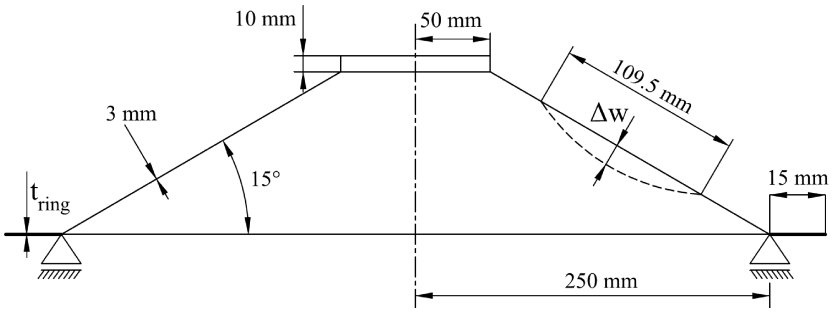

(c)

Figure 5.14. Schematic illustrations of the conical shells with a base angle 15° and shell thicknesses. (a) 0.6 mm, (b) 1.4 mm, and (c) 3 mm.

Figure 5.15 shows the dependence of reduction coefficient on the depth of imperfection Δ*w* for three different wall thicknesses. Schematic illustrations can be seen in the Figure 5.14 for these three conical shells that are performed in the numerical analyzes.

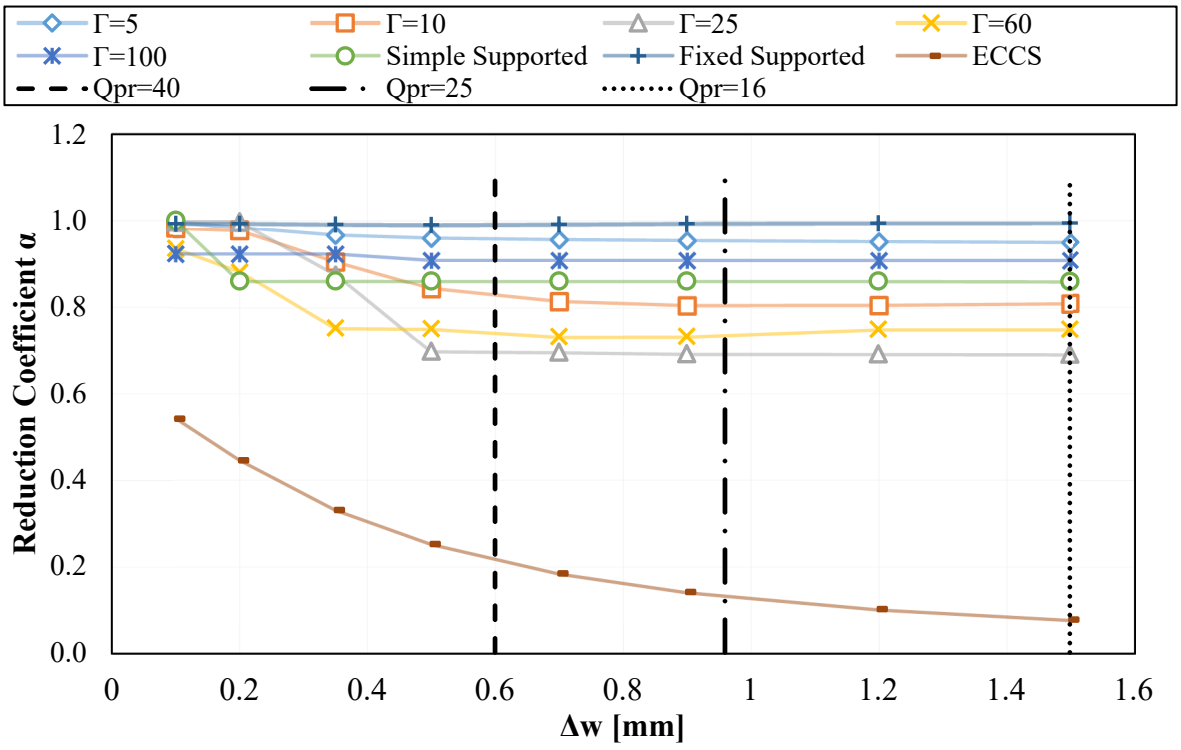

(a)

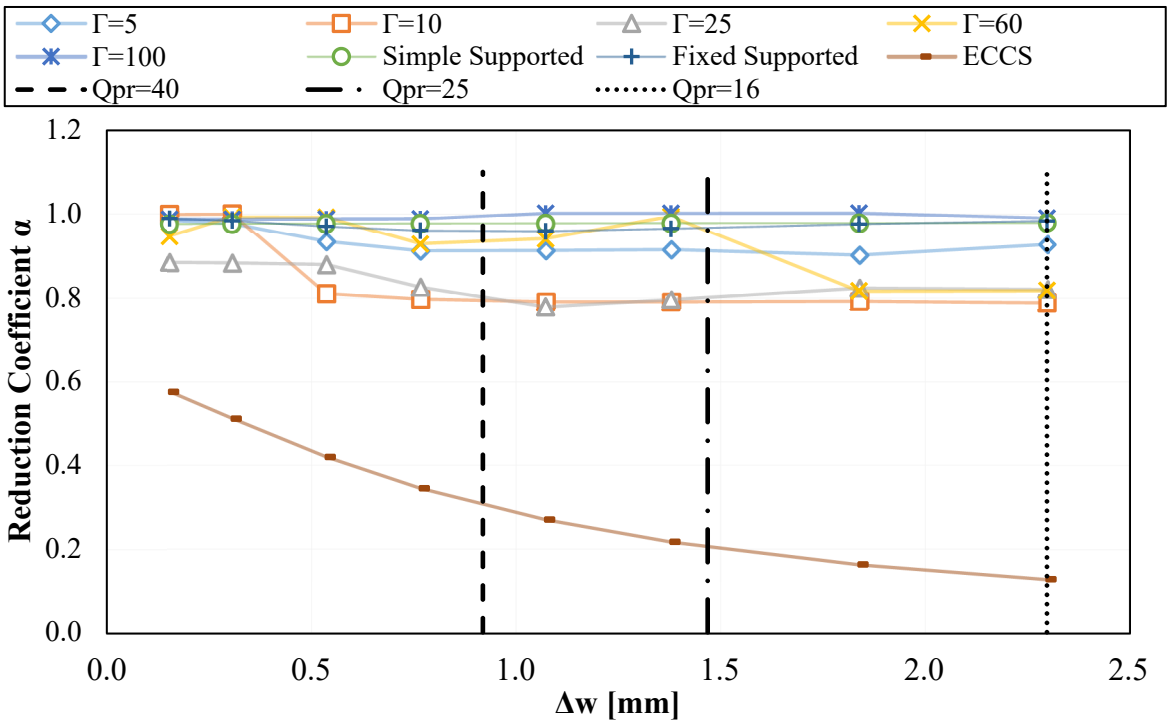

(b)

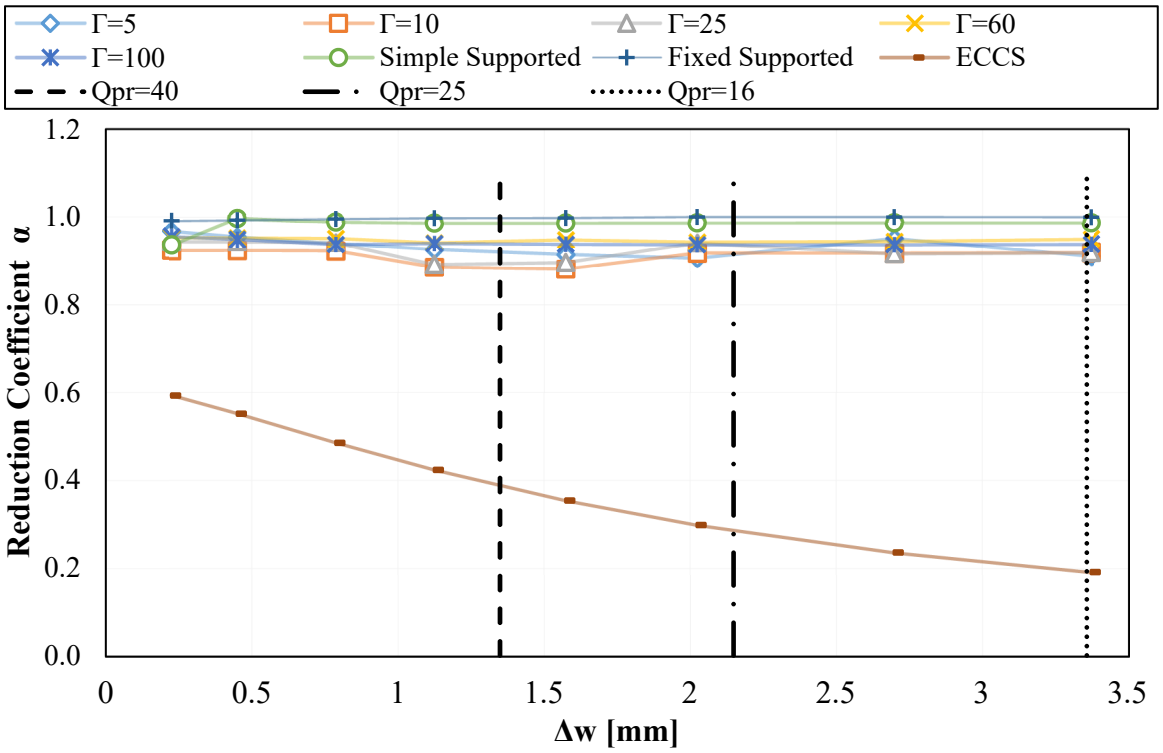

(c)

Figure 5.15. Reduction coefficient for different configuration of conical shells with a base angle 15°. (a) t_{shell} = 0.6 mm, (b) t_{shell} = 1.4 mm, and (c) t_{shell} = 3 mm.

The production quality classes (Table 4.7) and their respective reduction coefficients according to recommendation [5] are illustrated in the graphs (vertical lines nominated with Q_{pr}). Those lines also show the maximum permissible depth of the imperfection. The reduction coefficient values that obtained from ECCS are too conservative for conical shells even for the quality class A. Hence, this value could be replaced by $\alpha = 0.70$.

It is also interesting to see from the curves in Figure 5.15 that the increment in the depth of imperfection can result in a reduction of its effect on the load carrying capacity. The reduction coefficient may tend to increase after a point in some cases. In those cases, the dimple starts to act as a stiffener.

According to the European Recommendation, the value of the reduction coefficient for conical shells under axial loading is calculated using Eq. 4.64. The proposed calculation methodology by ECCS to estimate load carrying capacity of the conical shells is originated from the cylindrical shells. In contrast to the cylindrical shells, the conical shells have a significant bending stress. Therefore, the influence of initial imperfections, which represents an additional bending effect, is less significant in conical shells with base angle is lower than 25°. From this point of view, it can be assumed that the reduction coefficient that is determined based on the cylindrical shell is considerably conservative for conical shells. The reduction coefficient does not drop below $\alpha = 0.70$ for different combinations of shell thickness and radial stiffness. Thus, the new value of the reduction coefficient is determined in this chapter as a constant value of $\alpha = 0.70$.

6 COMPARISON OF CALCULATION METHODS

The load carrying capacity estimations for the conical shells are compared in this chapter. Obtained results from the ECCS recommendations, the proposed method in the present study and the numerical analyzes are examined. The load carrying capacity values of the conical shells with diverse types of boundary conditions are considered. Influence of the initial imperfections is taken into account using the reduction coefficient that is proposed as α=0.70 in Section 5.6.

6.1 Fixed supported conical shells

The dimensions of the conical shell are shown in Table 6.1. The geometry of the cylinder, which originates from the geometry of the conical shell, falls within the area of medium length cylindrical shells (Table 4.8). For this reason, the influence of boundary conditions, which is expressed by the C_x factor, assigned to 1. According to the relationships in Section 4.5, it is assumed that the loss of stability occurs in the elastic region for the randomly selected conical shells. Therefore, the effect of the elastic-plastic behavior of the material is not applied for the solutions. The reduction coefficient is determined according to the ECCS recommendation by a_x (Eq. 4.64). In this study, a new value of the reduction coefficient is proposed as $a = 0.70$. (for reasons of clarity, the reduction coefficients are indicated with the corresponding indices as a_{NM} and a_{ECCS} in the following sections).

Table 6.1. Fixed supported conical shell dimensions.

a_c[°]	r_1[mm]	r_2[mm]	t_{shell}[mm]	r_e[mm]	r_e/t_{shell}[-]	C_x[-]	a_{ECCS}[-]	a_{NM}[-]
10	200	600	2	3455	1728	1	0.21	0.7

Calculation according to ECCS

The solution procedure is described in Section 4.5. Critical elastic stress for the conical shell is expressed by the relation,

$$\sigma_{xRcr} = 0.605EC_x\frac{t_{shell}}{r_e} = 0.605x2E5x1x\frac{2}{3455} = 70[MPa]$$

Characteristic imperfection depth for production quality class A and the reduction coefficient are determined as follows,

$$\Delta w_k = \frac{1}{Q_{pr}}\sqrt{\frac{r_e}{t_{shell}}}t_{shell} = \frac{1}{40}\sqrt{\frac{3455}{2}}2 = 2.08\ [mm]$$

$$\alpha_{ECCS} = \frac{0.62}{1 + 1.91(\Delta w_k/t_{shell})^{1.44}} = \frac{0.62}{1 + 1.91(2.08/2)^{1.44}} = 0.21$$

The factor C_x is determined using Table 4.8 from the relationship for a medium length cylindrical shell regarding to the dimensionless length parameter ω.

$$\omega = \frac{l_e}{\sqrt{r_e t_{shell}}}$$

It is assumed that the loss of stability will occur for this conical shell structure in the elastic area (see Table 4.5, i.e. $\lambda_x \geq \lambda_p$). The characteristic buckling stress is given by the relation,

$$\sigma_{xRk} = \chi_x f_{y,k} = \frac{\alpha}{\lambda_x^2} f_{y,k} = \alpha_{ECCS}\sigma_{xRcr} = 0.21x70 = 14.7\ [MPa]$$

Limit load is calculated with Eq. 4.48 for the conical shell,

$$F_{lim,ECCS} = 2\pi r_e t_{shell}\sigma_{xRk}cos^2\beta_c = 2x\pi x3455x2x14.7xcos^2(80) = 19245[N]$$

then if the limit load is normalized using geometrical parameters and modulus of elasticity,

$$F_{Normalized,ECCS} = \frac{F_{lim,ECCS}}{2\pi r_2 t_{shell}E} = \frac{19245}{2x\pi x600x2x2E5} = 12.76x10^{-6}\ [-]$$

GNA type numerical analysis

Load carrying capacity of the conical shell with dimensions of Table 6.1 obtained using GNA type numerical analysis. The numerical result is seen below. The influence of initial imperfections is taken into account by means of the proposed reduction coefficient value α_{NM}=0.70.

$$F_{lim,GNA} = 68171.5\ [N]$$

when the effect of initial imperfections is considered the limit load decreases to $F_{lim,GNA,\alpha}$,

$$F_{lim,GNA,\alpha} = \alpha_{NM}F_{lim,GNA} = 0.70x68171.5 = 47720\ [N]$$

and it is normalized,

$$F_{Normalized,GNA,\alpha} = \frac{F_{lim,GNA,\alpha}}{2\pi r_2 t_{shell}E} = \frac{47720}{2x\pi x600x2x2E5} = 31.64x10^{-6}\ [-]$$

Proposed method

The proposed method calculates the load carrying capacity by means of Eq. 5.2 as given below,

$$F_{Normalized} = a\left({}^{r_e}/_{t_{shell}}\right)^{-b}$$

The coefficients of the regression curve of the fixed supported conical shell are shown in Table 5.7.

Table 6.2. Regression curve coefficients

a	b
0.0696	0.995

$$F_{Normalized} = a\left({}^{r_e}/_{t_{shell}}\right)^{-b} = 0.0696\left({}^{3455}/_{2}\right)^{-0.995} = 41.82x10^{-6}\ [-]$$

and the effect of initial imperfections reduces the calculated value using reduction coefficient α_{NM},

$$F_{Normalized,\alpha} = \alpha_{NM} F_{Normalized} = 0.70x41.82x10^{-6} = 29.28x10^{-6}\ [-]$$

Comparison of the results

A summary of the previous results is shown in Table 6.3.

Table 6.3. Comparison of results for the fixed supported conical shell.

Fixed Supported Conical Shell	ECCS	GNA Analysis	Proposed Method
$F_{Normalized}$*10^6 [-]	12.76	31.64	29.28

The value of the reduction coefficient α_{ECCS} is relatively low in the calculation of ECCS. Thus, the calculation with respect to ECCS is quite conservative in the case of the fixed supported conical shell.

6.2 Simple supported conical shell

The results of the load carrying capacity of a simple supported conical shell with the dimensions given in Table 6.4 are compared in this section.

Table 6.4. Simple supported conical shell dimensions.

a_c[°]	r_1[mm]	r_2[mm]	t_{shell}[mm]	r_e[mm]	r_e/t_{shell}[-]	C_x[-]	a_{ECCS}[-]	a_{NM}[-]
15	150	400	4	1545	386.4	1	0.264	0.7

Calculation according to ECCS

$$\sigma_{xRcr} = 0.605EC_x\frac{t_{shell}}{r_e} = 0.605x2E5x1x\frac{4}{1545} = 313[MPa]$$

Characteristic imperfection depth for production quality class B and the elastic imperfection reduction coefficient are determined as follows,

$$\Delta w_k = \frac{1}{Q_{pr}}\sqrt{\frac{r_e}{t_{shell}}}t_{shell} = \frac{1}{25}\sqrt{\frac{1545}{4}}4 = 3.145\ [mm]$$

$$\alpha_{ECCS} = \frac{0.62}{1 + 1.91(\Delta w_k/t_{shell})^{1.44}} = \frac{0.62}{1 + 1.91(3.145/4)^{1.44}} = 0.264$$

The factor C_x is determined regarding to dimensionless length parameter ω from Table 4.8. Since, the assumption is the loss of stability occurs in the elastic area for this example (see Table 4.5, i.e. $\lambda_x \geq \lambda_p$), the characteristic buckling stress can be written as seen below,

$$\sigma_{xRk} = \chi_x f_{y,k} = \frac{\alpha}{\lambda_x^2} f_{y,k} = \alpha_{ECCS}\sigma_{xRcr} = 0.264x313 = 82.6\ [MPa]$$

Limit load is calculated using Eq. 4.48 for the conical shell,

$F_{lim,ECCS} = 2\pi r_e t_{shell} \sigma_{xRk} cos^2\beta_c = 2x\pi x1545x2x82.6xcos^2(75) = 107426[N]$

when it is normalized,

$$F_{Normalized,ECCS} = \frac{F_{lim,ECCS}}{2\pi r_2 t_{shell} E} = \frac{107426}{2x\pi x400x4x2E5} = 106.8x10^{-6}\ [-]$$

GNA type numerical analysis

The limit load is computed via GNA type numerical analysis for the conical shell with the dimensions stated in Table 6.4. The result is given below,

$F_{lim,GNA} = 160323\ [N]$

when initial imperfection is considered, the limit load reduces to,

$F_{lim,GNA,\alpha} = \alpha_{NM} F_{lim,GNA} = 0.70x160323 = 112226\ [N]$

and it is normalized,

$$F_{Normalized,GNA,\alpha} = \frac{F_{lim,GNA,\alpha}}{2\pi r_2 t_{shell} E} = \frac{112226}{2x\pi x400x4x2E5} = 55.82x10^{-6}\ [-]$$

Proposed method

The proposed method calculates the load carrying capacity by means of the Eq. 5.2 as given below,

$$F_{Normalized} = a\left({}^{r_e}/_{t_{shell}}\right)^{-b}$$

The coefficients of the regression curve of the simple supported conical shells are shown in Table 5.7.

Table 6.5. Regression curve coefficients.

a	b
0.0289	0.998

$$F_{Normalized,\alpha} = a\left({}^{r_e}/_{t_{shell}}\right)^{-b} = 0.0289\left({}^{1545}/_{4}\right)^{-0.998} = 75.71x10^{-6}\ [-]$$

and the effect of initial geometrical imperfections leads to a reduction in the calculated value using the reduction coefficient of α_{NM},

$F_{Normalized,\alpha} = \alpha_{NM} F_{Normalized} = 0.70x75.71x10^{-6} = 52.99x10^{-6}\ [-]$

Comparison of the results

A summary of the previous results is shown in Table 6.6.

Table 6.6. Comparison of results for the simple supported conical shell.

Simple Supported Conical Shell	ECCS	GNA Analysis	Proposed Method
$F_{Normalized}$*10^6 [-]	106.8	55.82	52.99

The ECCS estimates the load carrying capacity of this structure relatively higher than the numerical analysis and proposed method. The reason of this case can be explained with the calculation methodology of the ECCS. The methodology assumes the structure has infinite radial stiffness. Since a simple supported conical shell structure is considered, the assumption of the ECCS is not suitable in this case. Nevertheless, the proposed method in the present study is well matched with the result of GNA type numerical analysis.

6.3 Conical shells with a circumferential ring

The results of a conical shell which has a circumferential ring with the dimensions given in Table 6.7 are compared in this section.

Table 6.7. Dimensions of the conical shell with a circumferential ring.

a_c[°]	r_1[mm]	r_2[mm]	t_{shell}[mm]	r_e[mm]	r_e/t_{shell}[-]	C_x[-]	a_{ECCS}[-]	a_{NM}[-]	Γ [-]
20	100	800	2.8	2339	835.4	1	0.1132	0.7	5

Calculation according to ECCS

The factor C_x is determined regarding to dimensionless length parameter ω from Table 4.8.

$$\sigma_{xRcr} = 0.605EC_x\frac{t_{shell}}{r_e} = 0.605x2E5x1x\frac{2.8}{2339} = 144.8[MPa]$$

Characteristic imperfection depth for production quality class C and the reduction coefficient are calculated as follows,

$$\Delta w_k = \frac{1}{Q_{pr}}\sqrt{\frac{r_e}{t_{shell}}}t_{shell} = \frac{1}{16}\sqrt{\frac{2339}{2.8}}2.8 = 5.06\ [mm]$$

$$\alpha_{ECCS} = \frac{0.62}{1 + 1.91(\Delta w_k/t_{shell})^{1.44}} = \frac{0.62}{1 + 1.91(5.06/2.8)^{1.44}} = 0.1132$$

For the case of $\lambda_x \geq \lambda_p$, the characteristic buckling stress is calculated as follows,

$$\sigma_{xRk} = \chi_x f_{y,k} = \frac{\alpha}{\lambda_x^2}\ f_{y,k} = \alpha_{ECCS}\sigma_{xRcr} = 0.1132x144.8 = 16.4\ [MPa]$$

Limit load is calculated for the conical shell,

$$F_{lim,ECCS} = 2\pi r_e t_{shell}\sigma_{xRk}cos^2\beta_c = 2x\pi x2339x2.8x16.4xcos^2(70) = 78943[N]$$

Then this load is normalized,

$$F_{Normalized,ECCS} = \frac{F_{lim,ECCS}}{2\pi r_2 t_{shell} E} = \frac{78943}{2x\pi x800x2.8x2E5} = 28.05x10^{-6}\ [-]$$

GNA type numerical analysis

The result that is obtained from GNA type numerical analysis is,

$F_{lim,GNA} = 515433\ [N]$

$F_{lim,GNA,\alpha} = \alpha_{NM} F_{lim,GNA} = 0.70x515433 = 360803\ [N]$

and

$$F_{Normalized,GNA,\alpha} = \frac{F_{lim,GNA,\alpha}}{2\pi r_2 t_{shell} E} = \frac{360803}{2x\pi x800x2.8x2E5} = 128.2x10^{-6}\ [-]$$

Proposed method

The proposed method calculates the load carrying capacity by means of the Eq. 5.2 as given below,

$$F_{Normalized} = a\left({}^{r_e}/_{t_{shell}}\right)^{-b}$$

The coefficients of the regression curve of the fixed conical shells are shown in Table 5.7. Linear interpolation is used to get coefficients if the certain value of Γ is not found in Table 5.7.

Table 6.8. Regression curve coefficients.

a	b
0.2036	1.033

$$F_{Normalized,\alpha} = a\left({}^{r_e}/_{t_{shell}}\right)^{-b} = 0.2036\left({}^{2339}/_{2.8}\right)^{-1.033} = 195.2x10^{-6}\ [-]$$

To consider initial imperfections, the reduction coefficient α_{NM} is used,

$F_{Normalized,\alpha} = \alpha_{NM} F_{Normalized} = 0.70x195.2x10^{-6} = 136.6x10^{-6}\ [-]$

Comparison of the results

A summary of the previous results is shown in Table 6.9.

Table 6.9. Comparison of the results for the conical shell with a circumferential ring.

Conical Shell with Circumferential Ring	**ECCS**	**GNA Analysis**	**Proposed Method**
$\boldsymbol{F_{Normalized}*10^6}$ **[-]**	28.05	128.2	136.6

The calculation of ECCS is quite conservative in the case of the conical shell with the circumferential ring. It is due to the value of the elastic imperfection reduction coefficient α_{ECCS}. On the other hand, the result of the proposed method is well matched with the results of the numerical analysis.

According to ECCS, if the conical shell stays in the elastic region regarding its geometry, the material nonlinearity does not affect to load carrying capacity. In the elastic region, the value of load carrying capacity is multiplied by the elastic imperfection reduction coefficient, α. The effect of nonlinear material behavior is not considered. Nevertheless, the influence of the material nonlinearity could arise especially in the relatively low dimensionless parameter of r_e/t_{shell} (see Figure 4.18). In this case, the proposed method may overestimate the load carrying capacity. The influence of the material nonlinearity is described in the ECCS for cylindrical shells in terms of $\alpha, \beta, \lambda,$ and η (see Table 4.5). It is suggested that the determination of the boundaries of the plastic and elastic-plastic region for the conical shells under axial loading should be investigated in further studies. It is out the scope of this study.

7 CONCLUSION

In this study, the load carrying capacity of the conical shell structures which have different radial stiffnesses is examined. The base angle of the conical shell structures is kept less than 25° to contribute to filling the deficiency in the literature. A new method is proposed to estimate the load carrying capacity for mentioned conical shell structures. Results which are obtained from the nonlinear FEM analyses are stated below.

In order to predict load carrying capacity of the conical shell structures under the axial load with lower base angles (i.e. 10, 15 and 20°), normalized design parameters (Γ and r_e/t_{shell}) are derived. Based on these parameters, a similarity approach is proposed which estimates load carrying capacity of the shells of different shell geometry configurations at the same base angle. This similarity approach tells that the two different shell configurations having the same Γ, r_e/t_{shell} and base angle have the same normalized loads. Practically, this provides an enormous advantage of estimating load carrying capacity of the conical shells from small to large structures. Therefore, there is no need to perform some series of the experiments to determine the load carrying capacity of the structures.

A simple expression is proposed to calculate the normalized load of the conical shell structure as a function of the dimensionless geometrical shell parameters and two constant coefficients of "a" and "b" which are selected considering the base angle, rigidity parameter, and range of the r_e/t_{shell} values of the given intervals from Table 5.7. In this way, it enables an appropriate prediction of the load carrying capacity of the conical shell structures under the axial load for a variety of the shell configurations without performing some complex non-linear FEM analysis or numerical solutions. Furthermore, the discrepancy of the proposed new method and FEM results of the normalized load is found out to be the maximum 15% which can be considered in the acceptable limits for a highly nonlinear shell behavior of the lower base angles (10, 15 and 20º).

Implementation of the linear theory in the load carrying capacity calculations concludes with the high amount of deviations due to the presence of the circumferential ring and highly nonlinear shell response of the shell structures which is encountered at low base angles such as 10, 15 and 20º. The proposed expression for the normalized load minimizes this aforementioned deviation and keeps the results within the acceptable limits. Since particular equation coefficients of "a" and "b" are selected for a specific shell geometrical parameter range from the Table 5.7 in order to characterize the non-linear response of the corresponded shell geometry.

In the scope of the thesis, the value of r_1 is kept constant to be 50mm. Because the influence of the upper shell radius r_1 on the load carrying capacity can be neglected for a wide range of upper-to-bottom shell radius ratios "r_1/r_2" as a result of performed FEM simulations. However, the influence of the upper shell radius on the load carrying capacity of the shell structure is observed to be more apparent as the upper-to-lower shell radius ratio "r_1/r_2" approaches its extremities which are r_1/r_2=0 and 1.

The influence of initial imperfections, which represents an additional bending effect, is less significant in conical shells with base angle is less than 25°. From this point of view, it can be assumed that the reduction coefficient that is determined based on the cylindrical shell is considerably conservative for conical shells. The reduction coefficient does not drop below $\alpha = 0.70$ for different combinations of shell thickness and radial stiffness. Thus, the new value of the reduction coefficient is proposed as a constant value of $\alpha = 0.70$.

Circumferential ring implementation and its radial stiffness make a contribution to the load carrying capacity of the structure under the axial loading. The influence of the radial stiffness increases as r_e/t_{shell} parameter decreases. The results show that application of circumferential ring in lower r_e/t_{shell} dimensionless parameter value becomes more advantageously.

7.1 Scientific Contribution of the Doctoral Dissertation

The influence of the circumferential ring on the load carrying capacity of a conical shell under axial loading has not been involved fully in the European Recommendation ECCS [5]. Also, relationships in the recommendation are not applicable to the conical shells structures that have a base angle less than 25°.

Evaluation of the load carrying capacity of the fixed supported shell structures is outlined in the ECCS [5]. Nevertheless, this calculation may give higher values for the real application because of the flexible radial restrains. The results are presented in the study in order to complement the current state of knowledge of science and technology.

Determination of the limit load for the nonstandard conical shell structures with a circumferential ring has not been resolved yet. Validating the numerical results of the experimental study is necessary. After validation process, the study will be put on authorities display.

7.2 Implementation of the Results in Practice

This study proposes a new method to predict load carrying capacity of a conical shell structure and it suggests similarity parameters. By means of these parameters, experiments can be performed with small-scaled structures for simulation the real one. Additionally, the method allows estimation the load carrying capacity without any need of numerical analysis and avoids time-consuming. Thus, efforts have been made to contribute to the design process in fields such as transport, machinery and civil engineering where thin-walled shells are widely used. For this purpose, further studies should be accomplished primarily.

7.3 Future Works

For the further parts of the current study, the following evaluations and statements are to be completed, respectively which are;

- A validation methodology will be conducted in order to ensure that how the numerical study approaches the experimental results. Hereby, a specimen will be manufactured, and it will be loaded by a hydraulic press. A load history concerning vertical deformation will be extracted to make a comparison of proximity.
- The influence of the material nonlinearity is described in the ECCS for cylindrical shells in terms of $\alpha, \beta, \lambda,$ and η (see Table 4.5). It is suggested that the determination of the boundaries of the plastic and elastic-plastic region for the conical shells under axial loading should be investigated in further studies.

8 REFERENCES

[1] Orion Spacecraft NASA https://www.nasa.gov/exploration/systems/orion/gallery/index.html?id=368774

[2] Viertürmiger slowakischer Staubsilowagen vom Einsteller WAGONSERVIS spol.s.r.o. http://karow900.startbilder.de/bild/gueterwagen~slowakei~behalterwagen-mit-druckluftentladung-zb-zementstaubsilowagen/91164/viertuermiger-slowakischer-staubsilowagen-vom-einsteller-wagonservis.html

[3] Ars Technica and WIRED http://arstechnica.com/science/2013/04/how-nasa-brought-the-monstrous-f-1-moon-rocket-back-to-life/

[4] Meridian Manufacturing http://www.meridianmfg.com/hopper-bottom-galvanized-bins/

[5] ECCS TC8 TWG 8.4 Buckling of Steel Shells. European Design Recommendations. 5th Edition, ECCS, (2008), ISBN: 92-9147-000-92.

[6] EN 1993-1-6 (2007) Eurocode 3: Design of Steel Structures - Part 1-6: Strength and Stability of Shell Structures, The European Union, ISBN: 978 0 580 50669 7

[7] Středová D., Stabilitní Prolomení Kuželových Skořepin S Malým Vzepětím. Doctoral Thesis, Jan Perner Transport Faculty, 2012.

[8] Teng J.G. and Rotter J.M., Buckling of Thin Metal Shells, Spon Press, London, 2004, ISBN 0–419–24190–6.

[9] FEM Computer program COSMOS/M GeoStar 2010, SRAC (Structural Research and Analysis Corporation), Santa Monica, California.

[10] Seide P., Axisymmetrical Buckling of Circular Cones Under Axial Compression, Journal of Applied Mechanics, 1956;78:625-628.

[11] Donnell L. H., Stability of Thin-Walled Tubes Under Torsion, NACA, Technical Report, No. 479, Washington, 1933.

[12] Batdorf S. B., A Simplified Method of Elastic-Stability Analysis for Thin Cylindrical Shell, NACA, Technical Report, No. 874, Washington, 1947.

[13] Lackman L, Penzien J., Buckling of Circular Cones Under Axial Compression, Journal of Applied Mechanics, 1960:458-460.

[14] Seide P., Buckling of Circular Cones Under Axial Compression, Journal of Applied Mechanics, 1961.

[15] Weingarten VI, Morgan EJ, Seide P., Elastic Stability of Thin- Walled Cylindrical and Conical Shells Under Axial Compression, AIAA J, 1965;3:500-05.

[16] Weingarten VI, Morgan EJ, Seide P., Elastic Stability of Thin-Walled Cylindrical and Conical Shells Under Combined Internal Pressure and Axial Compression, AIAA J, 1965;3:1118-25.

[17] Singer J., Buckling of Circular Conical Shells Under Uniform Axial Compression, AIAA J, 1965;3:985-87.

[18] Tani J, Yamaki N., Buckling of Truncated Conical Shells Under Axial Compression, AIAA J, 1970;8:568-71.

[19] Pariatmono N, Chryssanthopoulos MK., Asymmetric Elastic Buckling of Axially Compressed Conical Shells with Various End Conditions, AIAA J, 1995;33:2218-27.

[20] Tavares SA., Thin Conical Shells with Constant Thickness and Under Axisymmetric Load, Computer & Structures, 1996;60:895-921.

[21] Teng JG, Barbagallo M., Shell Restraint to Ring Buckling at Cone-Cylinder Intersections, Engineering Structures, 1997;19:425-31.

[22]Chryssanthopoulos MK, Spagnoli A., The Influence of Radial Edge Constraint on The Stability of Stiffened Conical Shells in Compression, Thin-Walled Structures, 1997;27:147-63.

[23] Gupta NK, Easwara Prasad GL, Gupta SK., Plastic Collapse of Metallic Conical Frusta of Large Semi-Apical Angles. International Journal of Crashworthiness, 1997;2(4):349-366.

[24] Chryssanthopoulos MK, Poggi C, Spagnoli A., Buckling Design of Conical Shells Based on Validated Numerical Models, Thin-Walled Structures, 1998;31:257-270.

[25] Spagnoli A, Chryssanthopoulos MK., Elastic Buckling and Postbuckling Behaviour of Widely-Stiffened Conical Shells Under Axial Compression, Engineering Structures, 1999;21:845-55.

[26] Chryssanthopoulos MK, Poggi C., Collapse Strength of Unstiffened Conical Shells Under Axial Compression, Journal of Constructional Steel Research, 2001;57:165-84.

[27] Yu TX, Xue P, Tao XM., Flat-Topped Conical Shell Under Axial Compression, International Journal of Mechanical Sciences, 2001;43:2125-45.

[28] Thinvongpituk C, El-Sobky H., The Effect of End Conditions on The Buckling Load Characteristic of Conical Shells Subjected to Axial Loading, ABAQUS Users' Conference, Munich, 4-6 June 2003.

[29] Gupta NK, Sheriff NM, Velmurugan R., A Study on Buckling of Thin Conical Frusta Under Axial Loads, Thin-Walled Structures, 2006;44:986-996.

[30] Błachut J, Ifayefunmi O, Corfa M., Collapse and Buckling of Conical Shells, Proceedings of the Twenty-first (2011) International Offshore and Polar Engineering Conference, Maui, Hawaii, USA, June 19-24, 2011.

[31] Shakouri M, Kouchakzadehn MA., Stability Analysis of Joined Isotropic Conical Shells Under Axial Compression, Thin-Walled Structures, 2013;72:20-27.

[32] Gere J.M. and Goodno B.J., Mechanics of Materials, Global Engineering, Stamford, 2012, ISBN: 978-1-111-13602-4

[33] Jenike & Johnson Science Engineering Design

http://jenike.com/files/2012/10/BlueSiloCollapsing-41.jpg

[34] Trains Magazine http://cs.trains.com/trn/f/111/t/81033.aspx

[35] Caitríona de Paor, Buckling of Thin-Walled Cylinders: Experimental and Numerical Investigation, The Boolean, 2010.

[36] MPRNEWS http://www.mprnews.org/story/2010/12/12/snowstorm-sunday-metrodome-roof

[37] Tomek P., Vliv Počátečních Imperfekcí Na Pevnost A Stabilitu Tenkostěnných Skořepinových Konstrukcí. Doctoral Thesis, Jan Perner Transport Faculty, 2012.

[38] Brush, D.O. and Almorth, B.O., Buckling of Bars Plates and Shells, 1st Edition, McGraw Hill, New York, 1975, ISBN: 978-0-070-85028-6.

[39] Timoshenko, S.P. and Gere, J.M., Theory of Elastic Stability, McGraw Hill, New York and London, 1961, ISBN: 978-0-486-42207-2.

[40] Chajes, A., Principles of Structural Stability Theory, Prentice-Hall, Inc., Englewood Cliffs, New Jersey, 1974, ISBN: 978-0-137-09964-1.

[41] COSMOS/M User's Guide. Structural Research and Analysis Corporation. 2001.

[42] Lavasani A., Simple Solutions for Buckling of Conical Shells Composed of Functionally Graded Materials, Journal of Solid Mechanics, 2009;1:108-117.

[43] Ifayefunmi O., A Survey of Buckling of Conical Shells Subjected to Axial Compression and External Pressure, Journal of Engineering Science and Technology Review, 2014;7:182-189.

[44] Bushnell D., Computerized Buckling Analysis of Shells. Kluwer Academic Publishers, 1989, ISBN 90-247-3099-6.

[45] Bushnell D., Computerized Analysis of Shells – Governing Equations, Computer & Structures, 1984;18:471-536.

[46] Simulia, D. S., Abaqus 6.13, Getting Started with Abaqus Interactive Edition, Dassault Systems, Providence, RI, 2013.

[47] EN ISO. 6892-1. metallic materials-tensile testing-part 1: Method of test at room temperature. International Organization for Standardization, 2009.

9 STUDENT PUBLICATIONS

- Yilmaz H., Ozyurt E., Pascenko P., (2015) Elastic buckling of thin conical caps with edge ring constraint under uni-axial compression, International Journal of Scientific and Technological Research Vol 1, No.9, 1-9

- Ozyurt E., Yilmaz H., Pascenko P., (2015) An investigation on dynamic response of truncated thick walled cones with edge ring under axial compressive impact load, International Journal of Scientific and Technological Research Vol 1, No.9, 21-30

- Yilmaz, H., Ozyurt, E. Tomek, P, (2017) A Comparative study between numerical and analytical approaches to load carrying capacity of conical shells under axial loading, International Journal of Engineering Trends and Technology (IJETT), Vol 52, No.l

- Yilmaz H., Kocabas I., Ozyurt E, (2017) Empirical equations to estimate non-linear collapse of medium-length cylindrical shells with circular cutouts, Thin-Walled Structures, Vol 119, 868-878.

- Ozyurt, E.Yilmaz, H., Tomek, P, (2018) Prediction of the influence of geometrical imperfection to load carrying capacity of conical shells under axial loading. Sigma Journal of Engineering and Natural Sciences, Vol 36, 11-20.

10 APPENDICES

Table 10.1. Results of the numerical analyses and theoretical calculations for base angle 10°.

	r_e/t_{shell}													
	360	**480**	**576**	**720**	**800**	**900**	**1028**	**1200**	**1440**	**1600**	**1800**	**2057**	**2399**	**2879**
A_{ring} [mm]	**Limit Load F_{lim} [kN]**													
6	77.5	46.2	33.7	23.4	19.9	16.7	13.9	11.2	8.79	7.58	6.38	5.21	4.10	3.09
9	84.8	53.8	41.0	29.9	25.7	21.7	17.9	14.1	10.6	8.99	7.42	5.96	4.56	3.18
12	95.7	63.64	49.2	35.3	30.0	24.9	20.2	15.5	11.5	9.69	7.97	6.20	4.57	3.19
15	108	72.70	55.5	38.8	32.5	26.6	21.5	16.3	12.1	10.21	7.93	6.20	4.58	3.20
30	146	92.42	67.5	45.3	37.5	30.5	24.2	17.9	12.5	10.18	8.02	6.12	4.46	3.21
45	157	99.00	72.3	48.7	40.4	31.9	24.3	17.9	12.5	10.17	8.04	6.15	4.49	3.18
60	163	103.7	76.2	51.3	40.6	31.8	24.3	17.9	12.5	10.19	8.05	6.19	4.50	3.20
90	173	112.3	83.5	50.9	40.7	31.9	24.4	17.9	12.5	10.16	8.05	6.19	4.58	3.21
150	190	117.4	82.9	50.8	40.7	32.0	24.4	17.9	12.5	10.17	8.06	6.20	4.58	3.21
300	209	119.3	81.1	50.7	40.8	32.0	24.5	18.0	12.5	10.12	8.05	6.20	4.58	3.22
***F_{cr}**	365	205.6	142	91.3	74.0	58.4	44.78	32.90	22.85	18.51	14.62	11.20	8.23	5.71

*F_{cr} values are calculated via theoretically and represent critical load.

	r_e/t_{shell}									
	360	**480**	**576**	**720**	**900**	**1200**	**1440**	**1800**	**2399**	**2879**
Γ	**Limit Load F_{lim} [kN]**									
1	207.4	128.8	85.15	51.5	32.28	17.98	12.44	7.93	4.46	3.11
5	203.9	128.8	85.14	51.46	32.01	17.91	12.44	7.93	4.46	3.11
10	176.2	107.8	76.78	49.7	31.69	17.82	12.44	7.95	4.46	3.11
20	160.1	96.47	68.39	44.25	28.59	16.55	11.77	7.73	4.46	3.11
40	144.4	85.83	60.6	39.09	25.15	14.34	10.07	6.5	3.7	2.58
60	128.5	75.16	52.62	33.67	21.44	12.02	8.34	5.3	2.96	2.04
80	112.8	64.88	44.98	28.65	18.05	10.02	6.9	4.38	2.43	1.67
100	100.9	52.08	39.49	24.95	15.79	8.76	6.05	3.83	2.14	1.48

Table 10.2. Results of the numerical analyses and theoretical calculations for base angle 15°.

	r_e/t_{shell}													
	241	**322**	**386**	**483**	**537**	**604**	**690**	**805**	**966**	**1073**	**1207**	**1380**	**1610**	**1932**
A_{ring} [mm]	**Limit Load F_{lim} [kN]**													
6	174	102	74.7	51.8	44.1	37.0	30.5	25.0	19.6	17.05	14.49	11.99	9.53	7.13
9	189	118	89.7	65.7	57.0	48.5	40.2	32.2	24.3	20.79	17.17	13.95	10.85	7.66
12	212	138	107	78.6	68.1	56.3	45.9	36.1	26.9	22.66	18.78	14.68	10.88	7.65
15	240	159	122	88.4	75.3	61.5	49.5	38.5	28.5	24.04	18.99	14.68	10.82	7.26
30	341	210	153	107	90.1	72.6	58.5	42.8	29.6	24.03	19.04	14.63	10.89	7.67
45	377	227	165	113	95.8	76.1	58.3	42.6	29.6	23.97	19.07	14.61	10.89	7.62
60	397	239	174	118	96.1	76.1	58.3	42.7	29.6	23.97	19.05	14.69	10.86	7.61
90	426	259	185	118	96.3	76.2	58.2	42.7	29.6	24.04	19.03	14.61	10.80	7.63
150	475	272	185	119	95.9	76.2	58.2	42.7	29.6	24.0	19.02	14.62	10.84	7.57
300	507	272	186	118	96.2	76.2	58.2	42.6	29.6	24.0	19.07	14.66	10.85	7.64
***F_{cr}**	816	459	318	204	165	130	100	73.4	51.0	41.3	32.66	25.00	18.37	12.76

*F_{cr} values are calculated via theoretically and represent critical load.

	r_e/t_{shell}									
	241	**322**	**386**	**483**	**604**	**805**	**966**	**1207**	**1610**	**1932**
Γ	**Limit Load F_{lim} [kN]**									
1	513	277.5	190.6	120.7	76.45	42.39	29.22	18.6	10.5	7.31
5	512.6	277.8	188.2	119.6	76.45	42.45	29.22	18.6	10.5	7.31
10	434	249.8	175.9	116	76.43	42.51	29.22	18.6	10.5	7.31
20	385.6	224.4	155.5	101.7	66.96	38.94	27.54	18.1	10.5	7.31
40	335.9	193	135.4	88	57.22	32.71	22.9	14.8	8.4	5.88
60	290.2	165.4	115.3	74.1	47.49	26.64	18.45	11.7	6.6	4.53
80	250.6	141.3	97.8	62.3	39.57	22.04	15.17	9.6	5.4	3.71
100	222.6	124.5	86	54.6	34.73	19.34	13.37	8.5	4.8	3.3

Table 10.3. Results of the numerical analyses and theoretical calculations for base angle 20°.

	r_e/t_{shell}													
	183	**244**	**292**	**365**	**406**	**457**	**522**	**609**	**731**	**812**	**914**	**1044**	**1218**	**1462**
A_{ring} [mm]	**Limit Load F_{lim} [kN]**													
6	309	181	132	91.6	77.4	64.9	53.7	43.95	34.59	30.20	25.72	21.44	17.79	13.10
9	333	207	156	115	102	85.2	71.0	57.42	44.04	37.69	31.53	25.24	20.20	14.32
12	371	242	189	138	120	101	82.7	65.26	49.16	41.57	34.09	27.23	20.24	14.32
15	417	279	218	156	133	113	89.7	73.28	52.47	44.33	35.28	27.48	20.25	14.32
30	604	381	284	193	162	133	107	78.63	54.73	44.41	35.28	27.50	20.22	14.32
45	675	411	304	212	178	140	106	78.59	54.55	44.45	35.27	27.41	20.25	14.32
60	713	435	322	222	179	140	107	78.67	54.67	44.45	35.29	27.20	20.23	14.32
90	769	483	345	221	178	140	106	78.63	54.73	43.95	35.08	27.21	20.24	14.31
150	855	495	346	221	178	140	106	78.43	54.73	44.22	35.03	27.19	20.22	14.29
300	888	499	347	221	178	140	107	78.70	54.71	44.32	35.08	27.22	20.14	14.03
***F_{cr}**	1425	801	556	356	288	228	174	128	89.1	72.1	57.0	43.6	32.1	22.27

*F_{cr} values are calculated via theoretically and represent critical load.

	r_e/t_{shell}									
	183	**244**	**292**	**365**	**457**	**609**	**731**	**914**	**1218**	**1462**
Γ	**Limit Load F_{lim} [kN]**									
1	920.3	511.9	352.9	223.1	140.6	77.8	53.6	34.1	19.2	13.4
5	909.5	503.6	351.3	223.7	140.8	77.7	53.6	34.1	19.2	13.4
10	783.8	455.4	325.9	216.9	141.1	77.7	53.6	34.1	19.2	13.4
20	691	398.9	283.2	186.4	122.3	71	50.3	33.1	19.2	13.4
40	593.1	342	241.6	157.5	102.3	58.4	40.94	26.4	15	10.5
60	504.9	288.9	202.2	130.2	83.3	46.7	32.4	20.6	11.5	8
80	434.2	245.4	170.4	108.7	69.1	38.5	26.6	16.9	9.46	6.6
100	386.5	199.7	150.2	95.58	60.9	34	23.5	15	8.43	5.9

Whole results in the appendices were obtained for the conical shell having r_1=50mm and r_2=250mm.